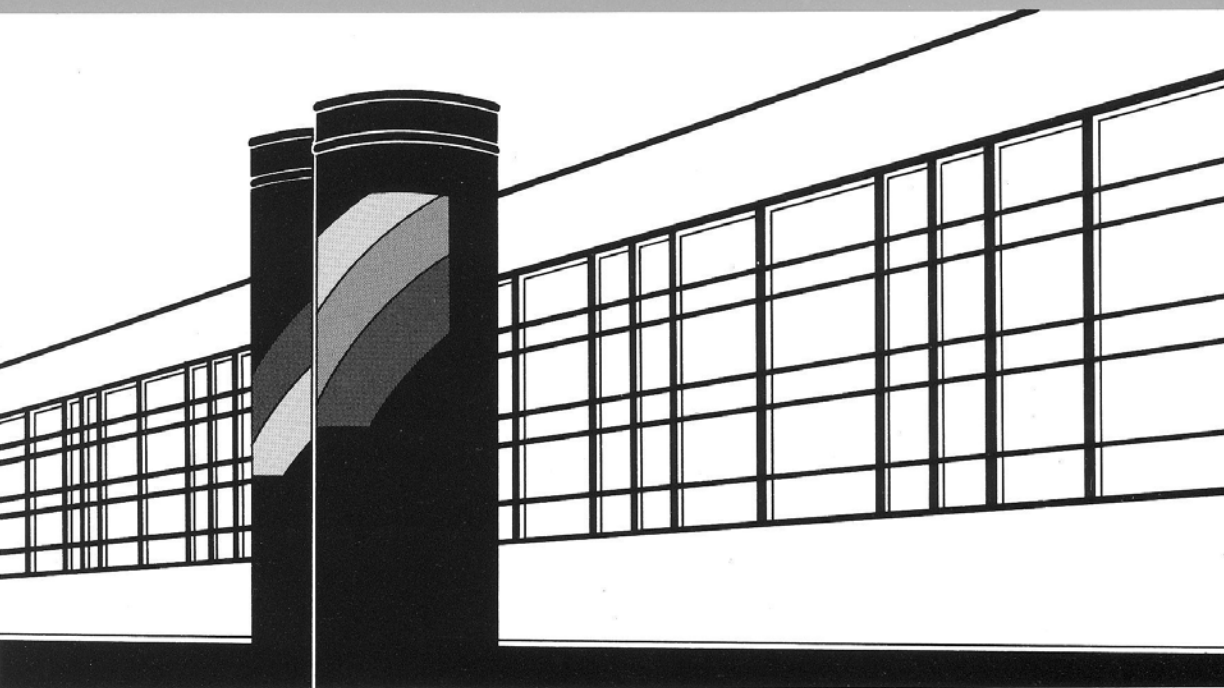


Institut für Wasserbau · Universität Stuttgart

Mitteilungen



Heft 98

Yichun Xu

Numerical Modeling of Suspended
Sediment Transport in Rivers

Numerical Modeling of Suspended Sediment Transport in Rivers

Von der Fakultät Bau- und Umweltingenieurwissenschaften der
Universität Stuttgart zur Erlangung der Würde eines
Doktor-Ingenieurs (Dr.-Ing.) genehmigte Abhandlung

Vorgelegt von
Yichun Xu
aus VR China

Hauptberichter:	Prof. Dr.-Ing. Bernhard Westrich
Mitberichter:	Prof. Dr. h.c. Helmut Kobus
	Prof. David Stephenson, MSc (Eng.) PhD, Dsc (Eng.)

Tag der mündlichen Prüfung: 24. Juli 1998

Institut für Wasserbau der Universität Stuttgart
1998

Heft 98 Numerical Modeling of
Suspended Sediment
Transport in Rivers

von
Dr.-Ing.
Yichun Xu

D93 Numerical Modeling of Suspended Sediment Transport in Rivers

Titelaufnahme der Deutschen Bibliothek

Xu, Yichun:
Numerical Modeling of Suspended Sediment Transport in Rivers / von Yichun Xu
Institut für Wasserbau, Universität Stuttgart. - Stuttgart: Inst. für Wasserbau,
1998

(Mitteilungen / Institut für Wasserbau, Universität Stuttgart: H. 98)

Zugl.: Stuttgart, Univ., Diss., 1998)

ISBN 3-933761-00-X

NE: Institut für Wasserbau <Stuttgart>: Mitteilungen

Gegen Vervielfältigung und Übersetzung bestehen keine Einwände, es wird lediglich um Quellenangabe gebeten.

Herausgegeben 1998 vom Eigenverlag des Instituts für Wasserbau

Druck: Sprint-Druck, Stuttgart

Vorwort

Der Ausbau der Flüsse für die Belange der Energiewirtschaft und des Schiffsverkehrs hat mitunter Aufstaumaßnahmen erforderlich gemacht, die zu starken Sedimentationserscheinungen geführt haben. In Flußstauhaltungen, Talsperren und Rückhaltebecken kommt es teilweise zu starken Schwebstoffablagerungen, die sowohl aus quantitativer wie auch qualitativer Sicht zu Problemen führen. Für die Gewässermorphologiesi sind Erosions- und Sedimentationsprozesse von großer Bedeutung. Mathematisch numerische Transportmodelle sind geeignete Instrumentarien für die Beurteilung morphologischer Entwicklungstendenzen und können einen wichtigen Beitrag liefern für Gewässerentwicklungskonzepte, Gewässerunterhaltung und Sedimentmanagement.

Großräumige Transportprobleme in Fließgewässern werden häufig mit 1-dimensionalen Modellansätzen beschrieben, wobei auf eine laterale Differenzierung der Transportprozesse innerhalb des Fließquerschnittes verzichtet wird. Mit dem in der vorliegenden Arbeit weiterentwickelten Stromröhrenmodell kann das Strömungsfeld erfaßt und die damit verbundenen Sedimentations-, Erosions- und Transportprozesse quasi 2-dimensional beschrieben werden. Das Verfahren ist besonders geeignet zur Quantifizierung der Sedimentation auf überfluteten Vorländern und in ufernahen Strukturen, wie beispielsweise Bühnenfeldern. Die Modellierung des Erosions- und Sedimentationsverhaltens von Suspensionsmischungen wird mit probabilistischen Ansätzen für die einzelnen Schwebstofffraktionen weiterentwickelt und mit experimentellen Daten anderer Autoren überprüft und verifiziert.

Die Anwendung des quasi 2-dimensionalen Schwebstofftransportmodells zur Vorhersage der Sedimentationsprozesse in dem weltweit bekannten Stausee des 3-Schluchten-Projekts am Jangtze in China zeigt eindrucksvoll die räumliche und zeitliche Entwicklung des Verlandungsprozesses sowie den Anteil der einzelnen Kornfraktionen des Schwebstoffgemisches an der Gesamtssedimentation. Für den prognostizierten Zeitraum von 76 Betriebsjahren zeigt sich eine außerordentlich gute Übereinstimmung mit den an der Tsinghua Universität in Peking durchgeführten flußhydraulischen Modellversuchen. Darüber hinaus wurde für die Stauhaltung Lauffen am Neckar auf der Basis einer hydrologisch generierten Zeitreihe eine Langzeitprognose der Stauraumverlandung durchgeführt und die Entwicklung des Sedimentationsvolumens dargestellt. Für eine ausgewählte Abflußperiode von 1989 bis 1994 wurde eine Sedimentbilanz erstellt und hierbei die Schwebstoffablagerungen auf dem überfluteten Vorland rechnerisch zu 1,3 zeigt, daß mit dem Modell wichtige Teilbilanzen erstellt werden können, die für morphologische und gewässerökologische Auswirkungen der Sedimentation von Bedeutung sind.

Die Arbeit liefert wichtige Ansatzpunkte für die Berücksichtigung des korngrößenabhängigen Erosions- und Sedimentationsverhaltens und stellt damit eine wichtige Ausgangsbasis dar für eine weitergehende Beschreibung des korngrößenspezifischen partikulären Schadstofftransportes in Fließgewässern.

Stuttgart, im September 1998

Bernhard Westrich

Danksagung

Die vorliegende Arbeit entstand während meiner Tätigkeit als wissenschaftliche Mitarbeiterin am Institut für Wasserbau der Universität Stuttgart.

Herrn Professor Westrich möchte ich für die finanzielle Unterstützung und für die Übernahme des Hauptberichts herzlich danken.

Herr Professor Kobus hat mich nach Stuttgart eingeladen. Dies ermöglichte es mir hier zu Arbeiten und zu Studieren. Hierfür und für die Übernahme des Koreferats möchte ich mich herzlich bei ihm bedanken.

Mein Dank gilt Herrn Professor Stephenson für die Übernahme des zweiten Koreferats und die Durchsicht meines Dissertations.

Besonderer Dank gebührt Herrn Dr. Kern für seine Hilfsbereitschaft und die kritische Durchsicht des Manuskriptes. Mein Dank gilt auch Herrn Dr. Cirkpa für die sorgfältige Durchsicht des Manuskriptes und seine Anregungen. Allen Kolleginnen und Kollegen des Instituts danke ich für die gute Zusammenarbeit und die Unterstützung, die sie mir jederzeit bereitwillig gewährten. Mein Dank gilt M.Sc. Birks für sprachliche Verbesserungen in der Dissertation.

Contents

List of Figures	III
List of Tables	VIII
Notation	X
Zusammenfassung (Summary in German)	XIV
1 Introduction	1
1.1 Problem	1
1.2 Purpose of the work	3
1.3 Organization of the present work	3
2 State of the art	5
2.1 Suspended sediment transport	5
2.1.1 Suspended sediment load	5
2.1.2 Diffusion and Dispersion of particles	9
2.1.3 Suspended sediment transport for uniform sediments	16
2.1.4 Suspended sediment transport for nonuniform sediment mixtures	20
2.1.5 Flood plain sedimentation	28
2.2 Model research situation	34
2.2.1 General remarks	34
2.2.2 Overview of present models	38
3 Numerical models	45

3.1	Stream tube model	46
3.1.1	Model concept	46
3.1.2	Application of the stream tube model	48
3.1.3	Governing equations in the flow calculation	57
3.1.4	Stream tube computation	58
3.2	Suspended sediment transport model for uniform sediments	60
3.2.1	Natural orthogonal curvilinear coordinate system	60
3.2.2	Governing equations for suspended sediment transport	63
3.2.3	Numerical method	66
3.3	Suspended sediment transport model for nonuniform sediment mixtures . .	73
3.3.1	Probabilistic approach to nonuniform suspended sediment transport	74
3.3.2	Governing equations of suspended sediment transport for nonuniform sediment mixtures	83
4	Model test and application	88
4.1	Model test by physical model studies	88
4.1.1	Sediment transfer from main channel to flood plains	89
4.1.2	Transport model of nonuniform sediment mixtures	91
4.2	Field study in the Lauffen Reservoir on the River Neckar	98
4.2.1	Description of study reach	99
4.2.2	Calibration of the flow model	101
4.2.3	Calibration and application of transport model for uniform sediments	103
4.2.4	Investigation of selective transport of nonuniform sediment mixtures	124
4.3	Sediment exchange between the stream and the dead water zones	132
4.3.1	Lateral exchange	132

4.3.2 Case study	133
5 Conclusions and proposals	135
5.1 Conclusions	135
5.2 Proposals	137
Reference	138

List of Figures

1.1	Framework of the present work.	4
2.1	River channel adjustment upstream and downstream a dam	6
2.2	Longitudinal development of sedimentation in a river with a constructed dam. After Westrich, B. (1988) [167]	6
2.3	Sediment transport mode	7
2.4	Turbulent boundary layers on the plane walls. a. Burst-sweep cycles of turbulence and associated patterns of shear stress, deposition and erosion. According to Allen (1983) [3] and Leeder (1983) [78]. b. Position of the interface between marked and unmarked fluid showing the sweep-bursting may be controlled by the movement past the bed of large horseshoe vortices of outer flow, according to Falcon (1977) [35].	8
2.5	Relationship between the turbulent flow and sediment transport in open channel. After Nezu and Nakagawa (1993) [100]	9
2.6	Dispersion in natural channels	10
2.7	Vertical distribution of suspended sediment concentration. After Vanoni (1963)[156].	14
2.8	Velocity profile for sediment-laden and clear-water flow. After Vanoni et al. (1960) [160] *.	15
2.9	Critical shear stress for erosion and suspension. After van Rijn (1984) [154]	17
2.10	Definition sketch, suspended sediments interacting with losse bed	27
2.11	Secondary current vectors. After Tominage and Nezu (1991) [147] (experiment) and Naot et al. (1993) [99] (computation). a. $h_m/h_p = 0.5$, $\frac{W_{max}}{\langle W \rangle} = 1.24$. and b. $h_m/h_p = 0.25$, $\frac{W_{max}}{\langle W \rangle} = 1.28$. solid line: $\frac{W}{W_{max}}$, dashed line: $10^3 \frac{\psi}{\langle W \rangle H}$	29
2.12	Dispersion coefficient at the interaction zone between the main channel and the flood plains. After Ashida et. al. (1988) [8]	31

2.13 Bottom shear stress distribution in a compound section. After Pasche (1985) [107]	33
2.14 Framework of sediment transport modeling	35
3.1 Open-channel flow	49
3.2 Compound channel flow configuration. After Rajaratnam and Ahmadi (1981) [118]	50
3.3 Stream tube distribution	51
3.4 Mass exchange between the main stream and the groyne fields	55
3.5 Definition of hydraulic variables	56
3.6 Flow chart showing the steps for calculation of stream tube locations	59
3.7 Definition of metric coefficients	61
3.8 Control volume with the center point P	66
3.9 Schematic element and node arrangement used to evaluate the sediment concentration variables	67
3.10 Schematic convection and diffusion terms	68
3.11 Selective transport: particle size sorting and critical velocity for particle sedimentation along a river course	74
3.12 Gaussian distribution of instantaneous bottom shear stress and critical shear stress.	75
4.1 Sketch of flume experiment set-up of James.	90
4.2 Comparison of deposition distribution on the flood plain calculated and measured by James [58].	91
4.3 Sketch of flume experiment set-up of Samaga et al. (1986).	92
4.4 Cumulative grain size distribution of original bed material used for flume experiments by Samaga et al. (1986).	93

4.5	Comparison between computed and measured grain-size distributions of suspended load in flume experiments of Samaga et al. (1986).	9
4.6	Sketch of the TGP Reservoir showing the calculation domain in present work. After Zhou (1995) [185].	9
4.7	Median diameter and grain size distribution of suspended sediment inflow used for present work.	9
4.8	Comparison of accumulated deposition volumes over the 76-year period of calculation predicted and measured in the river model.	9
4.9	Changes in cross sectional areas along the river course below 145 m (FCL) during operation.	9
4.10	Changes in the cross sectional areas below 145 m (FCL) during operation.	9
4.11	Plan of the Lauffen Reservoir from Besigheim to Lauffen.	10
4.12	Measured deposition volumes (from 125.2 to 130.0 km) during the period of 1973 - 1994. After Kern (1997) [62].	10
4.13	Reproduction of water surface profiles for the greatest discharges over the floods of 1978, 1990, 1993 and 1994. Solid line: model calculation, open squares: field measurement.	10
4.14	Reproductions of water surface elevation at the gauge of Besigheim during the flood events from 1978 to 1994.	10
4.15	Hydrograph and suspended sediment concentration at Besigheim over the calibration period, from 1973 to 1994 [62].	10
4.16	Characteristics of flow variables: a. Water surface and river bed profiles in the study reach, b. Velocity distribution along the river ($Q = 500m^3/s$); c. Bottom shear stress increasing with discharge.	10
4.17	Critical shear stress of cohesive sediment. After Tsai and Lick (1987) [148].	10
4.18	Scheme of the two layer sediment model.	11
4.19	Comparison of calculated concentration profiles of suspended sediment with the data measured at 23/11/1992.	11

4.20	Comparison of calculated lateral concentration distribution of suspended sediment with the data measured at 07/03/1994 and 08/03/1994.	112
4.21	a. Concentration distribution of suspended sediment calculated, b. Grid for computation.	113
4.22	Comparison of the calculated and measured data: a. Changes in average river bed elevation; b. Changes in the minimum river bed elevation; c. Changes in cross-sectional area; d. Changes in bankfull cross-sectional area over the calibration period, from 1973 to 1994.	114
4.23	Relationship of discharges, deposition and erosion rates along the river centerline.	117
4.24	Deposition volume versus time during the prediction period.	120
4.25	Comparing the calculated and measured data: a. Changes in the average river bed elevation; b. Changes in the minimum river bed elevations; c. Changes in cross-sectional area; d. Changes in the bankfull cross-sectional area over the prediction period, from 1995 to 2045.	121
4.26	Characteristics of overbank flow and calculation of sediment deposition on the flood plains from 1989 to 1994: a. Hydrograph over the calculated period; b. Total deposition volume on the flood plains; c. Maximum water surface width of overbank flow; d. Maximum deposition volume on the flood plains; e. Maximum deposition height from 1989 to 1994.	123
4.27	Measured grain size distribution of bed material in the Lauffen Reservoir. .	124
4.28	Measured grain size distribution of suspended sediment load in the Lauffen Reservoir. After Kern [64].	125
4.29	Evaluation of the grain size distribution of suspended sediment inflow according to measured data.	126
4.30	Grain size distributions of suspended sediment inflow used for computation.	126
4.31	Original grain size distribution of bed material assumed for computation. .	127
4.32	Hydrograph of the flood 1993.	127
4.33	Influence of discharges on the grain size distributions of active layer material and eroded material.	128

4.34 Grain size distributions of the active-layer material along the river varying with time.	128
4.35 Grain size distributions of eroded and active-layer material at selected locations.	129
4.36 Longitudinal distribution of the median diameter of the active sediment layer after the flood 1989.	129
4.37 Lateral grain size distribution of bed material after the 81-hours calculation.	130
4.38 Effect of selective transport on the erosion volume.	130
4.39 Grain size distribution of suspended sediment load at the station 125.2 km on the River Neckar.	131
4.40 Influence of mass exchange coefficients between the stream and dead water zone on the sediment concentration distribution.	133
4.41 Sediment concentration distribution under the condition of a high erosion rate in the groyne field.	134

List of Tables

2.1	Critical flow conditions for sediment suspension	18
2.2	Formulae to determine entrainment rates for nonuniform sediment mixtures	24
2.4	Expressions of the turbulent shear stress	31
2.5	Convection-diffusion equations used by different models	38
2.6	Selected existing models	39
4.1	Flow variables used in the simulations of James' flume study (1985).	89
4.2	Hydraulic parameters of the flume experiment of Samaga et. al. (1986)	92
4.3	Comparison between measured and computed grain size distribution of suspended sediment load in the flume study by Samaga et. al (1986)	94
4.4	Mean deviation of the water surface elevations calibrated from measured.	103
4.5	Transported suspended sediment volume (in $10^6 m^3$) over the calibration period	105
4.6	Balance of sediment volume based on the measured profiles	107
4.7	Parameters used for the model calibration	108
4.8	Change in average river bed elevation in the Lauffen Reservoir from 1973 to 1994.	115
4.9	Changes in bankfull cross-sectional areas (in m^2) in the Lauffen Reservoir from 1973 to 1994.	116
4.10	Influence of the number of stream tubes selected on the calculated total sed- iment volume and the calculated water surface level for different discharges varying with time.	118
4.11	Formulae to describe flow, particle exchange, deposition and erosion within groyne fields.	132

Notation

Dimensions

L	Length
M	Mass
T	Time

Variable	Physical Meaning	Dimension
A_i	Local area of strip or stream tube in cross section i	$[L^{-2}]$
A_T	Cross-section area	$[L^2]$
B	Width of channel, length of the interaction zone between the main channel and the flood plain	$[L]$
$B_{i,k}$	Width of the i th stream tube at the k th cross-section	$[L]$
C	Courant number	
C	Depth-averaged local suspended sediment concentration	$[ML^{-3}]$
C_a	Suspended sediment concentration at a reference level a	$[ML^{-3}]$
C_n	Suspended sediment concentration of size fraction n	$[ML^{-3}]$
d	Grain size of sediment	$[L]$
d_{16}	Grain size for which 16% of sediment by weight is finer	$[L]$
d_{50}	Median grain size	$[L]$
d_{84}	Grain size for which 84% of sediment by weight is finer	$[L]$
D_e	Mass diffusion rate through the east face of a control volume	$[MLT]$
d_m	Mean grain size of sediment	$[L]$
D_x	Dispersion coefficient in x direction	$[L^2T^{-1}]$
D_z	Dispersion coefficient in z direction	$[L^2T^{-1}]$
D_*	Dimensionless sediment parameter	
\dot{E}	Erosion rate	$[ML^{-2}T^{-1}]$
F_e	Mass flow rate through the east face of a control volume	$[MLT]$
g	Gravitational acceleration	$[MT^{-2}]$
h	Local average water depth	$[L]$

h_m	Water depth in the main channel	[L]
h_p	Water depth on the flood plain	[L]
J_T	Energy slope	
$L_{i,k}$	Distance between the k th and $(k - 1)$ th cross-sections along the i th streamline	[L]
$L_{L,k}$	Distance between the k th and the $(k - 1)$ th cross-sections along the longitudinal coordinate which are coincided with the right river bank	[L]
$L_{R,k}$	Distance between the k th and the $(k - 1)$ th cross-sections along the longitudinal coordinate which are coincided with the left river bank	[L]
M	Erosion parameter	[ML ⁻² T ⁻¹]
m_x	Metric coefficient in x direction	
m_z	Metric coefficient in z direction	
N	Total number of computation nodes	
P	Peclet number	
p_{an}	Percentage of eroded material of grain size fraction n	
p_{bn}	Percentage of material of grain size fraction n in the bed surface	
R_T	Hydraulic radius of a cross section	[L]
q	Lateral discharge	[L ⁻³ T ⁻¹]
Q	Discharge	[L ⁻³ T ⁻¹]
R_i	Hydraulic radius of a strip	[L]
\dot{S}	Deposition rate	[ML ⁻² T ⁻¹]
t	Time	[T]
T_k	Sedimentation coefficient	
T_a	Thickness of the active layer	[L]
u	Local depth-averaged velocity in the longitudinal (streamline) direction	[LT ⁻¹]
u_m	Flow velocity in the main channel	[LT ⁻¹]
u_p	Flow velocity on the flood plain	[LT ⁻¹]
u_*	Shear velocity	[LT ⁻¹]
v	Local depth-averaged velocities in the lateral direction	[LT ⁻¹]
w	Vertical velocity	[LT ⁻¹]
w'	Vertical velocity deviation from time average	[LT ⁻¹]

w_s	Fall velocity of sediment	[LT ⁻¹]
$w_{s\ n}$	Fall velocity of sediment of size fraction n	[LT ⁻¹]
x, y, z	Spatial coordinates	[L]
y_{bnl}	Thickness of size fraction n in the layer l	[L]
z	Distance from the interface to the main channel in the transverse direction	[L]
α	Coefficient used for determining the lateral dispersion of mass between the main channel and the flood plain	
α_n	The ratio of mean effective velocities for fractional sediment re-suspension and deposition	
α_s	Coefficient of the vertical concentration distribution	
$\alpha_{s\ n}$	Coefficient of the concentration distribution of size fraction n	
β	Boussinesq coefficient	
β_x	Longitudinal dispersion coefficient	
β_z	Lateral dispersion coefficient	
Δ	Bedform height	[L]
Δx	Distances along the axes x	[L]
Δy	Change in bed elevation	[L]
Δz	Distances along the axes z	[L]
κ	Coefficient or von Kármán constant, $\kappa = 0.4$ for clear water	
∇	Vector gradient operator	[L ⁻¹]
∇^2	Laplacian scalar operator	[L ⁻²]
ν	Kinematic viscosity	[MLT]
ψ	Stream function	
ρ	Water* density	[ML ⁻³]
ρ_p	Bulk density of sediment	[ML ⁻³]
ρ_s	Sediment density	[ML ⁻³]
σ_g	Gradation coefficient for nonuniform sediment mixture $\sigma_g = \frac{\sigma_{84}}{\sigma_{16}}$	
σ_{st}	Turbulent-Schmidt number	
σ_w	Standard deviation of the distribution of w' and $\sigma_w = \sqrt{w'^2} = u_*$	
τ	Bottom shear stress	[ML ⁻¹ T ⁻¹]
$\tau_{0\infty}$	Undisturbed bottom shear stress on the flood plain	[ML ⁻¹ T ⁻¹]
τ_{crf}	Critical shear stress of erosion for fresh deposition	[ML ⁻¹ T ⁻¹]

τ_{cr_o}	Critical shear stress of erosion for old deposition	$[ML^{-1}T^{-1}]$
$\tau_{cs\ n}$	Critical shear stress of size fraction n	$[ML^{-1}T^{-1}]$
τ_{zx}	Shear stress at the interface between the main channel and the flood plains	$[ML^{-1}T^{-1}]$
ε	Convergence criterion	
ε_m	Molecular diffusion coefficient	$[L^2T^{-1}]$
ε_s	Diffusion coefficient of sediment particles	$[L^2T^{-1}]$
ε_t	Diffusion coefficient of turbulent flow	$[L^2T^{-1}]$
$\varepsilon_x, \varepsilon_y, \varepsilon_z$	Diffusion coefficients of turbulent flow in x, y, z direction	$[L^2T^{-1}]$
ζ	Rouse number	

super-/subscripts

b	River bed, dead water zone
I	ith computation section along the flow direction
k	jth stream tube along the cross section
l	Layer number
m	Main stream
n	Grain size fraction
p	Flood plain
s	Sediments

Zusammenfassung

(Summary in German)

Einführung

Der Ausbau und die Regulierungen von Flußläufen zur menschlichen Nutzung stellt eine wichtige Aufgabe dar. Ein alluvialer Fluß ist ein selbstregulierendes System. Er reagiert auf das durch menschliche Eingriffe wie z.B. Stauanlagen, Dammbau, Uferschutz gestörte dynamische Gleichgewicht durch morphologische Gegenentwicklungen. Zu diesen Prozessen zählen Veränderungen des Sohlgefälles, der Korngrößenverteilung des Sohlmaterials, der Fließquerschnitte und des Flußverlaufs. Der Anpassungsprozeß läßt sich an den morphologischen Veränderungen und dem Fließverhalten des Flusses erkennen. Die Beurteilung und Vorhersage der morphologischen Veränderungen stellt somit eine wichtige Aufgabe für das Flußmanagement dar.

Hochwasserereignisse spielen für die Flußmorphologie eine herausragende Rolle, da Sedimente meistens während Hochwasserperioden transportiert und umgelagert werden. Im Falle von Ausuferungen haben die Vorländer einen großen Einfluß auf den Feststofftransport. Die Erosion an der Flußsohle wird gebremst und auf den Vorländern kommt es zur Ablagerung von Sedimenten.

Die morphologischen Veränderungen eines Flusses hängen von den Einwirkungen von Strömung und Sedimenttransport ab. Für den Sedimenttransport sind die Ablagerung und Erosion von Feststoffen die maßgebenden Prozesse. Diese Prozesse werden von den Eigenschaften und der Kornverteilung des Sohlmaterials beeinflusst. Die unterschiedliche Partikelgröße der verfügbaren suspendierten Partikel und die davon abhängige Sinkgeschwindigkeitsverteilung führen zu einer selektiven Sedimentation. Entsprechendes gilt für das verfügbare Material an der Sohle und die davon abhängige Verteilung der kritischen Erosionsschubspannung hinsichtlich einer selektiven Erosion.

Die selektiven Transportmechanismen haben zur Folge, daß sich die Kornzusammensetzung der Sohle entlang eines Flusses verändert. Bei ungleichförmiger Kornverteilung während des Transport- und Sedimentationsprozesses findet eine Kornsortierung nach der Größe statt. Die Suspension der feineren Partikel führt zu einer Anreicherung von grobkörnigem Material an der Sohle, deren Erosionsfähigkeit dadurch verringert wird. Die feinen Sedimente lagern sich in Stauhaltungen und anderen Stillwasserzonen ab. Durch die weitergehende Sedimentkonsolidierung erhöht sich die Erosionsstabilität der Flußsohle im Laufe der Zeit. Feinsedimente können als Träger von Schadstoffen fungieren. Die Ablagerung von Feinsedimenten führt in Stauräumen daher oft zu Kontaminationsproblemen.

Um die Prozesse des Sedimenttransports unter Berücksichtigung des selektiven Transports realitätsnah zu simulieren, ist ein Mehrkorn-Sedimenttransportmodell erforderlich, das die Transportdynamik von Korngrößengemischen beschreibt und die Transportrate der einzelnen Korngrößenfraktion ermittelt. Auf der Grundlage von deterministischen Verfahren wurden bereits einige Methoden zur direkten Berechnung von fraktionsweisen Erosionsraten oder des gesamten Feststofftriebes entwickelt. Probleme bei der Anwendung solcher Verfahren sind die Bestimmung der entsprechenden Koeffizienten und der eingeschränkte Gültigkeitsbereich der jeweiligen Verfahren. Eine andere Möglichkeit zur Simulation des selektiven Sedimenttransports bieten die probabilistischen Methoden, die oft für die Berechnung der Erosion eingesetzt werden. Diese Methoden basieren auf der statistischen Beschreibung der momentanen Sohlschubspannung der turbulenten Strömung und der Verfügbarkeit von Material an der Sohle. Die effektive Sohlschubspannung und der Anteil der Fraktion im Sohlmaterial bestimmen den Beginn und das Ausmaß der Erosion einer Kornfraktion. Bei diesen Methoden müssen nur wenige Koeffizienten bestimmt bzw. kalibriert werden.

Die numerische Modellierung findet in der Ingenieurpraxis zur Simulation von Strömung und Sedimenttransport breite Anwendung. Mit eindimensionalen numerischen Modellen konnten Erfolge bei der Simulation der langfristigen Veränderungen für ausgedehnte Flußstrecken erzielt werden. Ein eindimensionales Modell kann aber nur die durchschnittlichen Parametergrößen in den Fließquerschnitten ermitteln. Zweidimensionale Modelle sind erforderlich, um Informationen über die morphologischen Veränderungen in Flüssen zu erhalten.

Auf der Grundlage dieser Überlegungen wurde ein Stromröhrenmodell als ein quasi zweidimensionales Modell zur Simulation des Schwebstofftransports in einer Flußstrecke entwickelt. Für dieses Stromröhrenmodell wird die Annahme getroffen, daß die tiefengemittelte Strömungsgeschwindigkeit quer zur Hauptfließrichtung vernachlässigbar ist. Im allgemeinen gelten solche Voraussetzungen für eine stationäre Strömung in einer geraden Flußstrecke. Für Flußabschnitte mit Sekundärströmungen, die durch Kurven oder lokale geometrische Veränderungen verursacht werden, ist das Stromröhrenmodell nur beschränkt anwendbar. Durch einen Zusatzterm, der die Partikeldispersion quer zur Strömungsrichtung berücksichtigt, wird die Anwendungsmöglichkeit des quasi zweidimensionalen Transportmodells erweitert.

Das Hauptziel der vorliegenden Arbeit besteht in der Entwicklung eines Modells zur Simulation des Sedimenttransports. Hierbei sind Teilziele zu bearbeiten:

- Entwicklung von numerischen Methoden zur Beschreibung des zweidimensionalen Ein- und Mehrkorn- Schwebstofftransports und der morphologischen Veränderungen

in Flüssen. Die Sedimenttransportmodelle sind mit einem Stromröhrenmodell gekoppelt, das die für die Berechnung des Sedimenttransports erforderlichen Strömungsparameter liefert.

- Untersuchung des lateralen Schwebstoffaustausches zwischen dem Gerinne und der Vorländern. Eine Formel zur Quantifizierung des Massenaustausches wird abgeleitet um das Anwendungsfeld des quasi zweidimensionalen Modells zu erweitern.
- Untersuchung des Mechanismus der Sedimentsuspension. Eine Methode zur Abschätzung der fraktionsweisen Resuspension (Erosion) wird entwickelt. Mit deren Hilfe soll der Effekt des selektiven Transports auf den Sedimenttransport, die Kornzusammensetzung an der Flußsohle und die morphologischen Veränderungen untersucht werden.
- Anwendung der Modelle. Angestrebt wird die Analyse und Prognose langzeitiger morphologischer Veränderungen von Flüssen anhand von Fallbeispielen.

Entwicklung und Anwendung numerischer Modelle

Strömungsmodell

Es wurde ein eindimensionales Stromröhrenmodell entwickelt, mit dem ein zweidimensionales Strömungsfeld nachgebildet werden kann. Der Fluß wird in Stromröhren mit gleichem Teildurchfluß q_s aufgeteilt. Die Strömungsrichtung verläuft parallel zu den Stromröhren. Bei instationärem Abfluß werden die Stromröhren den Veränderungen des Strömungsfeldes entsprechend angepaßt. Dem Modell liegen die Kontinuitäts- und Impulsgleichung zur Berechnung der Strömung zugrunde. Das erzeugte diskretisierte Gleichungssystem wird mit der Finiten Differenzen-Methode gelöst.

Die Stromlinien, die die Ränder der Stromröhren markieren, und die Fließquerschnitte bilden ein natürliches orthogonales krummliniges Koordinatensystem. Sie bilden gleichzeitig das systemeigene Gitter, das in das Sedimenttransportmodell übernommen wird. Die x-Achse liegt auf der Mittellinie des Flusses bzw. die z-Achse auf dem ersten Fließquerschnitt am oberstromigen Modellrand. Die Abstände der Gitterzellen sind sowohl in x-Richtung als auch in z-Richtung veränderlich und entsprechen somit nicht den Gitterabstand auf den Achsen. Für die numerische Umsetzung werden zwei metrische Koeffizienten, m_x und m_z , als Korrekturfaktoren eingeführt. Die Werte von m_x variieren je nach Flußtyp zwischen 0,57 und 1,35.

Einkorn-Schwebstofftransportmodell

Auf dem natürlichen, orthogonalen, krummlinigen Koordinatensystem erfolgt im Anschluß an die Strömungsberechnung die Simulation mit dem entwickelten zweidimensionalen Schwebstofftransportmodell. Die tiefengemittelte Konvektions-Dispersions-Gleichung wird zur Beschreibung des Schwebstofftransports verwendet. Unter Berücksichtigung der metrischen Korrekturfaktoren kann die Konvektions-Dispersions-Gleichung wie folgt formuliert werden:

$$\frac{\partial m_x m_z h C}{\partial t} + \frac{\partial m_z h u C}{\partial x} + \frac{\partial m_x h v C}{\partial z} = \frac{\partial}{\partial x} \left(\frac{m_z}{m_x} h D_x \frac{\partial C}{\partial x} \right) + \frac{\partial}{\partial z} \left(\frac{m_x}{m_z} h D_z \frac{\partial C}{\partial z} \right) + \dot{E} - \dot{S}$$

wobei h die lokale Wassertiefe, u und v die tiefengemittelten Geschwindigkeitskomponenten in Fließrichtung x und Querrichtung z , C die tiefengemittelte Schwebstoffkonzentration, \dot{E} die Erosionsrate und \dot{S} die Sedimentationsrate sind. Die diskretisierte Konvektions-Dispersions-Gleichung wird über die Finite-Volumen-Methode (FVM) numerisch gelöst, wobei die Massenbilanz für jedes Kontrollvolumen vollständig erhalten wird.

Es wird angenommen, daß in turbulenter Strömung der Dispersionskoeffizient von Feststoffen dem Dispersionskoeffizient von gelösten Stoffen entspricht. Im Falle einer Ausuferung findet infolge des Geschwindigkeitsgradienten ein starker lateraler Massenaustausch zwischen dem Hauptgerinne und den Vorländern statt. Der Dispersionskoeffizient wird als Funktion der Differenzen der Geschwindigkeiten und der Wassertiefen zwischen Gerinne und Vorländern, $\alpha |u_m - u_p| (h_m - h_p)$ mit $\alpha = 0.12 - 0.24$, formuliert.

Anwendungsbeispiel:

Der Schwebstofftransport in der Stauhaltung Lauffen am Neckar wurde mit dem kalibrierten Transportmodell untersucht. Diese Stauhaltung enthält sowohl kohäsive als auch nicht kohäsive Sedimente. Die Kornzusammensetzung der Sohle unterliegt räumlich starken Veränderungen. Infolge der Sedimentkonsolidierung steigt die kritische Erosionsschubspannung der Flußsedimente mit der Ablagerungsdauer an. Es wird angenommen, daß sie den maximalen Wert nach 7 Tagen erreicht und danach konstant bleibt. Um die Erosion des Sediments naturnäher zu simulieren, wird ein Zwei-Schichten-Modell implementiert. In dem Modell werden zwei kritische Sohlschubspannungen als Grenzwerte für die Erosion angenommen. Eine ist die auf das innerhalb von 7 Tagen frisch abgelagerte Sediment bezogene durchschnittliche kritische Erosionssohlschubspannung, die andere ist die maximale kritische Erosionssohlschubspannung für das konsolidierte Feinsediment und das nicht kohäsive, gröbere Sediment.

Das Strömungsmodell und das Transportmodell wurden mit Felddaten über einen Zeitraum von 22 Jahren (1973-1994) kalibriert. Als Grundlage für die Kalibrierung des Strö-

mungsmodells dienten die gemessenen Wasserspiegellagen des Neckar bei Hochwasser. Für die Eichung des Transportmodells standen die Profildatensätze aus Sohlpeilungen der Jahre 1973 und 1994 zur Verfügung. Die Kalibrierung des Transportmodells wurde durch Variation der Sedimentations- und Erosionsparameter und der kritischen Erosionsschubspannungen des Sohlmaterials durchgeführt. Die Ergebnisse zeigen, daß das Schwebstofftransportmodell die gemessenen Höhenveränderungen der Sohle sowie den Stoffaustausch für den Neckar bei Lauffen mit gegliederten Querschnitten beschreiben kann.

Mit dem kalibrierten Modell wurde eine Prognoserechnung hinsichtlich der Veränderung der Flußsohle für einen Zeitraum von 50 Jahren (1995-2045) durchgeführt. Dazu wurde eine Abflußganglinie auf der Basis der vorliegenden Tagesabflüsse, die sich über den Zeitraum von 1950-1994 erstrecken, als Eingabedatei generiert. Das Volumen an abgelagertem Sediment nimmt bei kleinen Durchflüssen infolge Sedimentation zu und während der Hochwasserperioden infolge Erosion sprunghaft ab. Erosion findet bei Abflüssen über $600 \text{ m}^3/\text{s}$ statt. Dies geschieht im Mittel an ca. 4,5 Tagen pro Jahr. In dem untersuchten Zeitraum wurden insgesamt ca. $1100 \cdot 10^3 \text{ m}^3$ Sediment erodiert. Die für den Prognosezeitraum berechnete mittlere Erosionsrate liegt deutlich über der für den Kalibrierungszeitraum ermittelten mittleren Erosionsrate. Der Grund dafür liegt darin, daß der maximale Tagesabfluß ($1745 \text{ m}^3/\text{s}$) im Prognosezeitraum viel größer als der maximale Tagesabfluß im Kalibrierungszeitraum ($1490 \text{ m}^3/\text{s}$) ist. Die Prognoserechnung deutet an, daß der Schwebstofftransport sehr empfindlich auf das Abflußgeschehen, insbesondere auf die Abflußspitzen, reagiert.

Die abgeleitete Formel zur Bestimmung der Partikeldispersion in der Nähe der Trennflächen zwischen Hauptgerinne und Vorländern wurde mit Daten aus dem Laborversuch von James (1986) getestet. Anschließend wurde die Sedimentation auf den Vorländern mit dieser getesteten Formel für einen Zeitraum von 5 Jahren (1989-1994), in dem sich drei Hochwasserereignisse ereignet haben, untersucht. Die Simulationsergebnisse zeigen, daß eine Sedimentation auf den Vorländern nur dann stattfindet, wenn ein Abfluß von $600 \text{ m}^3/\text{s}$ überschritten wird. Dieser Abfluß hat ein Wiederkehrintervall von ca. 1,45 Jahren. Dieser Wert stimmt mit den Felddaten (Wiederkehrintervall: 1,5 Jahre) überein. Während der drei Hochwasserereignisse strömten insgesamt ca. $570 \cdot 10^3 \text{ m}^3$ Schwebstoffe in die Untersuchungstrecke ein. Dies entspricht 47,1% der insgesamt einfließenden Schwebstoffe innerhalb dieser fünf Jahre ($1,2 \cdot 10^6 \text{ m}^3$). 1,6% der durch Hochwasser eingetragenen Schwebstoffe kamen auf den Vorländern zur Sedimentation. Da die Feinsedimente Träger für umweltrelevante Schadstoffe sind, sollte das Ausmaß der Sedimentation zukünftig näher untersucht werden. Die abgeleitete Formel zur Berechnung der Dispersion an den Trennflächen erweitert die Anwendung des Stromröhrenmodells. Dadurch wird ein zuverlässiges Instrumentarium zur Simulation des Sedimenttransports in Flüssen mit komplexer Geometrie zur Verfügung gestellt.

Mehrkorn-Schwebstofftransportmodell

Im allgemeinen kann für Schwebstoffe und Sohlmaterial keine einheitliche Korngröße angenommen werden. Die Partikel in Suspension sind in der Regel wesentlich kleiner als die an der Sohle. Aufgrund des selektiven Transports verändert sich die Kornverteilung des Sohlmaterials in Fließrichtung. Mit einem Einkorn-Transportmodell ist es nicht möglich, diesen Kornsortierungsprozeß darzustellen. Nur ein Mehrkornmodell kann dieses Phänomen adäquat nachbilden.

Die Resuspension von abgelagerten Partikel einer bestimmten Korngröße kann als stochastischer Vorgang beschrieben werden. Der Vorgang ist von den folgenden Faktoren abhängig: den schwankenden Sohlschubspannungen, der verfügbaren Partikelmenge an der Sohle und der Schwebstoffkonzentration. Diese Faktoren können durch die Mobilität und Verfügbarkeit der Partikel beschrieben werden.

In der Arbeit wurde eine neue Methode zur Bestimmung der Korngrößenverteilung der erodierten Partikel abgeleitet, unter Berücksichtigung

- der Mobilität der einzelnen Korngrößenfraktion im Sohlmaterial, die von der turbulenten Sohlschubspannung, der kritischen Erosionsschubspannung und der Korngröße abhängt.
- der Verfügbarkeit jeder Korngrößenfraktion in der Sohle.
- der Schwebstoffkonzentration jeder Korngrößenfraktion, die von der Sinkgeschwindigkeit der Partikel und der fraktionsweisen Schwebstoffkonzentration in Sohlnähe abhängt. Die fraktionsweise Konzentration hängt wiederum von der Turbulenz und der Transportfähigkeit dieser Kornfraktion ab.

Die Sohlschubspannung unterliegt turbulenten Schwankungen. Die effektive Schubspannung für die Erosion ist die Differenz zwischen der Sohlschubspannung τ und der kritischen Schubspannung τ_c . Die zeitlichen Schwankungen der Sohlschubspannung können als eine Gaußsche Verteilung um den Mittelwert $\bar{\tau}$ mit einer Standardabweichung σ beschrieben werden. Für eine gegebene Strömung ist die turbulente Sohlschubspannung zu bestimmen. Die kritische Sohlschubspannung, bei der die Partikelbewegung einsetzt und ein Erosionsprozeß stattfindet, hängt von dem Durchmesser der Kornfraktion ab. Die Wahrscheinlichkeit, daß die momentane Sohlschubspannung die kritische Erosionssohlschubspannung überschreitet, ist für eine Fraktion mit kleinem Durchmesser größer als für grobkörniges Material. Somit besitzen Feinsedimente eine größere Mobilität.

Der unmittelbare Bereich nahe der Sohloberfläche kann in die folgenden Zonen untergliedert werden: sohlnahe Zone oberhalb der Sediment-Wasser-Grenze, mobiles Flußbett

und immobiles Bett. Das mobile Flußbett kann in Abhängigkeit vom Strömungsgeschehen in eine transportaktive Schicht und eine inaktive Schicht (tiefes Flußbett) untergliedert werden. In der aktiven Schicht findet der Austausch zwischen den Schwebstoffen und den Sohlmaterial statt. Die Partikel im tiefen Flußbett befinden sich bei der vorherrschenden Strömung in Ruhe, sie können aber möglicherweise bei stärkerem Strömungsangriff erodiert werden. Das immobile Flußbett ist nicht an der aktuellen Erosion beteiligt.

Die aktive Schicht und das tiefe Flußbett können weiter in Einzelschichten unterteilt werden. Solche Einzelschichten können unterschiedliche Eigenschaften besitzen, z.B. Korngrößenverteilung oder Sedimentdichte. Diese Unterschiede beruhen auf unterschiedlichen Sedimentationsbedingungen.

Bei der Ableitung der neuen Methode zur Bestimmung des Anteils jeder einzelnen Kornfraktion an der Gesamtkornverteilung des Erosionsmaterials werden folgende Annahmen und Überlegungen getroffen:

- Jede Kornfraktion besitzt einen charakteristischen Durchmesser d_n .
- Die effektive Sinkgeschwindigkeit ist als Differenz zwischen der vertikalen aufwärtsgerichteten turbulenten Geschwindigkeit und der Sinkgeschwindigkeit definiert.
- Die suspendierten Partikel der Fraktion n können nur dann sedimentieren, wenn die effektive Schubspannung kleiner als die kritische Schubspannung für den Sedimentationsbeginn der Partikel ist.
- Die Partikel der Fraktion n werden dann suspendiert, wenn die effektive Schubspannung die kritische Schubspannung für den Bewegungsbeginn überschreitet.
- Die momentane Sohlschubspannung kann mit einer Gaußschen Verteilung beschrieben werden. Die Wahrscheinlichkeit, daß die kritische Sohlschubspannung für die Erosion kleiner bzw. für die Sedimentation größer als die vorherrschende Schubspannung τ_{cn} ist, ergibt sich nach Integration der normierten Gaußschen Verteilung von τ_{cn} .
- Erreicht der Schwebstofftransport ein Gleichgewicht, so haben die Suspensa in der sohnahen Zone und das aus der aktiven Schicht erodierte Sediment die gleiche Kornverteilung.

Unter Berücksichtigung der oben genannten Überlegungen wurde eine Formel zur Ermittlung der Erosionsanteile für jede einzelne Kornfraktion des erodierten Sediments, p_{an} , abgeleitet.

$$p_{an} = \frac{p_{bn} \alpha_{vn} (1 - T_n \psi_n)}{\sum_{n=1}^N p_{bn} \alpha_{vn} (1 - T_n \psi_n)}$$

Hierbei bezeichnet p_{bn} den Anteil der Fraktion n in der aktiven Schicht, ψ eine Wahrscheinlichkeitsfunktion von $\frac{\tau}{\tau_{cn}}$, T_n den Transportparameter der Kornfraktion n und α_{vn} das Verhältnis zwischen der aufwärtsgerichteten Geschwindigkeit und der Sinkgeschwindigkeit der Partikel der Kornfraktion n . α_{vn} nimmt mit zunehmendem Partikeldurchmesser ab. Der Maximalwert von α_{vn} ist 1.

Aus der Formel folgt, daß

- p_{an} von p_{bn} und den hydraulischen Parametern beeinflusst wird,
- die Korngrößenverteilung des erodierten Sediments feiner als die der aktiven Schicht ist,
- sich die Verteilung von p_{an} bei gegebenem p_{bn} mit zunehmender Fließstrecke in Richtung größerer Kornfraktionen verschiebt.

Im Vergleich mit den existierenden Methoden ist diese abgeleitete Methode einfacher und ohne weitere Modifikation anwendbar. Die Formel berücksichtigt drei wichtige Faktoren zur Bestimmung der Korngrößenverteilung von erodiertem Sediment, nämlich die schwankenden Sohlschubspannungen, die Korngrößenverteilung der aktiven Schicht und diejenige der suspendierten Schwebstoffe. Der Selektionseffekt beim Transport von Korngemischen kann dadurch realitätsnah beschrieben werden.

In dem Mehrkorn-Schwebstofftransportmodell sind die bestimmenden Gleichungen der Kornfraktion n , die numerische Lösungsmethode und die Gittererzeugung identisch wie in dem Einkorn-Transportmodell. Zum Lösen des Gleichungssystems wird jede Fraktion mit einer entkoppelten Methode getrennt behandelt. Die gegenseitige Beeinflussung der Fraktionen wird nicht berücksichtigt, da die Konzentrationen niedrig sind und damit der resultierende Fehler vernachlässigbar ist. Hingegen wird die Verteilung der Schwebstofftransportkapazität der Strömung berücksichtigt, da dies die fraktionsweisen Erosionsraten maßgeblich beeinflusst.

Anwendungsbeispiele:

Das Mehrkorn-Sedimenttransportmodell wurde mit den Daten aus den Laborversuchen von Samaga (1986) und des physikalischen Modells der Tsinghua Universität (China, 1994) getestet. Die Simulation der Korngrößenverteilung der suspendierten Feststoffe wurde von Samaga unter stationären Strömungen durchgeführt. Das physikalische Modell der Tsinghua Universität beschreibt die Sedimentation in den Stauhaltungen des Drei-Schluchten-Projekts über 76 Jahre. Die Berechnungsergebnisse des Mehrkorn-Sedimenttransportmodells deuten an, daß in den ersten 45-50 Jahren eine große Menge an

Sedimenten in den Stauhaltungen zurückgehalten wird. Danach schreitet die Sedimentation langsamer voran. Eine gute Übereinstimmung zwischen gemessenen und berechneten Ergebnissen konnte sowohl bezüglich des Sedimentvolumens als auch der Querschnittsveränderungen erzielt werden.

Zum Nachweis der Leistungsfähigkeit des Mehrkorn-Schwebstofftransportmodells wurde der selektive Sedimenttransport untersucht. Das Ziel bestand darin, die Änderungstendenz der Korngrößenverteilung der suspendierten Feststoffe und des Sohlmaterials darzustellen. Da dafür keine Felddaten vorlagen, wurden allgemeine Daten der Stauhaltung Lauffen verwendet.

Es wurde die Veränderung der Kornverteilung und des mittleren Durchmessers des Sohlmaterials während des Hochwassers im Dezember 1993 untersucht. Es wurde angenommen, daß am Anfang der Berechnung das Sohlmaterial in der gesamten Strecke die gleiche Korngrößenverteilung hat. Die Ergebnisse der Modellberechnungen zeigten einen starken Selektionseffekt infolge des Hochwassers. Der mittlere Korndurchmesser nimmt entlang der untersuchten Fließstrecke ab. Die Kornverteilung verschiebt sich in Richtung unterstrom zu feineren Kornfraktionen. Die hochwasserbedingte Verschiebung der Kornzusammensetzung hin zu größeren Kornfraktion an der Flußsohle geht mit einem Anstieg der Erosionsstabilität der Flußsohle einher. Das Simulationsmodell berechnete beispielhaft für ein Hochwasserereignis, daß die Erosionsrate in der betrachteten Stauhaltung für $Q = 420 \text{ m}^3/\text{s}$ bei ablaufender Hochwasserwelle um 47% geringer ist als bei anlaufender Welle. Die Kornverteilung des suspendierten Sediments ist viel feiner als die in der aktiven Schicht des Flußbetts. Die ermittelte Korngrößenverteilung der suspendierten Feststoffe wurde mit den Felddaten verglichen. Es zeigt sich, daß nur mit dem numerischen Modell die fraktionsweise Erosionsrate bei variierenden Abflüssen unter Verwendung der gemessenen Kornverteilung des Sohlmaterials ohne weitergehende Modifikation der Koeffizienten berechnet werden kann.

Die abgeleitete Formel hat im Vergleich zu anderen bekannten Methoden deutliche Vorteile hinsichtlich der benötigten Eingangsdaten und der Anwendbarkeit. Das Mehrkorn-Sedimenttransportmodell liefert zuverlässige Informationen über die Veränderung der Sohlenhöhe und der Korngrößenverteilung der Schwebstoffe und des Sohlmaterials in Flußlängsrichtung.

Das Transportmodell für gleichförmige Sedimente ist geeignet für die Simulation und Prognose langfristiger Tendenzen der Flußmorphologie. Die Annahme eines repräsentativen Durchmessers der Sedimente weicht von den wahren Verhältnissen in der Natur ab. Zur Untersuchung der Auswirkungen des selektiven Transports auf die fraktionsweisen Erosions- und Sedimentationsraten bzw. die Änderung der Korngrößenverteilung des Sohlmaterials ist das Mehrkorn-Transportmodell erforderlich. Allerdings erfordert das Modell

einen größeren Speicherplatz bei der Berechnung. Aufgrund der rasanten Entwicklung im Bereich der Computertechnik verliert dieser Nachteil zunehmend an Bedeutung.

Ausblick

Die vorliegende Arbeit leistet einen Beitrag zur numerischen Untersuchung des Schwebstofftransports in Flüssen. Die entwickelten Transportmodelle für gleichförmige und ungleichförmige Sedimente sind praktisch von relevant und stehen für weitere Forschungsarbeiten als wichtige Hilfsmittel zur Verfügung. In weiteren Arbeiten sollten einige wichtige Problempunkte des Feststofftransports detailliert untersucht werden:

- Die Sedimentation auf den Vorländern wird von der Partikeldispersion an den Trennflächen zwischen dem Hauptgerinne und den Vorländern beeinflusst. Für eine genauere quantitative Einschätzung muß der in der abgeleiteten Berechnungsformel auftretende Koeffizient durch Experimente noch quantifiziert werden.
- Der selektive Transportprozeß verändert die Kornverteilung des Materials an der Flußsohle, wodurch sich ihr Reibungswiderstand verändert. Der Sohlreibungswiderstand übt großen Einfluß auf die Berechnung des Wasserspiegels und damit auch auf den Sedimenttransport aus. Deshalb sollte der Widerstandsbeiwert in Abhängigkeit von der Sohlzusammensetzung ausgedrückt werden.
- Die in dieser Arbeit entwickelten Transportmodelle berücksichtigen lediglich den Schwebstofftransport, nicht jedoch die Umlagerung von Geschiebe an der Flußsohle. Eine Erweiterung der Modelle um entsprechende Module für den Geschiebetransport stellt einen wichtigen Schritt dar, um den Sedimenttransport in Fließgewässern realitätsnah beschreiben zu können.

Chapter 1

Introduction

1.1 Problem

Rivers are important natural transport systems of both water and sediment. Sediment transport occurs due to natural variation of discharge and human interference. For example, hydraulic structures are built on rivers to decrease the risk of floods, produce electric power, improve navigation and protect river banks. These structures disturb the equilibrium of river flow and sediment transport and may result in considerable river bed aggregation and degradation.

Among natural factors, floods play an important role in river morphological changes, because most of the sediment is produced by strong rainfall and transported during following flood events. When overbank flow occurs in a river reach, sediment is exchanged between the main channel and the flood plains due to lateral dispersion. Suspended sediment deposition on the flood plains can cause great economic losses and serious environmental problems. An important aspect in river management is to be able to predict sediment transport, response of rivers in terms of morphological adjustment processes due to both natural and human interference.

Numerical modeling of river morphological changes has been developed and advanced with the progress in computer techniques in the last decades. Compared with physical models, numerical models have advantages with regard to space, time and costs. Furthermore, they are widely applicable and flexible, convenient for comparing alternative designs.

For simulating flow and sediment transport processes numerical modeling has been widely used in hydraulic engineering practice. Many one-dimensional numerical models have been successfully applied to simulate long-term changes in the morphology of long river reaches. In order to provide more detailed information of morphological changes compared to one-dimensional models, two-dimensional models are required.

Computational results of unsteady, two-dimensional open channel flow are greatly affected by the accuracy and stability of the calculation, since the general equation of flow for river channels is nonlinear. To describe two-dimensional sediment transport processes it is desirable to develop a numerical model that can address the difficulties in computation of

a two-dimensional flow field and can obtain two-dimensional river morphological changes with acceptable accuracy.

For this reason a stream tube model has been adopted for simulating suspended sediment transport in rivers with straight and curvilinear alignments. The applications for a stream tube model are restricted due to the elimination of depth-averaged lateral velocities. A few studies have been reported in the literature in which sediment particle transfer between the main channel and the flood plains was modeled during flood events.

In general, sediment transport models can be categorized into two types: those that simulate transport of uniform sediments and those that simulate transport of nonuniform sediment mixtures. In the uniform sediment transport model, the sediments are characterized by a single representative grain size. This kind of model is simple and is a useful tool for qualitatively evaluating and predicting sediment transport. However, it does not really describe the physical processes of sediment transport, since river bed material mostly contains nonuniform sediment mixtures, more or less graded sediment. Selective transport plays an important role in nonuniform sediment transport processes. It has been found that due to selective sedimentation fine sediment is accumulated in reservoirs and on flood plains, it may raise environmental problems when sediment particles are bound pollutants and they may be resuspended and transported during future flood events. Available suspended sediment concentration for deposition, that relates flow conditions, sediment inflow and particle fall velocities required for deposition, influences rates of reservoir sedimentation and effective storage of reservoirs. Selective erosion results in that sediment particles on river bed surfaces gradually coarsen, which may protect the underlaying material from movement and decrease erosion in depth. Resistance to flow and water depth vary with changes in friction resistance, as compositions of bed material changes.

Some attempts have been made to develop sediment transport models for nonuniform sediment mixtures to describe selective transport and downstream fining. However, because these physical processes are more complicated, the models still face the following difficulties: (1) unreliable friction factor formulas, which affect predictions of the resistance to a flow; (2) simplified sediment transport mechanisms, which cannot adequately describe selective transport, downstream fining, the interaction between flow and sediment and the exchange between suspended sediment and bed material.

To eliminate the first difficulty dedicated theoretical and experimental researches are still needed. The present work focuses on the second difficulty. A new method has been developed, which can describe selective transport and considers the effect of this process on changes in grain size distributions of river bed material, e.g. downstream fining, and changes in river morphology.

1.2 Purpose of the work

The purpose of this work is to develop numerical models to describe suspended sediment transport processes in rivers, including:

- Develop and validate the two-dimensional suspended sediment transport models for (a) uniform sediment and (b) nonuniform sediment mixtures to evaluate morphological changes in rivers. Each transport model is coupled with a stream tube flow model which provides essential flow parameters for computation of sediment transport.
- Study the lateral exchange of suspended sediment particles between the main channel and the flood plains and derive a formula to calculate the exchange quantities to improve the model's ability to simulate morphological changes in rivers with complicated geometries.
- Study the mechanics of sediment suspension and develop a method for the evaluation of fractional entrainment (erosion) to describe the effect of selective transport on sediment transport processes and on the river bed changes.
- Apply the models to predict river morphological changes due to sediment transport caused by natural or human interference. This will provide a basis for the assessment of the impacts of river drainage works, channel dredging and reservoir operations on long-term river morphology.

1.3 Organization of the present work

The present work is divided into 5 chapters. The framework is shown in Figure 1.1

Chapter 2 briefly reviews the theory of sediment transport and numerical methods. Based on a literature study, the reason for developing a new model and improving formulae for selective sediment transport simulation is further explained. The numerical flow model and transport models for uniform sediments and nonuniform sediment mixtures are given in **Chapter 3**. The stream tube flow model is introduced in this chapter. Applicability of a stream tube flow model for a natural river channel is also discussed. Based on Evers' assumption [34] and experimental results [118] a formula for calculating particle dispersion in the interaction zone is derived to consider the effect of overbank flow on dispersion at the interface between the main channel and the flood plains.

In this chapter, the relationships between selective transport and grain size distributions of suspended and bed sediment are investigated. A formula for calculating the grain size distribution of entrainment is derived using a probabilistic approach. The formula is derived for equilibrium transport conditions. It can be used as an approximate method for predicting fractional entrainment under non-equilibrium conditions.

In **Chapter 4**, the derived formulas for the lateral dispersion at/near the interface between the main channel and the flood plains and fractional entrainment are tested using the experimental data of James [58], Samaga [125] and the Tsinghua University [149]. The flow and suspended sediment transport models for uniform sediments are calibrated using field data in the Lauffen Reservoir on the River Neckar. The calibrated model is then used for predicting changes in the river morphology for the next 50 years. In order to verify the capability of the nonuniform sediment transport model to predict the effects of selective transport and downstream fining, field studies are also made using this transport model. As a special application of the uniform sediment transport model, the dispersion of sediment particles between the stream and the groyne fields (dead water zones) and deposition and erosion rates on the groyne fields are investigated.

Chapter 5 gives conclusions and recommendations for improving the models.

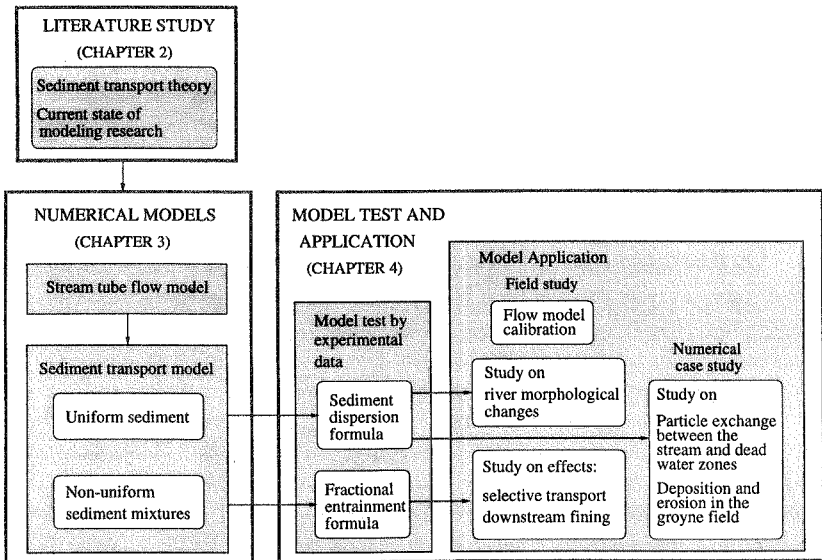


Figure 1.1: Framework of the present work.

Chapter 2

State of the art

2.1 Suspended sediment transport

2.1.1 Suspended sediment load

Rivers are a self-formed channel system. They carry rainwater towards topographic sinks. During flow sediment erosion and deposition arise when the momentum of the water is transferred to the solid boundary of the river. Therefore, the character and geometry of a river are controlled not only by the hydrology, but also by deposition and erosion which occur at all scales from local to basinal.

River water is rarely free of sediment, either at low flow conditions or at high flow conditions such as a flood. Although floods are not common events, they are very important factors for river morphology, because of increased sediment transport, sedimentation and erosion during these events. During sediment transport a fraction of the sediment may be deposited on the flood plains or on the convex bank of bends in meandering rivers. The transport of sediment by river flow is responsible for many environmental impacts.

Human interference can also change a river morphology. For example, above and below a recently constructed dam the channel gradient will be changed (Figure 2.1). A portion of the sediment load will be entrapped in the reservoir and consequently erosion may take place below the dam and the original channel gradient will be reduced [131].

In a reservoir flow velocity decreases with increase in depth along the river. Consequently the sediment transport capacity of flow also decreases and sediment deposition increases in the flow direction. The grain size of deposited particles is reduced as the flow transport capacity decreases, and as a result the median diameter of bed material decreases in the flow direction [93]. Coarser grains, transported as bed-load, are deposited close to the beginning of the backwater effect, in the far upstream region from the dam. Finer grains, transported as suspended load, are carried far downstream to the dam (Figure 2.2). Deposition takes place if the suspended sediment concentration is larger than the equilibrium concentration, $C > C_e$. This equilibrium concentration varies with flow conditions. As this concentration decreases along the flow direction deposition rate increases

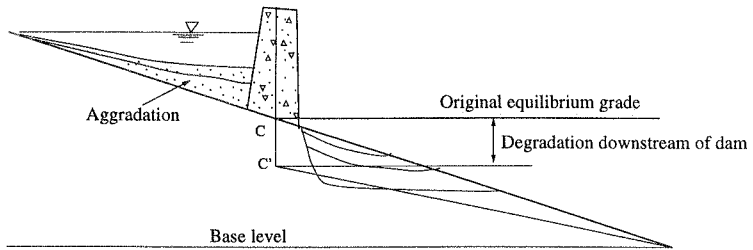


Figure 2.1: River channel adjustment upstream and downstream a dam

whereas erosion rate decreases. The maximum deposition is found at where the bottom shear stress is smaller than the critical shear stress for erosion, $\tau < \tau_{c,E}$. In the middle region, both sedimentation and erosion occur.

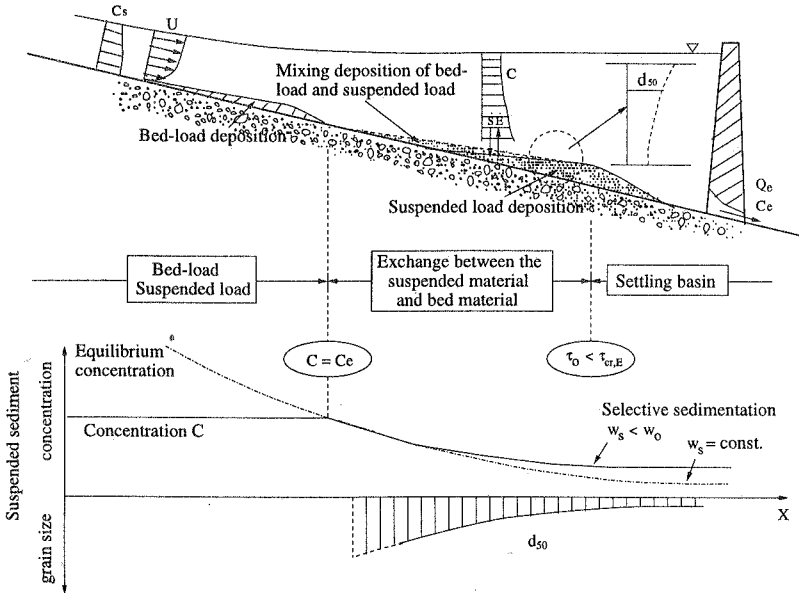


Figure 2.2: Longitudinal development of sedimentation in a river with a constructed dam.
After Westrich, B. (1988) [167]

Sediment transport can be classified as bed-load, suspended load or wash load based on the type of transport. Particles transported as bed-load or as suspended load is dependent not only on particle size but also on the local flow strength. This means that a particle may be carried as bed-load in one reach and as suspended load in another section, where the flow conditions are different (Figure 2.3).

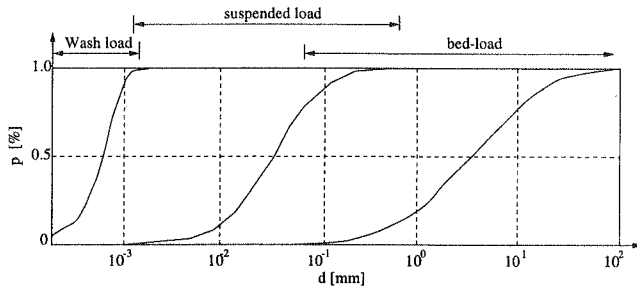


Figure 2.3: Sediment transport mode

In most rivers the suspended sediment load is the most significant in terms of quantity. This may be due to the fact that non-cohesive fine sediment, such as silt and fine sand, has lower critical shear stress of entrainment (erosion). Even at low flow suspended load almost always exists. During typical flow conditions, such as during the long period between two floods, suspended sediment concentrations greater than 0.1 kg/m^3 or more often occur [120]. For example, average annual sediment concentrations are 0.05 kg/m^3 in most of the rivers in Germany, 1.14 kg/m^3 in the Yangtze River and 36.9 kg/m^3 in the Yellow River in China. Their maximum sediment concentration are 4.5 kg/m^3 , 10.5 kg/m^3 and 590 kg/m^3 , respectively. In contrast, bed-load transport may contribute less than 1% of total sediment transport in some streams. Obviously, studying suspended sediment transport in rivers over the long period is important. The present research will focus on the long-term suspended sediment transport in rivers.

Effect of turbulence on sediment transport

Turbulence is a random motion of fluid. It plays a very important role in sediment transport. Turbulence can be described by statistical-dynamic methods. Kline et al (1967) [66] and Grass (1971) [49] studied the structure of the turbulent boundary layer. They divided a turbulent boundary layer into two regions: a wall region and an outer region. In the wall region flow is laminar and turbulence begins to develop. In the outer region the turbulence is well developed. Kline found that the fluid in the wall region was organized

into an array of streamwise high- and low-speed streaks. Periodically, at a fixed point, the fluid in the part of a high-speed streak became lifted up and swiftly ejected on a steeply inclined path into the outer flow, a process called streak bursting. Nakagawa and Nezu (1981) [94] found that the streamwise spatial separation of bursts formed under certain circumstance was two or three times the boundary layer thickness (Figure 2.4 b).

Grass (1971) [49] refined the concept of streak bursting in his experiment. He pointed out that the bursting streak is a jet of low momentum fluid ejected from near the wall into outer part of flow, determined not by the wall property but by the overall flow properties [119]. The turbulence is anisotropic. The fluctuating velocity component that is perpendicular to the wall is stronger than that parallel to the wall. So there exists a pure outward flow of momentum from the wall toward the outer region of the turbulent boundary layer.

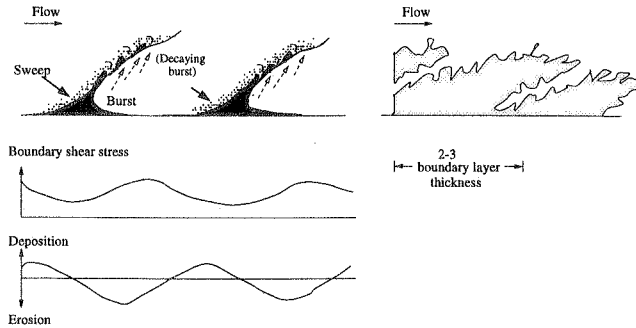


Figure 2.4: Turbulent boundary layers on the plane walls. a. Burst-sweep cycles of turbulence and associated patterns of shear stress, deposition and erosion. According to Allen (1983) [3] and Leeder (1983) [78]. b. Position of the interface between marked and unmarked fluid showing the sweep-bursting may be controlled by the movement past the bed of large horseshoe vortices of outer flow, according to Falcon (1977) [35].

Streak-bursting is significant for sediment motion near the river bed. It has been proved that the turbulence is responsible for particle suspension [29, 49, 139]. Turbulent eddies penetrate the laminar layer and hit the bed resulting in particle suspension. It is clear that turbulent intensity and the frequency of streak-bursting increases with the flow strength. The amount of particles in suspension drawn into turbulent eddies and ejected into flow by eddy bursts should also increase with the strength of flow.

The interaction between flow turbulence and bedforms exerts a strong influence on the

deposition and erosion processes [78, 100, 120] (Figure 2.5). Newly developed bedform adds resistance to the flow creating local turbulent intensity. Turbulent flow increases the sediment transport rate, while sediment transport has a damping effect on turbulence and also affects flow separation and bedform development. The range, size and character of bedforms are products of the balance between erosion and deposition at different points at a given turbulent flow condition. The direct result of these interaction is a change in the river morphology.

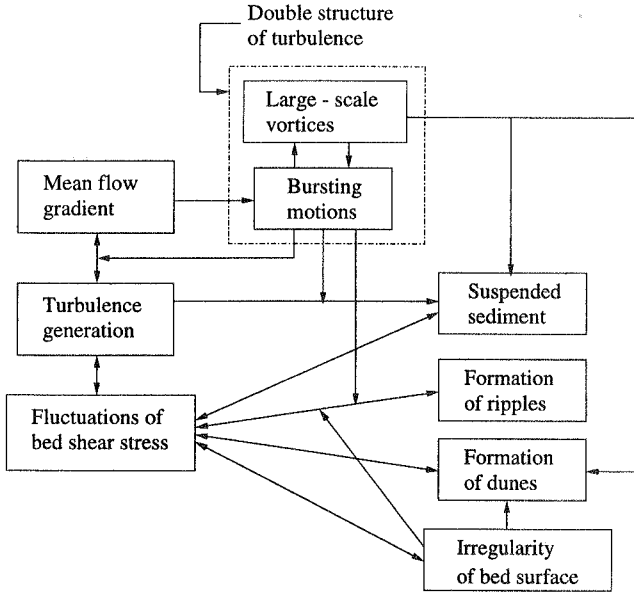


Figure 2.5: Relationship between the turbulent flow and sediment transport in open channel.
After Nezu and Nakagawa (1993) [100]

2.1.2 Diffusion and Dispersion of particles

Mass conservation

The general conservation equation describing the transport of pollutant or suspended sediment for a control volume can be written as

$$\frac{\partial C}{\partial t} + \vec{u} \cdot \nabla C = \varepsilon_m \nabla^2 C \quad (2.1.1)$$

where C is suspended sediment concentration, \vec{u} is three-dimensional vector velocity at a point and ε_m is molecular diffusivity, ∇ is vector gradient operator and ∇^2 is Laplacian scalar operator.

Particle dispersion

Particle dispersion in a natural channel results from a combination of (Figure 2.6 b4.)

- turbulent diffusion (Figure 2.6 a. and b.);
- differential convection caused by transverse variation of longitudinal velocity, (due for example to variable depths in a section, Figure 2.6 b2.);
- differential convection caused by centrifugal forces (Figure 2.6 b3.).

		Mass	Velocity	Mass diffusion / dispersion	Cross section	Mass	Velocity distribution	Mass diffusion / dispersion	Cross section
a.		Vertical dispersion							
Depth-averaged longitudinal and transverse dispersion	b1. Longitudinal diffusion only								
	b2. Differential convection only								
	b3. Differential convection with transverse diffusion								
	b4. Combined effects of b1. - b3.								

Figure 2.6: Dispersion in natural channels

Diffusion in turbulent flow In turbulent flow, the velocities and concentrations fluctuate with time. Using Reynolds' averaging principles to eq. 2.1.1 and according to Taylor's theory [39] that the particle diffusion due to turbulent convection can be represented as a gradient diffusion process,

$$\varepsilon \frac{\partial \bar{C}}{\partial x} = -\overline{u' C'}. \quad (2.1.2)$$

The time-averaged convection-diffusion equation can be obtained:

$$\frac{\partial \bar{C}}{\partial t} + \bar{u} \frac{\partial \bar{C}}{\partial x} + \bar{v} \frac{\partial \bar{C}}{\partial y} + \bar{w} \frac{\partial \bar{C}}{\partial z} = \frac{\partial}{\partial x} \left(\varepsilon_x \frac{\partial \bar{C}}{\partial x} \right) + \frac{\partial}{\partial y} \left(\varepsilon_y \frac{\partial \bar{C}}{\partial y} \right) + \frac{\partial}{\partial z} \left(\varepsilon_z \frac{\partial \bar{C}}{\partial z} \right) \quad (2.1.3)$$

where the overbar denotes an average over a period T , the prime denotes the instantaneous local deviations from the mean values over T , and ε_x , ε_y and ε_z are turbulent diffusion coefficients in x , y and z directions.

The molecular diffusion coefficient is of the order of $10^{-7} m^2/s$ and the turbulent diffusion coefficient is of the order $10^{-3} m^2/s$ [123].

Diffusion due to turbulent convection in shear flow In a natural channel, Taylor's theory describes turbulent transport of momentum as

$$\overline{u'v'} = -\varepsilon_t \frac{\partial \bar{u}}{\partial y} \quad (2.1.4)$$

where ε_t is the turbulent diffusivity for momentum transfer, $\varepsilon_t = \varepsilon_y / \sigma_{ct}$, σ_{ct} is a ratio of the turbulent viscosity, known as the Schmidt number. σ_{ct} has been found to equal approximately one.

According to Reynolds' analogy Elder used von Kármán's velocity distribution and a linearly varying shear stress in the analysis of vertical two-dimensional turbulent flows. He obtained the averaged vertical turbulent diffusion coefficient:

$$\varepsilon_y = \frac{\kappa}{6} u_* h \quad \text{and} \quad \varepsilon_y \simeq \varepsilon_x \quad (2.1.5)$$

Similarly, Rouse [122] suggested that particle diffusion is similar to the turbulent diffusion:

$$\varepsilon_s = \beta_s \varepsilon_t \quad (2.1.6)$$

in which β_s is a factor of proportionality. β_s is discussed later.

Dispersion due to differential convection in shear flow Taylor [143] investigated the longitudinal mass dispersion due to differential convection for the cross-sectional average concentration in a pipe. Based on his investigation, Elder obtained the dispersion coefficient due to differential convection:

$$D_x^T = \frac{1}{h} \frac{1}{e_m} \int_0^y u'_h \int_0^y \frac{1}{e_y} \int_0^y u'_h dy dy dy \quad (2.1.7)$$

where u'_h is the deviation of the local depth-averaged velocity from the average value of section. Based on it Elder obtained the dispersion coefficient due to the differential convection using $\varepsilon_y = hu_*\kappa\eta(1-\eta)$ and the logarithmic velocity distribution:

$$D_x^E = \frac{0.404}{\kappa^3} u_* h \approx 5.86 u_* h \quad (2.1.8)$$

where κ is von Kármán constant, $\kappa=0.4$ for clear water.

Adding the pure turbulent diffusion in eq. 2.1.8, Taylor wrote

$$D_x = D_x^E + \varepsilon_x = 5.86 u_* h + \frac{\kappa}{6} u_* h = 5.93 u_* h \quad (2.1.9)$$

By using Elder's longitudinal dispersion coefficient, the longitudinal dispersion of a cross-sectional average concentration in rivers is considerably underestimated. Fischer [38] hypothesized that in a natural river, the longitudinal dispersion of the cross-sectional average concentration is caused primarily by transverse rather than vertical deviations of velocity from the cross sectional mean velocity. Similar to the derivation of eq. 2.1.7, Fischer obtained the expression of longitudinal dispersion coefficient:

$$D_x^F = \frac{1}{A} \int_{z_L}^{z_R} h u'_s \int_{z_L}^{z_R} \frac{1}{h D_z} \int_{z_L}^{z_R} h u'_s dy dy dy \quad (2.1.10)$$

in which u'_s denotes the local deviations of the depth-averaged velocity, and D_z is the cross-sectional value of the transverse dispersion coefficient. For a straight channel without secondary flow, Elder found $D_z = \varepsilon_z = 0.23 u_* h$.

Under the assumption that longitudinal and transverse dispersion due to differential convection can be described as a gradient diffusion process, the expression of D_x and D_z can be used in a horizontal two-dimensional convection-diffusion equation of mass or particle transport. The longitudinal dispersion coefficient can be assumed as a constant along the river. For transverse dispersion coefficients there are three suggestions:

- (1) Assume a constant value along a channel [54, 183];
- (2) use a constant value in a cross section, since variations in D_z are smaller along a cross section than along a channel [54, 74];
- (3) use a value that varies both along the cross section and along the channel [171].

For uniform flow in a straight channel the term $D_z = \varepsilon_z = \beta u_* h$ can fully describe the transverse diffusion of mass where the transverse diffusion is only caused by bed friction and β varies in a range of 0.1 - 0.23 [31, 73]. In an irrigation channel β varies in a range of 0.2 to 0.3 and in a natural river it changes from 0.5 to 5.0 or more [74].

Secondary flow exists in rivers. In a river with curvilinear alignments or local irregularities, e.g. river bend reach or river reach with compound sections. The secondary flow increases the transverse mixing which is attributed to pure transverse convection and differential convection along a cross section. It is reported that if the total transverse mixing is described only by a transverse dispersion coefficient, this coefficient must be increased to take into account the effect of pure transverse convection [36, 97].

For a river reach with a compound section, the mass and particle dispersion between the main channel and the flood plains occur due to differential convection caused by local geometric changes. The dispersion is related to the effective shear stress, τ_{mp} , at the interface between the stream and the flood plains. A lot of effort has been put into studying such shear stress at the interface. Some of the results based on the different assumptions and considerations for turbulent transfer of momentum are given in the section titled 'Flood plan deposition'. The coefficient of sediment particle transfer at the interface, D_{zmp} , can be obtained by using Reynolds analogy and the turbulent-Schmidt number. The total transverse dispersion should include the pure turbulent diffusion (as in eq. 2.1.9) and D_{zmp} [8, 54]:

$$D_z = \varepsilon_z + D_{zmp} \quad (2.1.11)$$

Vertical distribution of suspended sediment concentration

The state of the particles in flow depends on their fall velocity and the turbulent intensity of flow. Considering the balance of forces acting on the particle in the vertical direction, it can be concluded that a concentration gradient exists in the vertical direction. The concentration will be much higher near the bed and will decrease rapidly with increasing distance to the bed.

Schmidt (1925) [127] first suggested the governing equation for vertical suspended sediment distribution in steady state flow: vertical net flux of particles must be zero everywhere. The downward flux due to gravity must then be exactly balanced by an opposite diffusive flux:

$$Cw_s + \varepsilon_s \frac{dC}{dy} = 0 \quad (2.1.12)$$

where C is a concentration; w_s is the fall velocity of particles and ε_s is a diffusion coefficient for sediments. Various options have been suggested for the coefficient ε_s . According to the assumption that sediment diffusivity is similar to the turbulent eddy diffusivity and the Prandtl-von Kármán velocity distribution Rouse [122] obtained the expression of a vertical particle diffusion coefficient, $\varepsilon_s = \beta u_* y (1 - \frac{y}{h})$. Based on this relationship he described the concentration profile as

$$C = C_a \left(\frac{h-y}{y} \frac{a}{h-a} \right)^\zeta \quad (2.1.13)$$

where $\zeta = \frac{w_s}{\beta \kappa u_*}$ is an exponent showing the relative relationship of the gravitational and turbulent effects, and a is a distance above the bed surface. The family of curves representing the values of $\frac{C}{C_a}$ with y and $a = 0.05h$ and $\beta = 1$, $\kappa = 0.4$ for various values of $\frac{w_s}{\beta \kappa u_*}$ is shown in Figure 2.7.

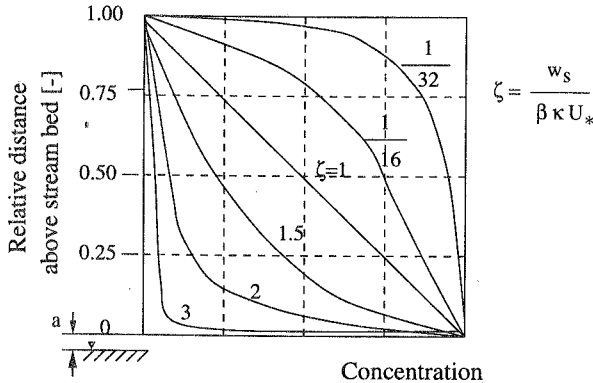


Figure 2.7: Vertical distribution of suspended sediment concentration. After Vanoni (1963)[156].

Comparison with experimental and field data showed that the form of eq. 2.1.13 describes the concentration distribution rather well and that only the exponent used differs from the theoretical value ζ cited by Graf [46]. Since turbulence and concentration affect the fall velocity and von Kármán constant, the theoretical concentration distribution differs from the observed if κ for clear water and a constant value w_s for still water are used. In addition, the assumption of $\varepsilon_s = \varepsilon_t$ with $\beta = 1$ does not take into account the difference between the diffusion of fluid and the diffusion of a discrete sediment particle.

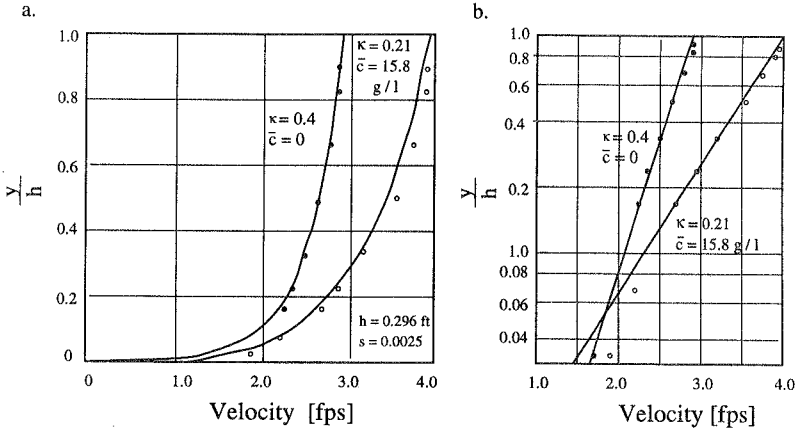


Figure 2.8: Velocity profile for sediment-laden and clear-water flow. After Vanoni et al. (1960) [160]

For the proportional value of β_s , some previous investigators believed $\varepsilon_s \leq \varepsilon_t$ ($\beta_s \leq 1$), and suggested that because sediment particles are larger than the fluid particles, they cannot fully follow the turbulent velocity fluctuations [17, 85, 87, 144]. This was verified by Vanoni [158]. Others concluded $\varepsilon_s > \varepsilon_t$ ($\beta_s > 1$) and reasoned that the centrifugal force acting on sediment particles would be greater than that acting on fluid particles in a turbulent flow, which could result in the sediments being thrown to the outside region of the vortices with a consequent increase in an effective mixing length and diffusion rate [132]. Van Rijn [154] analyzed the flume experiment results of Coleman [27] and suggested $\beta = 1 + 2(\frac{w_s}{u_*})^2$ for $0.1 < \frac{w_s}{u_*} < 1$.

Based on experimental work, Jobson and Sayre (1970) [59] concluded that the diffusion of the sediment particle is due to the tangential components of turbulent velocity fluctuation

and centrifugal force caused by the curvature of a fluid particle path line, described by

$$\varepsilon_s = \beta_t \varepsilon_t + \beta_c \varepsilon_c. \quad (2.1.14)$$

Diffusion due to the tangential components of turbulent velocity fluctuations appears to be the predominant turbulent mixing process for fine particles, β_t is less than or equal to 1 and β_t decreases with increase in particle size. This implies that the smaller the particle size, the closer are the transfer coefficients of fluid and sediment particles. Diffusion due to the centrifugal force appears to be significant for coarse particles in flow with strong vortex activity. The value of β_c can be assumed to reach a maximum value in zones of most intensive shear, and increases with particle size.

It was found that the value of κ in presence of sediment decreases with increase in sediment concentration [30, 165, 157]. The experiment presented by Vanoni (1960) [160] (Figure 2.8) demonstrated that for the same discharge, the average velocity for sediment laden flow is larger than that for the clear water flow. Vanoni (1963) [156] suggested that the decrease in the value of κ means that mixing is less effective and the presence of sediment damps the turbulence, which was also investigated by Einstein (1954) [30] and Hino (1963) [51].

Suspended sediment load According to the vertical distribution of concentrations, the suspended load rate in weight per unit time and width, for a given particle size can be obtained by:

$$q_s = \int_a^h u \cdot c \, dy \quad (2.1.15)$$

where q_s represents the suspended-load transport rate and h denotes the water depth. C_a denotes a reference concentration at a distance a above the bed surface (Figure 2.10).

2.1.3 Suspended sediment transport for uniform sediments

Critical shear stress for erosion (resuspension)

The criterion for initial instability of uniform bed grain was experimentally determined by Shields in 1936 [130], which is represented by the relationship between the critical mobility parameter

$$F_* = \frac{u_{*,cr}^2}{\frac{\rho_s - \rho}{\rho} \cdot g d_{50}} = \frac{\tau_c}{(\rho_s - \rho) \cdot g d_{50}}$$

and the particle parameter

$$D_* = d_{50} \left[\frac{\rho_s - \rho}{\rho} \cdot \frac{g}{\nu^2} \right]^{1/3}$$

(Figure 2.9). The critical shear stress in Shields' curve is defined as the flow stage where 50 percent of the bed material starts moving. From Figure 2.9 one can see that the critical mobility parameter strongly depends on the particle parameter. Sediments with very small values of D_* usually start moving in suspension from rest over the bed surface. Sediments with larger values of D_* are initially suspended from moving bed material, which is transported as bed-load near the bed surface.

A lot of effort has been given to investigate the initiation of suspension based on the different assumptions. A part of these research results are shown in Figure 2.9 and Table 2.1.

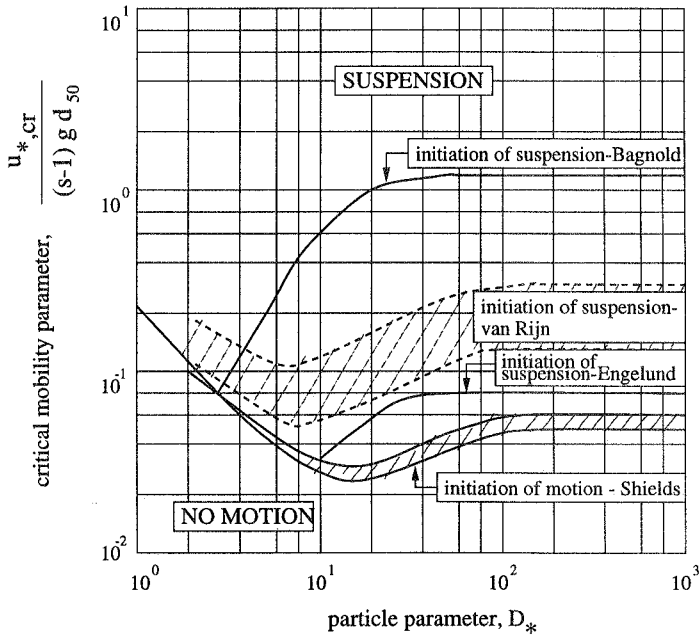


Figure 2.9: Critical shear stress for erosion and suspension. After van Rijn (1984) [154]

Critical flow condition	Author	Comments
$\sigma_w = \sqrt{w'^2} \geq w_s$	Bagnold (1966) [9]	Criterion: the vertical turbulent velocity is greater than the particle fall velocity
$u_{*,cr} = \alpha w_s$	Hinze (1975) [52]	Vertical turbulent intensity has the same order as the shear velocity u_* . Critical condition: $\alpha = 1$
$u_{*,cr} = 0.25 w_s$	Engelund (1967) [32]	Criterion: $\alpha = 0.25$ according to the stability analysis
$u_{*,cr} = 0.8 w_s$	Bridge (1981) [15]	with $\alpha = 0.8$
$u_{*,cr} = \frac{4w_s}{D_*}, \quad 1 < D_* \leq 10$ $u_{*,cr} = 0.4, \quad 10 < D_*$	van Rijn (1984) [154]	Criterion: the particle jumping height of 100 particle diameters observed in the experiment
$\frac{u_{*,cr}}{w_s} = \frac{2.5}{\log(\frac{U_* d}{\nu} - 0.06)}; \quad 1.2 < \frac{U_* d}{\nu} < 70$ $\frac{u_{*,cr}}{w_s} = 2.05; \quad 70 < \frac{U_* d}{\nu}$	Yang (1973) [176]	
σ : standard deviation, w_s : particle fall velocity, $u_{*,cr}$: critical shear velocity, $u_{*,cr} = \tau_c / \rho$		

Table 2.1: Critical flow conditions for sediment suspension

Erosion rate

Various formulae are available for calculating erosion rates. Generally the erosion rate is represented as a function of flow and river bed material conditions. For uniform sediment a total erosion rate is determined by using an equivalent diameter, usually the median diameter.

Parchure and Ashish [104] suggested a formula for determining the erosion rate which is related to the effective shear stress for erosion of fine and cohesive particles. The effective shear stress is given by the amount of the bottom shear stress, τ , that exceeds the critical shear stress for erosion, $\tau_{c,E}$. In other words, erosion occurs only when the bottom shear stress is greater than the critical shear stress. The critical shear stress is given as $\tau_{c,E} =$

ρu_{*cr}^2 . The expression of the erosion rate is then given by

$$\dot{E} = k \cdot (\tau_{c,E} - \tau), \quad \tau > \tau_{c,E} \quad (2.1.16)$$

A power-law expression was used to consider effect of consolidation of cohesive sediment on erosion rate [6, 28, 71]

$$\dot{E} = \begin{cases} M \left(\frac{\tau}{\tau_{c,E}} - 1 \right)^n & \tau > \tau_{c,E} \\ 0 & \tau \leq \tau_{c,E} \end{cases} \quad (2.1.17)$$

M is a parameter to be calibrated. M has the same unit as erosion rate and varies with the critical shear stress [6]. It has a range of $1.6 \cdot 10^{-5} \text{ kg/m}^2.s$ to $1.38 \cdot 10^{-3} \text{ kg/m}^2.s$ [90]. The value of n used varies between 1 and 4. This means that the erosion rate is not linear with the effective shear stress, $\tau - \tau_{c,E}$.

Eq. 2.1.17 is available for calculating the erosion rate of fine cohesive sediments. It can be also used for determining the erosion rate of non-cohesive sediments since this expression includes the main factor, effective shear stress which dominates erosion.

Sedimentation rate

The sedimentation rate, \dot{S} , is related to the reference concentration of suspended sediment at a distance, a , above the bed surface, C_a , the particle fall velocity, w_s , and the bottom shear parameter:

$$\dot{S} = \begin{cases} w_s C_a \left(1 - \frac{\tau}{\tau_{c,S}} \right) & \tau < \tau_{c,S} \\ 0 & \tau \geq \tau_{c,S} \end{cases} \quad (2.1.18)$$

where, $\tau_{c,S}$ is the critical shear stress required to initial deposition of suspended sediment particles. Deposition occurs only when the bottom shear stress is smaller than the critical shear stress $\tau_{c,S}$. Considering that the flow capacity for suspended sediment transport is closely related to the energy of turbulent motion, the expression for the critical shear stress $\tau_{c,S}$ is experimentally determined [169]:

$$\tau_{c,S} = \frac{\rho_s - \rho}{\rho_s} \frac{g h w_s C}{T_K U} \quad (2.1.19)$$

where T_K is an efficiency parameter related to the boundary condition, movable or non-erodible boundaries, permeable bed and non-permeable walls. For non-erodible bed conditions, a value of 0.0018 for T_K has been suggested by Westrich and Juraschek [169].

Many researchers have suggested that the reference concentration, C_a , is a function of hydraulic parameters and sediment properties. Some researchers have proposed that the reference concentration is proportional to the bed-load rate within the near-bed layer, using the assumption that there is a continuous exchange between the bed-load and suspended-load [16, 29, 154]. The proportional coefficient can be determined experimentally. Others believe that the reference concentration is related to the excess bed shear stress or shear velocity [18, 19, 135, 177].

There are also several hypothesis about the concentration reference height, a . Some researchers believe that a is related to the water depth, ($a = 0.05h$), the characteristic bed roughness, ($a = k_s$ [154]), half the bed-form height, ($a = \frac{1}{2}\Delta$ [53]), or two grain diameters ($a = 2d$ [29]). Others supposed that a may be related to the effective shear stress with a grain diameter and characteristic bed roughness [135].

2.1.4 Suspended sediment transport for nonuniform sediment mixtures

Sediments in a natural river are non-uniform with the sediment gradation varying continuously. For most river systems a pattern within downstream reaches containing more fine sediments is often found due to selective transport. For example this pattern was found at the Lauffen Reservoir on the River Neckar [88, 92], even though the sediments included cohesive clay the entrainment of which may be limited by consolidation.

Selective transport plays an important role in nonuniform sediment transport processes. It affects the changes in river morphology by varying the compositions of bed material and transported sediment. For several decades, considerable effort has been given to the study of size selectivity in the entrainment and transport of nonuniform sediments for gravel bed load [43, 44, 56, 82, 115, 140, 164] and fine suspended sediments [26, 86, 93, 174, 175].

Methods for calculation of fractional entrainment

Many approaches have been suggested for calculating the entrainment rate for sediment mixtures (here some formulae for calculating bed load transport rates are also introduced for comparison). To calculate the entrainment of nonuniform sediment both the amount

and the grain size distribution of entrained particles need to be determined. Generally, there are two methods to obtain these values: the probabilistic method (PROBM) and the deterministic method (DETM).

Einstein (1950) [29] was the first to introduce the probability concept, in sediment transport research and to use the concept to develop the bed-load and suspended-load formulae for nonuniform sediment. He found that the hydrodynamic lift caused by turbulent flow is attributed to the particle movement and entrainment. In a study on the armor-ing effects developed at the bed surface Gessler (1970) [44, 45] developed an incipient motion model in which the shear stress fluctuations and critical shear stress were correlated. In this model, Gessler assumed that fluctuating bottom shear stress can be described by a Gaussian distribution and erosion occurs only when the instantaneous bottom shear stress exceeds a critical shear stress. He defined the probability of the local shear stress, τ , not exceeding the critical shear stress, τ_c , $q_{\tau c}$, as:

$$q_{\tau c}(\frac{\tau}{\tau_c} < 1) = \frac{1}{\sqrt{2\pi}\sigma} \int_{-\infty}^{\frac{\tau_c}{\tau} - 1} \exp(-\frac{x^2}{2\sigma^2}) dx \quad (2.1.20)$$

in which σ is standard deviation of the shear stress fluctuation. For coarse material $\sigma = 0.57$. Considering a given sediment grain size fraction n , the probability that the instantaneous bottom shear stress does not exceed the critical shear stress for erosion of that size fraction of sediment mixture is represented by $q_{\tau cn}$. Thus, $(1 - q_{\tau cn})$ represents the probability of local bottom shear stress exceeding this critical value, τ_{cn} . If p_n represents the percentage of size fraction n in the sediment mixture, the percentage of eroded material for this size fraction n at the cross section considered can be defined as

$$P_{n,E} = \frac{\int_{n_{\min}}^n (1 - q_{\tau cn}) p_{bn} dn}{\int_{n_{\min}}^{n_{\max}} (1 - q_{\tau cn}) p_{bn} dn}, \quad (2.1.21)$$

The grain size distribution of the armor coat can then be defined by

$$P_{n,A} = \frac{\int_{n_{\min}}^n q_{\tau cn} p_{bn} dn}{\int_{n_{\min}}^{n_{\max}} q_{\tau cn} p_{bn} dn} \quad (2.1.22)$$

where n_{\max} and n_{\min} denote the maximum and minimum grain size of a mixture, respectively, and p_{bn} is the percentage of grain size fraction n on the bed surface.

Based on the sediment-mixture experiments of Yen (1988) [181, 182], Hsu and Holly (1992) [56] suggested that the percentage of a given grain size fraction in the transported material

is proportional to the joint probability of two factors: the mobility of this size fraction for the prevailing hydraulic conditions and the availability of this size fraction on the bed surface. The availability of a given size fraction n on the bed surface is represented by p_{bn} . They used the same assumptions as Gessler. In their model the grain size distribution of the eroded material is given by

$$P_{n,E} = \frac{q_{\tau_{cn}} p_{bn}}{\sum_{D_{\min}}^{D_{\max}} q_{\tau_{cn}} p_{bn} d(D)}, \quad (2.1.23)$$

where D_{\max} and D_{\min} are the representative diameters of the largest and smallest size fractions, and $q_{\tau_{cn}}$ is the probability of the local shear stress exceeding τ_{cn} , expressed by

$$q_{\tau_{cn}}\left(\frac{\tau_{cn}}{\bar{\tau}} > 1\right) = \frac{1}{\sqrt{2\pi}\sigma} \int_{\frac{\tau_{cn}}{\bar{\tau}} - 1}^{\infty} \exp\left(-\frac{x^2}{2\sigma^2}\right) dx \quad (2.1.24)$$

Similarly, Li suggested a formula to describe the sedimentation and erosion for sediment mixtures considering fluctuating velocity of turbulent flow (cited by Zhou [185]). In addition to use the probability theory to take into account turbulent flow properties in the previous examples many deterministic methods have also been developed to calculate the entrainment rates for nonuniform sediments. Based on field and flume data, Samaga et al. (1986) [124, 125] and Holtroff (1983) [55] introduced some modifications to Einstein's method. Swamee and Ojha (1991) [141] studied the properties of grain-size distribution curves and extended the formulae for calculating transport rate for uniform sediments to the nonuniform sediment mixtures. Some researchers directly apply the formulae for uniform sediment to the calculation of nonuniform sediment transport [116]. Table 2.2 summarizes some of the formulae presented here.

A variety of sediment transport formulae are available. Vanoni (1975) [159] used several formulae to predict sediment transport on the Colorado River and the Niobrara River. He found large differences between the estimated sediment discharges. A given formula predicted sediment discharge adequately for one river, but very poorly for the other river. Yang and Molinas (1982) [177], Shen and Hung (1983) [129], van Rijn (1984) [153, 154] and Nakato (1987, 1990) [95, 96] also compared predicted and measured flow and sediment data in natural rivers. They all concluded that a few formulae could predict the sediment discharge reasonably well for the flow conditions tested but that all the other formulae were found to over- or underpredict the sediment discharge. It is extremely difficult to find one formula that is widely applicable. The selection of formulae for predicting sediment discharge in movable-bed rivers must be related not only to the physical phenomena of interest but also to the range over which the selected formula is valid [96].

Variation	Method & Load	Author	Comments
$q_T = \sum_i p_i q_{Bi} (1 + P_E I_1 + I_2)_i \quad q_S = \sum_i p_i q_{Bi} (P_E I_1 + I_2)_i$ $p_i = 1 - \frac{1}{\sqrt{\pi}} \int_{-B_* \Psi_* - \frac{1}{\eta_0}}^{B_* \Psi_* - \frac{1}{\eta_0}} e^{t^2} dt = \frac{A_* \phi_*}{1 + A_* \phi_*}$ $\Phi_* = \frac{p_i q_{Bw}}{p_{bi} q_{\rho s}} \sqrt{\frac{\rho}{\rho_s - \rho}} \sqrt{\frac{1}{g D^3}} \quad \Phi_* = \Psi_* = \zeta Y \left(\frac{\beta^2}{\beta_x} \right) \Psi$ $\Psi = \frac{\rho_s - \rho}{\rho} \frac{D}{R_{0S}} \quad \beta_x = \log(10.6X) \quad P_E = 2.303 \log \frac{30.2d_i}{\Delta}$	PROBM Suspended & bed load	Einstein 1950	Theory analysis
$q_B = \sum_i q_{Bi} = p_i Q_{Bi} \quad p_i = \frac{\int_{i_{min}}^{i_{max}} (1 - q(\tau)) p_{bi} d\tau}{\int_{i_{min}}^{i_{max}} (1 - q(\tau)) p_{bi} d\tau}$	PROBM Bed load	Gessler 1970	Theory analysis; Armoring coat
$q_B = \sum_i \sum_j q_{Bij} = \sum_i \sum_j \sum_{k=e}^{k=f} p_{bij} P_k Q_{bk} \quad P_k = \int_{\tau_k - \frac{1}{2} \frac{6\sigma\tau}{N}}^{\tau_k + \frac{1}{2} \frac{6\sigma\tau}{N}} q(\tau_k)$ $q_S = \sum_i \sum_j q_{Sij} = \sum_i \sum_j \int_a^h u C_{ij} dy \quad C_{ij}(a) = \frac{q_{Bij}}{U_{bij} a g}$	PROBM Suspended & bed load	van Nierkerk 1992	
$q_B = \sum p_{bi} q_{Bi} = \sum p_{bi} \rho g d_i \sqrt{\frac{\rho_s - \rho}{\rho}} g d_i \zeta_B$ $q_S = \sum p_{bi} q_{Si} = \sum p_{bi} \rho g d_i \sqrt{\frac{\rho_s - \rho}{\rho}} g d_i \zeta_S$ $\zeta_{B,S} = f\left(\frac{\tau}{\tau_{ci}}, \frac{\tau}{(\rho_s - \rho) g d_i}, M\right)$	DETM Suspended & bed load	Samaga 1986	Flume experiment
$\Phi_B = \frac{q_B}{d \sqrt{\frac{\rho_s - \rho}{\rho}} g d} \quad \Phi_S = \frac{q_S}{d \sqrt{\frac{\rho_s - \rho}{\rho}} g d}$ $\Phi_B = \left[\left(\frac{0.8}{M} \right)^{4.75} + M^{0.004} 1.75 \left(\frac{0.9871}{\tau_*^{M^{0.25}}} \right)^9 + \left[\left(\frac{0.01}{M} \right)^{0.6} + M^{3.35} \right] 1.2 \left[\frac{0.339}{\tau_*^{8M/(8M^2+1)}} \right]^{1.6} \right]^{-1}$ $\Phi_S = \left[\left(\frac{0.073}{M} \right)^4 + M^{3.8} \left[\left(\frac{0.567}{\tau_*^{M^{0.635}}} \right)^6 + \left[\left(\frac{0.177}{M} \right)^2 + M^{1.45} \right] 2 \left[\frac{0.538}{\tau_*^{8M/(7M^{1.425}+1)}} \right] 3 \right]^{-1}$	DETM Suspended & bed load	Swamee & Ojha 1991	Empirical equation
$q_{Bplane} = \frac{(\tau - \tau_c) u}{3(1+n') \rho g \frac{\rho_s - \rho}{\rho} \tan \phi} \quad R_* = \left(1 - \frac{1}{1+n'} \right) \frac{u d \rho}{3\nu}$ $q_{Bbf} = q_B (1 - c) \quad c = f(\text{bedform})$ $q_S = \frac{\tau_{f,k} u}{p g \frac{\rho_s - \rho}{\rho}} \sum_i p_{si} a_{si} \left(\frac{\tau_{s,k}}{\tau_{f,k}} \right)_i \left(\frac{u}{u_w} \right)_i \quad \frac{\tau_{s,k}}{\tau_{f,k}} = f(\kappa) \quad a_s = \frac{\bar{C}}{C_a}$	DETM Suspended & bed load	Holtroff 1983	Modification of Einstein's method
$q_T = \sum_i p_{bi} Q_{Ti}$	DETM Total load	Yang 1982	formulae for uniform sed- iment used
$q_B = \sum_i p_{bi} \eta_i Q_{Bi} \quad \eta_i = \left(\frac{d_i}{d_{50}} \right)^{0.85}$	DETM Bed load	Rahuel 1989	for each size fraction

$q_{Bi} = M_i(2d_i)^{(1+\eta_v-0.785z_i)}$ $q_{S_{ui}} = \int u C_i dy = \int u \cdot C_{ui}(\frac{y}{h})^{-1.5z_i} dy$ $q_{S_{mi}} = \int u \cdot C_{mi}(\frac{y}{h})^{-1.5z_i} dy$ $\eta_v = 0.1198 + 0.00048T$	$u = (1 + \eta_v)U(\frac{y}{h})^{\eta_v}$ $q_{S_{Li}} = \int u \cdot C_{Li}(\frac{y}{h})^{-0.756z_i} dy$ $z_i = \frac{w_i u}{C_s d S}$	DETM	Toffaletti 1969	
		Suspended & bed load		

Tabelle 2.2: Formulae to determine entrainment rates for nonuniform sediment mixtures

The explanation of symbols used in Table 2.2 are listed in the following.

$C_{U,i,M,i,L,i}$	the concentration distributions for the lower, middle and upper zones in Toffaletti's method,
d_i	grain size diameter for size fraction i,
I_1, I_2	integrals from Einstein,
M	Kramer's uniform coefficient for a sediment mixture, $M = [0.1769\sigma_g + 1]^{-10}$ $M = 0.84\sigma_g^{-1.34}$,
N	interval number,
P_k	proportion of time kth shear stress interval is active,
p_{bij}	volumetric proportion of grain size fraction i and mineral density j on the surface (or in the active layer),
p_{bi}	volumetric proportion of grain size fraction i on the bed surface (or in the active layer),
p_{Bi}	percentage of erosion rate for size fraction i,
P_E	transport parameter,
$q(\tau)$	probability that particles of grain size fraction i will not be removed,
Q_{Bi}	fractional bed-load per unit width and time calculated by a formula for uniform sediments,
q_B	bed-load per unit width and time,
Q_{Si}	fractional suspended load per unit width and time calculated by a formula uniform sediments,
q_S	suspended load per unit width and time,
q_T	total load per unit width and time,
S	slope of a stream,
T	water temperature,
η_i	hiding factor,

Φ	transport rate function,
Ψ	shear intensity parameter.
σ_g	geometric standard deviation,
σ_τ	standard deviation,
τ_*	grain shear stress for nonuniform sediment

The total sediment transport includes the bed-load and the suspended load. Bed-load transport is saturated sediment transport, whereas suspended sediment transport is unsaturated. The continuity equation of total-load transport is:

$$\frac{\partial(G_b + G_s)}{\partial x} = \rho_p \frac{\partial z}{\partial t} + \frac{\partial hC}{\partial t} \quad (2.1.25)$$

where G_b and G_s are transport rates for bed-load and suspended load, respectively. The difference between these two kinds of transport loads can be understood by comparing their continuity equations of sediment transport. The continuity equation for fractional bed-load transport is

$$\frac{\partial G_{bn}}{\partial x} = -\rho_p \frac{\partial y_n}{\partial t}. \quad (2.1.26)$$

$$G_{bn} = f(h, \tau, \tau_{cn}, d_n, \gamma_s, \gamma, g) \quad (2.1.27)$$

The river bed changes, sedimentation and erosion, are included in the value Δy_n , which is determined by the difference in transport capacities between two adjacent sections. The sectional transport rate is related to the flow and bed conditions. A positive value of Δy_n indicates sedimentation and a negative value of Δy_n indicates erosion. The mass balance of the control volume between two adjacent cross sections is used for calculating the bed change within Δx , by summing sedimentation and erosion. For a fractional erosion the transport rate is limited by the mobility and availability of bed material of a given size fraction, which depends only on the local flow and bed conditions.

However, suspended sediment transport is unsaturated, fractional entrainment (erosion rate) is not only related to sediment inflow and outflow and the mobility and availability of bed material, but also to suspended sediment concentration. Sediment deposition depends on the sediment fall velocity and the suspended sediment concentration near the bed surface. The continuity equation for suspended sediment transport is expressed by:

$$\frac{\partial G_{sn}}{\partial x} = -\frac{\partial hC_n}{\partial t} + \rho_p \frac{\partial y_n}{\partial t}, \quad (2.1.28)$$

$$\rho_p \frac{\partial y_n}{\partial t} = -(\dot{S}_n - \dot{E}_n). \quad (2.1.29)$$

The concentration and the sedimentation rate must be determined by the convection-dispersion equation of suspended sediment transport. Obviously, the fractional entrainment can not be determined using the method for bed-load transport. As pointed out by Rahuel et al. (1989) [116], in some earlier efforts, the lack of success in modeling the sediment transport processes could be related to over simplified treatment of sediment transport. Considering effect of turbulence on sediment transport, Nezu and Nakagawa (1994) [100] stated that 'the classical stochastic model and its extension formula cannot be universally applied to rivers carrying suspended sediment. Their weakness is that they do not incorporate modern turbulence knowledge. The random character of the motions of sand particles is regarded as more significant than the flow in such stochastic models. As a result, they are not based on the mechanics of turbulence but use only the continuity equation for sediment transport and the parametric probability density functions. In this sense these stochastic models are not hydrodynamic model, but are really only kinematic models.' The present work will derived a new method to describe nonuniform sediment transport process bases on probability theory. It relates fractional erosion of a sediment mixture to (1) the turbulent flow condition, (2) the joint probability of mobility and availability of bed material to entrainment and (3) the suspended sediment concentration.

Sediment exchange near the bed surface

In sediment transport, exchange between transported sediments and river bed material occurs when the bottom shear stress exceeds the critical shear stress. To describe the exchange one usually divides the bed into several horizons according to the moving manner and position of sediment particles (Figure 2.10) [4, 10, 12, 77, 105, 116, 121, 133, 152].

- (1) Flow zone, in which the suspended load is transported along with water flow;
- (2) Bottom layer, in which bed-load is transported. In this region the particles move mainly by rolling and sliding.
- (3) Active layer, from which sediment particles may be entrained into the bottom layer or the flow zone as suspended sediments. Because of the existence of exchange between the bottom layer and this layer, it is also called the mixing layer in some models;

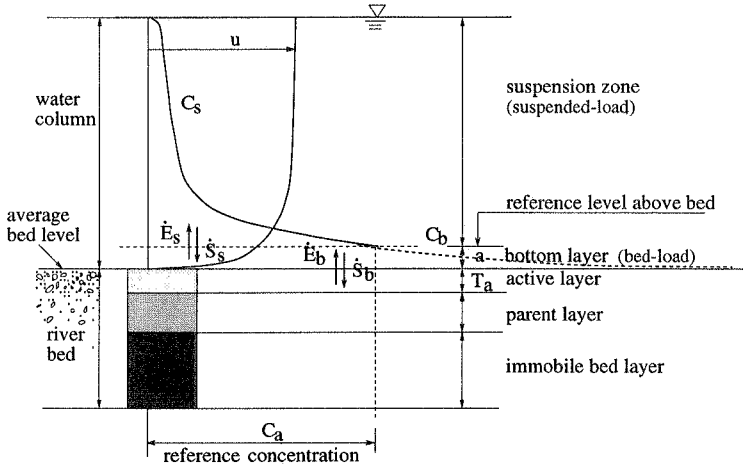


Figure 2.10: Definition sketch, suspended sediments interacting with losse bed

- (4) Parent layer, beneath the active layer. The bed material in this layer is not involved in transport calculations in the current time step, but supplies the material to the active layer to which the calculation may refer;
- (5) Immobile layer, in which bed material is not eroded in the flow transport process.

Moving particles in the bottom layer can enter the flow at the interface between the bottom and the suspension layers, i.e., bed-load and suspended load layer. Although in reality it is hard to position this interface, it is useful to define a boundary between the bed-load and suspended load layers for numerical calculation.

The parent layer may need to be further divided into layers if the bed material is mixed with partial cohesive clay. This is because the compaction and consolidation of cohesive sediments varies with depth under the bed surface and age of the deposited sediments. The compaction and consolidation influence the cohesive sediment entrainment [90, 106, 145, 148, 106].

Rahuel et al. (1989) [116] used the concept of the mixing layer in their fractional bed-load transport model to deal with the effects of sorting and bed armoring. They used a hiding factor to correct the overestimation of entrainment of fine bed material. The sediment exchange between the particles in the bottom layer (transported bed-load) and mixing layer is considered only in the current time step of calculation. The material exchange

between the mixing layer and the underlying parent layer depends on the difference in the thickness of the mixing layer, T_a , and the erosion thickness, E_a . When $T_a < E_a$, some of the underlying layer material will fill the mixing layer. Conversely, when $T_a > E_a$, some of the mixing layer material will appear in the underlying layer. Such a mixing layer has a quasi fixed upper boundary at the bed surface and a moving lower boundary. Its thickness is determined by flow conditions and the grain size distribution of bed material. This kind of model has been widely used [12, 13, 14, 60]

Rahuel et al. [116] stated that the mixing layer thickness is strongly dependent on the time scale considered. For short time scales, the mixing layer can be thought of as a thin surface layer, in which particles are susceptible to entrainment into the flow due to the fluctuation of the bed shear stress. For longer time scales, the mixing layer can be treated as a zone of bedform movement (dunes and ripples), or a layer of eroded or deposited material.

Silvio, G. D. (1991) [133] proposed a four-layer model for total load transport calculation. He defined the four layers as: water stream, bottom layer, mixing layer and intrusor layer. The last two layers correspond to the active layer. He reasoned that since the surface of gravel rivers has a coarser composition than the material underneath, the composition of transported material should be related to that of the material beneath under non-equilibrium transport condition. An alternative method is to consider a hiding and exposure effect. He concluded that this method may be more useful for the study of sediment transport of widely graded sediment mixtures.

The height of the bottom layer is usually defined as a proportion of the water depth, e.g. 0.05h, or as a thickness of transported bed-load [154]. The height of an active layer is generally related to the thickness of bedforms [53, 77], the representative diameter of bed material [14] or the critical shear stress for erosion [152].

2.1.5 Flood plain sedimentation

Interaction between the flow in the main channel and on the flood plains

When overbank flow occurs in a channel with compound cross-sections, the flow velocity in the deeper main channel will be significantly different from that on the shallower flood plains. This yields strong interactions between the flow in the main channel and the flood plains. Momentum is transferred from the main channel to the flood plain. It results in a decrease of the velocity in the main channel and an increase of that over the flood plain and generates turbulent shear at the interface. In the interaction zone there exist vortices

with longitudinal axis, called secondary currents observed by [2, 40, 112, 114, 138, 134, 142]. In trace experiments Wood and Liang (1989) [172] observed that the tracer moved either onto or off the flood plain. Imamoto and Ishigaki (1992) [57] demonstrated this phenomenon by using the visualization technique. These secondary currents are driven by the anisotropy and inhomogeneity of turbulence [147].

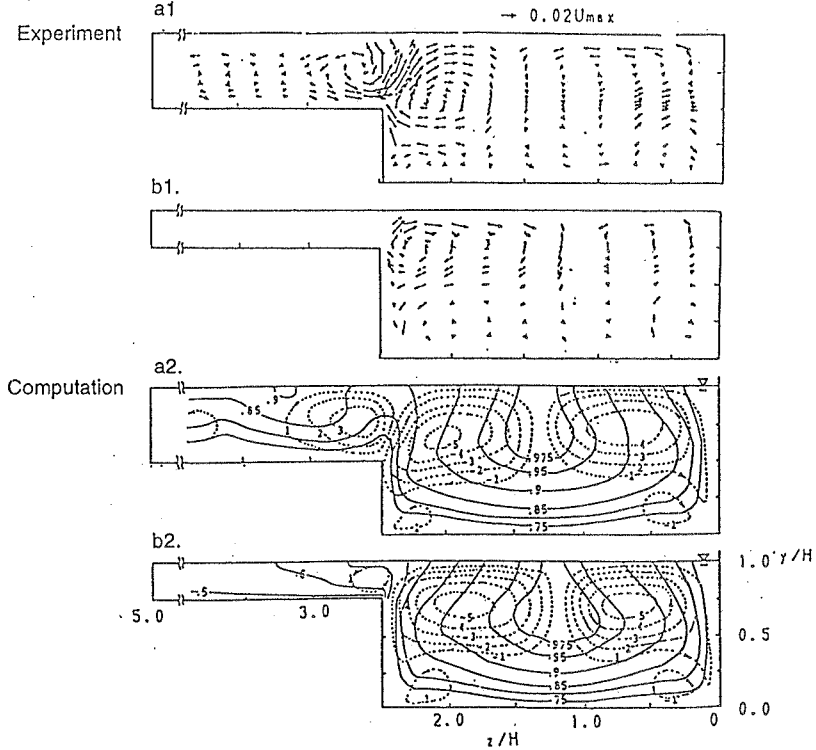


Figure 2.11: Secondary current vectors. After Tominage and Nezu (1991) [147] (experiment) and Naot et al. (1993) [99] (computation). a. $h_m/h_p = 0.5$, $\frac{W_{max}}{\langle W \rangle} = 1.24$. and b. $h_m/h_p = 0.25$, $\frac{W_{max}}{\langle W \rangle} = 1.28$. solid line: $\frac{W}{W_{max}}$, dashed line: $10^3 \frac{\psi}{\langle W \rangle H}$

At the interface between the main channel and the flood plain, the turbulent shear stress, τ_{zx} , generated by the difference in velocity between the main channel and the flood plain can be described by the Reynolds shear stress formula as follows

$$\tau_{zx} = -\rho \epsilon \frac{\partial u}{\partial z}. \quad (2.1.30)$$

The turbulent diffusion coefficient is usually related to a horizontal length scale and the velocity which may vary across the shear layer [2]. It can be expressed by

$$\tau_{zx} = -\rho \varepsilon_{mp} \frac{u_m - u_p}{B}. \quad (2.1.31)$$

An expression to determine ε_{mp} was suggested by Evers (1983) [34], in which the difference of velocities between the main channel and the flood plain, $u_m - u_p$, is taken as a velocity scale and the width of the interaction zone, B_{mp} , as length scale. Then, the turbulent diffusion coefficient ε has the following form

$$\varepsilon = 2 \kappa (u_m - u_p) \frac{\partial \bar{u}}{\partial z} B_{mp} \quad (2.1.32)$$

where κ is a proportional factor. Under the assumption that τ_{zx} has a linear distribution in the lateral direction, integrating the above equation on the x-z plane the turbulent shear stress, τ_{zx} , can be obtained

$$\tau_{zxT} = 2\rho\kappa (u_m - u_p) |u_m - u_p|, \quad (2.1.33)$$

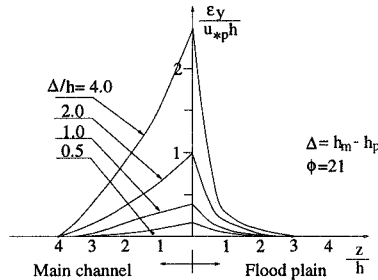
For practical application, the coefficient κ is experimentally suggested as 0.01 by Evers and proposed as 0.01-0.02 by Kohane (1991) [67].

Other investigators have proposed expressions of the turbulent shear stress, some of which are tabulated in Table 2.4.

Ogink (1985) [103] used a two-dimensional flow model to determine the discharge in the main channel and in the flood plains using different values of τ_{mp} , including the expressions of Nicollet, Evers, Rajaratnam and Ahmadi, Hanxiang and Könemann. He found that for $\frac{h_m}{h_p} < 8$ the results calculated by Nicollet, Evers and Könemann are in good agreement. To obtain a similar distribution of discharge for the river and the flood plain using the formula of Rajaratnam and Ahmadi a smaller value of τ_{mp} should be used. Xie's results deviate slightly from Evers.

The theoretical curves of the turbulent diffusion coefficient, ε_{mp} , in the interaction zone for a turbulent flow according to Ashida et al. (1988) [8] are shown in Figure 2.12, in which the ϕ is the diameter of cylindrical wooden rods used to simulate non-submerged vegetation roughness on the flood plains. It can be seen that the maximum value of ε_{mp} occurs at the interface between the main channel and the flood plain. ε_{mp} is much larger than the pure transverse turbulent diffusion coefficient, ε_t . At the interface, ε_{mp} increases

Expression	Investigator
$\tau_{xzT} = 2\rho\kappa (u_m - u_p) u_m - u_p $	Evers 1983 [34]
$\tau_b c_K (h_m - h_p)/(h_p - h_{po})$	Könemann 1980 [68]
$(1 - a_2^2) \frac{\rho g A_r S_o}{2h_p} \approx \tau_{bm} (1 - a_2^2) \frac{B_r}{2d}$ $a_2 = 0.9(stk_m/stk_p)^{\frac{1}{6}}$	Nicollet and Uan 1977 [101]
$0.15(\frac{h_m}{h_p} - 1)^2 \tau_{bp}$	Rajaratnam 1979, 81 [117][118]
$0.874(u_m - u_p)(\frac{h_m}{h_p})^{-1.129} (\frac{W_m}{W_p})$	Prinos and Townsend, 1984 [113]
$\rho \frac{\beta H_m^*}{2} \frac{\gamma}{\gamma+1} (u_m^2 - u_p^2)$ $H^* = \frac{4.8gh}{C(0.6+C)} \quad \gamma = f(C)$ C: Chezy coefficient	Xie 1980 [173]

Table 2.4: Expressions of the turbulent shear stress**Figure 2.12:** Dispersion coefficient at the interaction zone between the main channel and the flood plains. After Ashida et. al. (1988) [8]

with the ratio of the flood plain height and water depth on it. In the interaction zone, ε_{mp} decreases exponentially with increasing distance from the interface.

The total transverse diffusion coefficient at the interface of the main channel and the flood plain contains contributions of two terms, ε_t caused by pure transverse turbulent diffusion and ε_{mp} due to the interaction between differential velocity and longitudinal

turbulent diffusion.

$$\varepsilon_T = \varepsilon_t + \varepsilon_{mp} \quad (2.1.34)$$

thus, τ_{zx} should be written as

$$\tau_{zx} = \rho(\varepsilon_t + \varepsilon_{mp}) \frac{\partial u}{\partial z} \quad (2.1.35)$$

Yen (1985) [180] derived a quasi-one-dimensional method for backwater computation in a compound channel. He used the continuity and momentum equations for the main channel and the flood plains separately and took into account the effect of the lateral discharge and interfacial shear stress between them. Based on his experimental results, he concluded that the effect of interfacial shear stress on the backwater profile is insignificant compared to the effect of lateral discharge. The lateral diffusion coefficient has a range of 10^{-3} to $10^{-5} \text{ ft}^2/\text{s}$. Kohane [67] predicted the effect of the interfacial shear stress on the backwater profile for a 32 km reach upstream of the River Neckar using Yen's method. Comparing the results with a one-dimensional model, he found that the water surface calculated by Yen's method was higher than that calculated by the one-dimensional model. The maximum difference between them is at the sections with large changes in cross-sectional geometry or strong diverging flow. He concluded that in these cases the computation of a water surface by a one-dimensional model was not accurate enough. A one-dimensional multiple strip model should be used, even though this model requires a great computational effort

Pasche [107] and Alavian [2] developed $k - \varepsilon$ models (two-dimension) to describe the exchange of momentum and mass between the main channel and the flood plains. Pasche found that the non-dimensional lateral depth averaged diffusion coefficients, defined as $\frac{\nu_t}{u_* h \sigma_t}$, are very different in the main channel and the flood plains, Figure 2.13.

Few attempts have been made to determine the transverse dispersion coefficients of sediment particles between the main channel and the flood plains. Rajaratnam and Ahmad [118] suggested that the value of ε_s in the interaction zone over the flood plain can be described by

$$\frac{\varepsilon_s}{h_p \cdot (u_m - u_p)} = \frac{0.3 \left(\frac{h_m}{h_p} - 1 \right)^3}{\left[\frac{(u_m - u_p)}{u_{* \infty}} (u_m - u_p) \right]^2} A \quad (2.1.36)$$

and

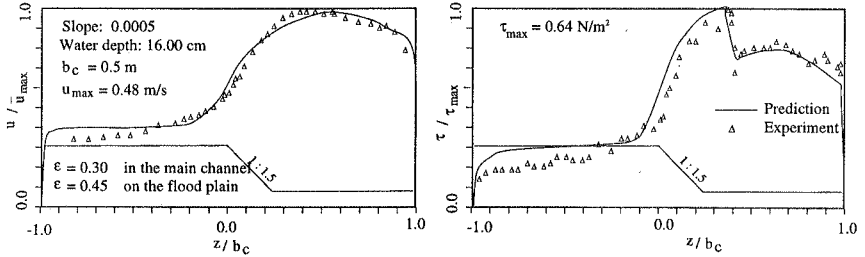


Figure 2.13: Bottom shear stress distribution in a compound section. After Pasche (1985) [107]

$$A = \frac{F(\eta)}{\eta F(\eta)}, \quad \frac{\tau}{\tau_{0\infty}} = 0.15 \left(\frac{h_m}{h_p} - 1 \right) F(\eta)$$

where $\frac{h_m}{h_p}$ is the ratio of water depths between the main channel and the flood plain, u_m and u_p are velocities of the main channel flow and undisturbed flood plain flow, A is a function of η , $\eta = \frac{z'}{b_p}$, and b_p is the length of the interaction zone on the flood plain, $b_p = z' = 0.64(h_m - h_p)$ where $(\tau - \tau_{0\infty})/(\tau_{0m} - \tau_{0\infty}) = 0.5$ [7]. τ , τ_{0m} , and $\tau_{0\infty}$ are the bottom shear stress within and beyond the interaction zone on the flood plain and at the interface, respectively. In the main channel, the length of the interaction zone can be determined using $b_m = 3.78(h_m - h_p)$. Rajaratnam's expression is not well suited for numerical modeling since it includes a function which has to be obtained from figures.

Many experimental results have shown that the interaction between the main channel and the flood plain flow significantly affects the transverse dispersion, and consequently lateral transport resulting in the sediment deposition on the flood plain. Therefore, it is desirable to derive an expression for the lateral diffusion coefficient in the interaction zone of the main channel and the flood plain. In the present work, an attempt is made to derive a method to evaluate such a diffusion coefficient. It will be presented in detail in Chapter 3.

Sediment deposition on flood plains

Overbank flow results in a transfer of mass, momentum and energy between the faster flow in the deep main channel and the slow flow on the shallow flood plain. On the flood plains transport capacity diminishes due to lower velocity and increasing flow resistance, and sediments rapidly settle [111].

The sediments deposited on the flood plains are generally finer than those occurring close to the active channel [120]. Flow patterns and deposition rates depend on the flood plain topography and vegetation [65]. Vegetation on the flood plains enhances deposition. The deposition rate and amount are of great environmental significance since sediment-bound pollutants can be deposited and accumulated on the flood plain and they may be resuspended and transported during flood events [84].

The sedimentation rates calculated by different methods range from 1 millimeter to a few centimeters per year. Measured sedimentation rates over 35-year period in southern Norway, were between 0 - 10 mm per year for the Culm River, and between 3 and 40 mm per year for the Severn River. For both cases, the greatest deposition occurred near the channel [161]. Obviously, there is considerable variation in the lateral sedimentation rate on the flood plain.

According to an analysis of river flow records, Leopold and Maddock (1953) [79] suggested that bankfull discharge had a recurrence interval of about 1.5 years. Overbank flow can therefore be expected to take place with about the same frequency. Because channel and flood plain sediments are distinctly different, this point on the magnitude-frequency plot is very significant. This means that for any river the channel geometry is adjusted to cope with floods of moderate magnitude with the same frequency. It has been proved that the formation of channel geometry is controlled by bankfull flows. The bankfull flow is frequent and powerful enough to erode banks and river beds. Floods have almost little effect on the channel form, as they rarely occur and overbanking flow greatly reduces the flow power to erode the river bed and the banks [80].

In fact, a flood plain represents a balance between the erosion energy and the alluvial resistance [98]. Leopold and Maddock suggested a general theory of flood plain formation related to both deposition on the flood plain and lateral bank erosion [80].

2.2 Model research situation

2.2.1 General remarks

The numerical simulation of sediment transport processes in river channels is an important tool to see how the channel characteristics and morphology respond to change caused by natural or human interference. The main objects of the simulation of sediment transport processes are shown in Figure 2.14. They involve: simulation of changes in river morphology, description of the effect of selective transport on the sediment transport process and

assessment of the impact of river drainage works.

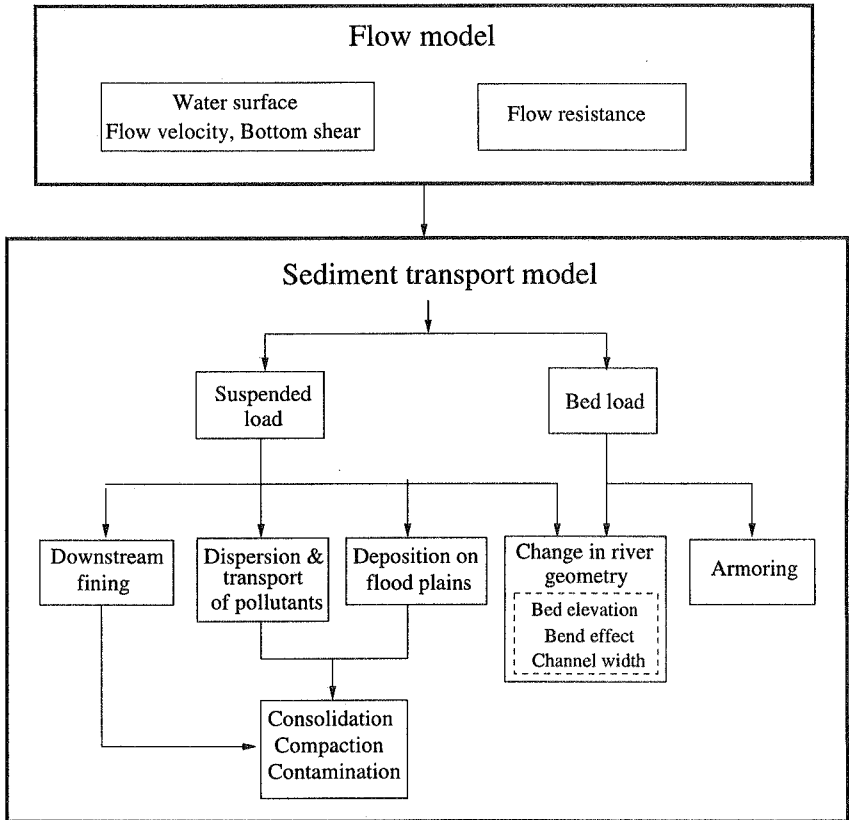


Figure 2.14: Framework of sediment transport modeling

In the past 30 years, modern computational techniques with enhanced computer capacity have rapidly advanced sediment transport modeling. Considerable effort has been given to develop numerical methods for simulating sediment transport processes in river channels. Different numerical models have been suggested. These models can be classified according to

- (1) numerical method: finite differential method (FFM), finite volume method (FVM), finite element method (FEM), characteristic method (CM);

- (2) dimension: one-, two-, three-dimensional models and quasi two- or three-dimensional models (multiple strip model and stream tube);
- (3) physical properties considered in the problems: two main classes in particle transport models: particle dispersion and sediment transport. The later can be further divide according to different transport loads (bed, suspended and total load) and/or different methods for treating bed material (uniform sediment and nonuniform sediment mixtures)

The selection of computational methods is usually connected with the selection of the model dimensions, and the model dimensions closely relate to the problems.

One-dimensional numerical models have been extensively applied to simulate long term river morphological changes, such as aggregation and degradation upstream and downstream of reservoirs. Most of the simulation for sediment transport in rivers used one dimensional models because of their shorter calculational time, lower cost and small data requirements. One-dimensional numerical models are usually sufficient, but they only give sectional averaged bed elevations. If more detailed information about river morphological changes are needed, two or three-dimensional models are required.

A frequently applied computational method for one-dimensional problems is the FDM. FDM may be explicit or implicit. An implicit scheme is unconditionally stable, so only the accuracy should be considered. An explicit scheme is conditionally stable and must satisfy the Courant criterion, $\Delta t \leq \frac{\Delta x}{c}$, where c is the shallow water wave velocity, which is equal to $c = \sqrt{gh} + U$. Generally, using the implicit scheme a longer time step is allowed whereas using the explicit scheme the time step is limited by the Courant criterion [128].

Two- and three-dimensional models are also known as horizontal and vertical models, respectively. Two dimensional depth-averaged flow and sediment transport model (horizontal models) have been widely developed for simulating river bed changes at river confluences and sediment deposition in reservoirs and lakes. Three-dimensional models are used for investigating the detailed changes at important positions. However, only a few studies based on the three-dimensional calculations have been reported because of the complicated mathematics and expensive computer time required.

Frequently used computation methods include FDM, FVM and FEM. The basic approximation principle of finite-difference and finite-volume methods is the same. In the finite difference method differential quotients of a differential equation are directly approximated. In the finite volume method, differential quotients are integrated over a control volume. In FVM, the calculation domain is divided into a number of non-overlapping control volumes, surrounding each grid point. Through integrating the differential equation over

control volume a conservative discretization equation is obtained, which contains the value of unknown variables for a group of grid points [109].

In the FEM the unknowns are approximated on the basis of nodes which are connected to each others by means of an element. Inside the elements the values of the unknown are evaluated by interpolation. Since the governing differential equation will not be met by the interpolated unknowns everywhere, a local residue occurs. By applying a weighting function and integrating over the volume of the element the residue inside the element is redistributed to the nodes. The sum of the weighted and integrated residues of all elements solved by a node must equal zero. Different choices for the functions of interpolation and weighting lead to different sub-schemes of the FEM such as the Galerkin method or the Petrov-Galerkin method [128].

The FEM is very flexible with respect to combining different element types such as triangles and quadrilaterals to unstructured grids, so irregularly shaped domains can be approximated by the method. In principle, this is also possible using the FVM. The most important disadvantage of the FEM is that mass-balance is not met locally, whereas the FVM is strictly conservative. Furthermore the derivation of equations is easier in the FVM than in the FEM.

Multiple-strip models and stream tube models are intermediary classes of models between the one- and two-dimensional models. In these models a river is divided into several parallel strips according to different principles. Multiple-strip models are generally used for simulation of water surface for overbank flow and deposition on the flood plains during flood events. Therefore they usually include three strips, one for the main channel and two for the flood plains. In stream tube model a river channel is divided into a certain number of stream tubes that have an equal portion of discharge. No flow is allowed to cross into the adjacent stream tubes. Hydraulic parameters and particle movement are simulated for each stream tube.

Quasi two-dimensional models consist of a stream tube flow model and a two-dimensional suspended sediment transport model. The stream tube flow model provides a quasi two-dimensional flow field. Based on this flow field two-dimensional phenomena of sediment and pollutant transport and can be described approximately.

The convection-dispersion equations of suspended sediment transport (or pollutant transport) used by the different models are summarized in Table 2.5.

Dimension	Flow model	Sediment transport model	Problem	Method	Convection-dispersion equation of suspended sediment transport
1 d	1 d		1-d open channel	FDM	$\frac{\partial c}{\partial t} + u \frac{\partial c}{\partial x} = \frac{\partial c}{\partial x} (D_L \frac{\partial c}{\partial x}) + \dot{E} - \dot{S}$
	Multiple strips		1-d open channel with compound section	FDM	$\frac{\partial c}{\partial t} + u \frac{\partial c}{\partial x} = \frac{\partial c}{\partial x} (D_x \frac{\partial c}{\partial x}) + \dot{E} - \dot{S}$
	Multiple stream tubes		1-d open channel with compound section	FDM	$\frac{\partial c}{\partial t} + u \frac{\partial c}{\partial x} = \frac{\partial c}{\partial x} (D_x \frac{\partial c}{\partial x}) + \dot{E} - \dot{S}$ (for each stream tube) $m_z h u \frac{\partial c}{\partial x} = \frac{\partial}{\partial x} (\frac{m_z}{m_x} h D_x \frac{\partial c}{\partial x})$
quasi 2 d	Multiple stream tubes	2 d		FDM FVM	$\frac{\partial c}{\partial x} = \frac{\partial}{\partial x} (m_x h^2 u D_z \frac{\partial c}{\partial z})$, $q_c = \int_{Z_L}^z m_x h u dz$ $m_x m_z \frac{\partial h c}{\partial t} + \frac{\partial m_x u h c}{\partial x} + \frac{\partial m_z v h c}{\partial z}$ $= \frac{\partial c}{\partial x} (\frac{m_z}{m_x} h D_x \frac{\partial c}{\partial x}) + \frac{\partial c}{\partial z} (\frac{m_x}{m_z} h D_z \frac{\partial c}{\partial z}) + \dot{E} - \dot{S}$ $\frac{\partial h c}{\partial t} + \frac{\partial u h c}{\partial x} + \frac{\partial v h c}{\partial z} = \frac{\partial c}{\partial x} (h D_x \frac{\partial c}{\partial x}) + \frac{\partial c}{\partial z} (h D_z \frac{\partial c}{\partial z}) + \dot{E} - \dot{S}$
2 d	2 d		2-d shallow flow: lake & estuaries	FDM FVM FEM	$\frac{\partial h c}{\partial t} + \frac{\partial u h c}{\partial x} + \frac{\partial v h c}{\partial z} = \frac{\partial c}{\partial x} (h D_x \frac{\partial c}{\partial x}) + \frac{\partial c}{\partial z} (h D_z \frac{\partial c}{\partial z}) + \dot{E} - \dot{S}$

c = concentration;

u, v = velocities in longitudinal and transverse directions, x and z , respectively;

h = averaged water depth;

m_x, m_z = metric coefficients in x and z directions;

D_L, D_x = dispersion coefficient in longitudinal direction;

D_z = dispersion in transverse direction;

\dot{S}, \dot{E} = deposition and erosion rates.

Table 2.5: Convection-diffusion equations used by different models

2.2.2 Overview of present models

In the past decades, many numerical models for the simulation of sediment transport in river channels have been developed. Some well-known models are given in the Table 2.6

Author	Model	Year	Load	Problem						Dimension
				changes in bed level	local scour	width variation	bend effect	Conso- lidation	pollution	
U.S. Army Corp of Engineers	HEC-6	1977 1990	Total (nonu.)	✓						1 d
Chang & Hill	FLUVIAL-11	1976 1982	Bed (nonu.)	✓	✓	✓	✓			1 d
Holly et al.	BRALLUVIAL CHARIMA	1985 1990	Bed (nonu.)	✓						1 d
Niekerk	MIDAS	1992	Bed & Susp. (nonu.)	✓						1 d
Yotsukura & Sayre		1976	Susp. (u.)	✓						2 d orthog. c.
Zegler et al.	SEDZL	1986	Bed & Susp. (nonu.)	✓				✓		2 d
Molinas & Yang	GASTARS	1986	Total (nonu.)	✓	✓	✓	✓			stream tube
Lee et al.	UGASTARS	1997	Bed & Susp. (nonu.)	✓						quasi 2d orthog. c.
Luk & Lau	MABOCOST	1987	Dye						✓	quasi 2d orthog. c. *
Lau		1990	Dye						✓	quasi 2d orthog. c.
Alavian		1987	Dye						✓	quasi 2d orthog. c.

Susp.

Suspended

u.

Uniform sediments

nonu.

Non-uniform sediment mixtures

orthog. c.

Using an orthogonal curvilinear coordinate system

*

Variable length element

Table 2.6: Selected existing models

One-dimensional models The HEC-6 model was developed by the U.S. Army Corps of Engineers in 1977, and refined in 1990 [146, 150]. It includes a steady-state hydrodynamic model and a transport model for total sediment load. The finite difference method with a 6-point iterative finite difference scheme is used to solve the sediment continuity equations. Nonuniform sediment properties and armoring effects in sediment transport processes are

taken into account. A wide gradation of sediment grain sizes from clay to gravel are included. For sediment routing it provides three transport relations to be selected.

FLUVIAL model was developed for water and sediment routing by Chang and Hill (1976 1977) [22, 23] and Chang (1982, 1987) [20, 21]. The model includes river bed sedimentation and erosion, width variation, and changes caused by the curvature effect. The last two terms are closely connected with changes in river morphology because of an interrelation between changes in channel width and channel-bed profile. The concept of minimum stream power is used to determine river width changes. After the banks are adjusted the remaining change in area is distributed to the river bed. For an aggregating section deposition is assumed to build up the bed in a horizontal layer. For a degrading section, the change is assigned in proportion to the effective tractive force, $\tau - \tau_c$. The water routing is assumed to be uncoupled from the sediment process. The FDM is used as computational method.

The models IALLUVIAL (1982) [61], CARICAR (1989) [116] and CHARIMA (1990) [53] were developed by Karim, Rahuel, Holly et al. at the institute of Hydraulic Engineering Iowa in the last twenty years. These models describe the bed evolution of branched and looped channel systems. A Preismann's finite difference approximation was used in the solution of the sediment transport equation. Armoring effects were considered in these models. In the model CARICAR, the concept of a mixing layer was used to treat non-uniform sediment mixtures and a hiding factor was introduced for bed-load transport. The flow and sediment transport equations are solved through a fully coupled, implicit finite difference scheme. It takes into account the interaction between flow hydrodynamics and sediment transport processes.

Another one-dimensional model was developed by van Niekerk, et. al. (1992) [152] to simulate river bed changes within a relative straight, non-bifurcating alluvial channel. The model includes density and size sorting of bed-load and suspended load for sediment mixtures. In the model the hydrodynamic model and the sediment transport model are uncoupled during each time step. Flow depth and velocities are determined from the gradually varied flow equation using the standard step method for backwater calculation. The transport of particles in suspension is modeled by a convection-dispersion sediment continuity equation, either explicitly solved by using the Rouse equation, or implicitly by using a finite-difference scheme. The vertical sediment distribution of the suspended load is computed in analogy to a parabolic distribution for momentum diffusion. A modified Bagnold formula [16, 33] was used for the determination of the bed load transport rate for each size-density fraction. The percentage of transport rate for each size-density fraction is calculated according to the efficient bottom shear stress, the difference of instantaneous bottom shear stress and critical shear stress.

One dimensional multiple strip model The one dimensional multiple strip model is an expansion of the one dimensional model. It is used for simulating water and sediment routing of a river channel with compound cross sections. Traditionally, the main channel and the flood plains were treated together as a single composite channel in computing backwater profiles of a flood flow. Yen (1984, 1985) [179, 180] developed a new quasi-one-dimensional backwater computation method that treated the main channel and the flood plain separately and considered lateral mass exchange, turbulent shear stress at the interface between the main channel and the flood plains and different bed roughness across the channel. His calculations showed that if the ratio of the flow depth in the flood plain and the main channel was smaller than one-half, the backwater profiles calculated by his new method differed from those generated using traditional methods. This difference was noticeable when the difference in bed roughness between the main channel and the flood plains was large and the width of the main channel was smaller than that of the flood plain.

Based on Yen's method, Kohane (1991) [67] developed a one-dimensional multiple strip flow model, in which the main channel and flood plains were taken as different strips. The momentum exchange and turbulent shear stress on the interface between the main channel and the flood plain and the variety of bed roughness for each strip were taken into account. Based on Evers' hypothesis (1983) [34], Kohane developed the following formula of the turbulent shear stress at the interface, $\tau = -2 \cdot \kappa \cdot \rho \cdot (u_m - u_p) \cdot |u_m - u_p|$.

Stream tube models and quasi two-dimensional models Fischer (1967) [38] was the first to use the stream tube model to simulate two-dimensional dispersion problems in streams. It was subsequently refined by Chang (1971) [24] and Sayre and Yeh (1973) [126]. Sayre and Yeh introduced a natural coordinate system in which a simplified equation was used to align the longitudinal coordinate surface perfectly in the direction of the depth-averaged local velocity vectors so that they form stream tube surfaces. They eliminated the lateral velocity in the two-dimensional depth-averaged convection-dispersion equation to simplify the computation. Yotsukura and Sayre (1976) [184] further improved the model by introducing cumulative discharge and metric coefficients. They proved that the surface corresponding to the constant cumulative discharge was tangential to the local velocity vector and thus acts as a stream tube surface. The significant feature of the cumulative discharge method is that it shifts the problem of calculating the transverse velocity from the convection-dispersion equation onto the coordinate system, whose configuration is constrained by the requirement that the water continuity equation is to be satisfied. This model was successfully used to simulate the solute dispersion in natural rivers.

GSTARS, Generalized Stream Tube model for Alluvial River Simulation, was developed

by Molinas and Yang (1986) [91] for solving river engineering problems. It takes into account the bed-load transport of nonuniform sediment mixtures. In the calculation of fractional erosion the formulae of total load for uniform sediment [1, 32, 176, 178] were used first to determine the erosion rate for each size fraction. Then the erosion rate of size fraction n is determined by multiplying this determined erosion rate of size fraction n and the availability of that size fraction in the bed material.

GSTARS can be used to simulate the complicated response of a river channel in terms of width and depth adjustment processes. It can also describe different types of channel development which could happen during the morphological adaptation process of a river channel.

GSTARS has been successful in simulating and predicting local scours as well as deposition across and along natural rivers with movable beds and fixed widths. For example, it was applied in the study on the Mississippi River Lock and the study on the local scour along the Willow Creek Dam unlined emergency spillway. The computation results demonstrated that GSTARS was able to simulate complicated morphological processes of natural rivers and might have the potential to simulate the process of river meandering.

GSTARS treated the total load as if it was an equilibrium transport conditions. In reality suspended sediment transport is not an equilibrium sediment transport process. Lee et al. [76] modified the model of GSTARS by considering bed-load and suspended load separately, creating USTARS. For entrainment and deposition of suspended load the expressions of van Rijn [154] and Holly and Rahuel [53] were used. USTARS uses the same method as GSTARS to determine the fractional entrainment. The convection-dispersion equation of suspended sediment transport was solved by FVM and the split operator approach. The equation is separated into four portions: convection-step, longitudinal dispersion-step, transverse dispersion-step and reaction-step. They were solved subsequently in one time step.

MABOCOST is a quasi-two-dimensional numerical model developed by Luk and Lau in 1987 [83]. It describes mixing in natural sinuous streams with non-uniform cross sections and velocity distributions and simulates localized sources or sinks due to chemical and biological reactions.

In order to eliminate longitudinal numerical dispersion completely, variable-length elements (developed by Beltaos [11]) were used in solving the sediment convection-dispersion equation. These elements were arranged in the parallel stream tubes. The length of each element is always equal to the product of the local velocity and the time step as to satisfy the Courant criterion, $\frac{u\Delta t}{\Delta x} = 1$.

Two- and three-dimensional models (horizontally and vertically) To predict small scale river bed changes, such as river bed changes near hydraulic structures, local scours at bridge crossing, scour and fill in curved channel reaches, two-dimensional or even three-dimensional models are required. With the advancement in computer technology, many two-dimensional models have been developed and have been widely used in the study of sediment transport processes, such as reservoir sedimentation, river morphological changes, the distribution of deposition and erosion [155, 185, 186], and in estuaries, bays and river mouths [72, 162, 163].

The two-dimensional sediment transport model, SEDZL, developed by Ziegler and Lick (1986) [186] simulates reservoir deposition. To improve accuracy an orthogonal curvilinear coordinate system, transformed from Cartesian coordinates, is adopted in the model. SEDZL considers the effect of flocculation and consolidation for mixing sediment, cohesive fine sediment and non-cohesive coarser sediment, in sedimentation and erosion processes.

In order to consider the effect of grain size variation, particles are classified based on their size fraction as either cohesive sediments and non-cohesive sediments. The expressions of Gailani et al. (1991) [42] and van Rijn [154] are used to determine the entrainment for these two size fractions, respectively. The percentages of bed material and entrainment for each size fraction are assumed as to be the same. The bed is vertically discretized into 7 layers to account for the fact that bed consolidation and compaction increases with depth [104, 148] within 7 days after deposition [148]. Each layer is composed of the deposition in one day. When the time after deposition of the layer exceeds 7 days, it is treated as the 7 days.

The model of SEDZL was used to simulate fine-grained, cohesive sediment transport in Watt Bar Reservoir, on the Fox and Pawtuxet Rivers [186, 187, 188]. The results proved that this model realistically predicts overall patterns of erosion and deposition throughout the reservoir.

In order to investigate the effect of the turbulent shear stress on the interface between the main channel and the flood plains, many two- and three-dimensional $\kappa - \epsilon$ models have been developed [25, 81, 102, 99, 172]. These models can simulate secondary flow and predict velocity fields and eddy diffusion.

A three-dimensional numerical model of solute transport in compound channel flow has been developed by Lin and Shiono (1995) [81]. The numerical model used linear and nonlinear $k - \epsilon$ models to evaluate turbulent parameters and used the simpler method of Patankar and Spalding (1972) [110] to solve the differential equations. According to the model, the transport behavior near the interface between the main channel and the flood plains showed that the secondary flow was significant. Tracer concentrations simulated

using nonlinear $k-\epsilon$ model agree with the experimental results better than those obtained by the linear model. The bed shear stress obtained by the two models agrees well with the experimental value by Wood and Liang (1989) [172].

Naot et al. [99] developed a three-dimensional turbulent model to simulate the hydrodynamic behavior of compound channels, which was originally advanced with reference to flow in a rectangular open channel. The approach of a second-order Reynolds stress closure is used to simulate secondary flow in this model. The computation results showed that the turbulent model can describe the main features of more complex flows by including the effects of asymmetry, flood-plain roughness, and sidewall inclination in compound channels. Without considering the vortices in the vertical direction, the close agreement obtained between the prediction and the measurement shows that this vertical eddy does not affect the process of momentum transport between the main channel and the flood plains (Figure 2.11).

A stream tube model, a quasi-two dimensional model and two-dimension model can be used for describing two-dimensional suspended sediment transport processes and pollutant dispersion in rivers (Table 2.5 and Table 2.6). In the stream tube model the depth-averaged transverse velocity is equal to zero. The sediment transport is considered only in a single stream tube and the dispersion between the neighboring stream tubes is ignored (Table 2.5 (c)). In a straight channel with a uniform flow the assumption and approximation are acceptable. However, for a river reach with secondary flow, caused by bend effects or local geometric changes, the application of the stream tube model is limited. A quasi two-dimensional model provides an improvement on the stream tube model by considering the transverse particle dispersion in the governing equation (Table 2.5 (f)).

The present work will attempt to improve a quasi-two-dimensional model based on the above considerations. Quasi-two-dimensional models are used not only for the ease of numerical computation, low cost, time and computer requirements, but also for their applicability in engineering practice. Two-dimensional horizontal models are often used for solving local problems. The simulation of river sediment transport is based on a long and narrow domain, thus, a two-dimensional model is not suitable for this case. In addition, the accuracy of computation by using quasi two-dimensional is acceptable for engineering purposes.

Chapter 3

Numerical models

In this chapter numerical models for simulating flow and suspended sediment transport processes in rivers are developed. The concept of stream tubes is used for the flow calculation. Based on this concept a quasi two dimensional flow field and a natural orthogonal curvilinear coordinates will be obtained. With this method the numerical difficulties associated with two dimensional flow models, such as numerical diffusion and instability, can be avoided. The suitability and applicability of the stream tube flow model to rivers is studied, especially for a river with compound flow cross sections or with groynes as bank protection. In order to describe the sediment dispersion in the interaction zone between the main channel and the flood plains a formula will be derived to calculate the dispersion coefficient, which is tested using flume data of James (Chapter 4 section 1).

Suspended sediment transport models are developed for uniform sediments and nonuniform sediment mixtures, respectively. The transport model for uniform sediments is relatively simple and practical. It can be used to make rough predictions in engineering practice. However, suspended load material and river bed material mostly consist of nonuniform sediments. Because of selective transport the grain-size distributions of suspended sediment load and bed material on river bed surfaces gradually change and sediment gradation varies continuously along the river course (Figure 3.11). The average grain size distribution in bed material is finer downstream than upstream. Selective erosion influences the sediment entrainment and the river morphology. In order to describe the effects of the selective transport and the downstream fining on the sediment transport processes, a new approach for evaluating the grain size distribution of entrainment is derived using a probabilistic approach.

Equations for the simulation of suspended sediment transport usually consist of momentum and continuity equations of flow, the convection-dispersion equation of suspended sediment transport and the continuity equation for river bed changes. These equations are coupled to each other and therefore must be solved simultaneously. However, for many practical applications, some useful simplifications can be made in order to grasp the essential trends of river movement and avoid involving some nonessential and complicated calculations. Since the sediment movement and morphological changes are slow compared with the time scale of flow hydraulics, the calculations of flow and sediment transport can be decoupled. In this case, sediment transport barely affects the behavior of the flow.

Flow parameters, such as velocity and water depth, need to be recalculated in much larger time steps.

The stream tube flow model and the transport model for uniform sediments will be calibrated using field data on the River Neckar at the Lauffen Reservoir from 1973 to 1994, a period of 22 years. The calibrated model is then adopted to predict the changes in river bed elevation over a 50-year period, from 1995 to 2045. The field data will be also used to test the capability of the nonuniform sediment transport model to describe the effect of selective transport (Chapter 4 section 2). The transport model for nonuniform sediment mixtures was tested using data from the physical model of Samaga and Tsinghua University [125, 149] (Chapter 4 section 1).

3.1 Stream tube model

The stream tube model is often used to simulate rivers that consist of single sections. However, natural rivers usually have compound sections with a main channel and flood plains. Flow structures are much more complicated in river channels with compound sections or groynes near banks than in simple compactive channels. It has been verified that a turbulent shear stress exists in the interaction zone between the main channel and the flood plains. This turbulent shear stress plays an important role in mass, momentum and energy exchange between the fast flow in the main channel and the slow flow over the flood plains.

In this section, a modified stream tube flow model is introduced to calculate flow parameters for rivers with compound sections. The use of computer models to examine flow parameters is much more convenient in terms of time and expense than the use of physical models. The calculated results will be used for simulating the sediment transport processes.

The mass exchange occurs between the main channel and the dead water zone in a river reach with the groynes and is similar to what happens at the interface between the main channel and flood plains. The mass exchange between the stream and dead water zones is considered in the flow model.

3.1.1 Model concept

A stream tube is bounded by two streamlines. A streamline is a line along which the velocity vectors are tangent. For a two-dimensional flow, the expression for a streamline

is

$$\frac{dx}{u} = \frac{dz}{v} \quad (3.1.1)$$

where u and v denote the depth averaged velocity components in the longitudinal and lateral directions, x and z , respectively.

Because streamlines form the boundaries of stream tubes and flow velocities are always tangents to streamlines, no flow can cross the boundaries of a stream tube. From the potential flow theory, we have the expressions:

$$d\psi = v dx - u dy = \frac{\partial\psi}{\partial x} dx + \frac{\partial\psi}{\partial y} dy \quad (3.1.2)$$

$$u = -\frac{\partial\psi}{\partial y}, \quad v = \frac{\partial\psi}{\partial x} \quad (3.1.3)$$

where ψ is the stream function. The velocity components can be determined from eq. 3.1.3 when the value and the location of ψ are known. From the condition of flow continuity, the following equations can be obtained

$$\frac{\partial u}{\partial x} + \frac{\partial v}{\partial y} = 0, \quad \nabla^2 \psi = 0. \quad (3.1.4)$$

The discharge between two streamlines or within a stream tube, Δq , can be described as:

$$\Delta q = \Delta\psi = \psi_1 - \psi_2. \quad (3.1.5)$$

Since river flow is not a potential flow, the concept of stream tubes differs from one defined by the potential flow theory. However, it still uses the assumptions that there is no flow across boundaries of the stream tube into its neighboring stream tubes and that the depth averaged flow velocities are parallel to the stream lines.

According to this stream tube concept, a river channel can be divided into several stream tubes along the river course. The boundary surfaces of stream tubes consist of the four surfaces: the water surface, the river bed surface and two vertical fictitious interfaces. The hydraulic variables of each stream tube can be determined by a flow momentum or energy equation with specific exchange terms.

In the stream tube flow model, the location of a stream tube is determined using:

- (1) A one-dimensional flow model used for calculating a water surface elevation. In the model each cross section is divided into an equal number of subsections. Strips are constructed by linking these subsections from upstream to downstream.
- (2) The total discharge can be equally assigned to each strip by adjusting the boundary surface of the strips. Thus, the boundary surfaces of the strips are a property of the surface of the stream tube and the strips can be then taken as stream tubes.

Locations and sizes of the stream tubes are determined by the river geometry, the total discharge and its transverse distribution. A quasi two-dimensional flow field with fixed as well as movable boundaries can be approximated with total discharge changes in the presented stream tube model. The detailed calculation procedure is described in the section 3.1.4.

3.1.2 Application of the stream tube model

Compound flow cross sections

The cross-sections of a river can be classified as either single sections or compound sections, with each section having different roughness and flow velocities. Typical forms of some river cross-sections are shown in Figure 3.1.

If gradually varying flow occurs in a river reach with prismatic sections, the stream lines are parallel to each other and there is no lateral flow through the stream tubes. The calculation using the stream tube method yields an excellent approximation of such a flow structure in a river reach.

In a river reach with single sections and with negligible small secondary flow effects or in a river reach with small curvature, the flow runs nearly parallel to the boundary of the river. In these case there may exist only minor lateral flow through the fictitious boundaries of the calculated stream tubes. Therefore, the hydraulic parameters obtained by the stream tube model are adequate. However, in a river reach with great curvature flow calculations by the stream tube flow model can only approximately reflect the real flow condition because of the secondary flow.

When overbank flow occurs in a river channel, a large difference in velocities exists within the deeper main channel and the shallower flood plains (Figure 3.2). This produces strong interactions and a large turbulent shear layer which results in secondary currents along the interface between the main channel and the flood plains. In the interaction zone, there

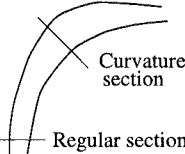
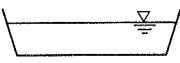

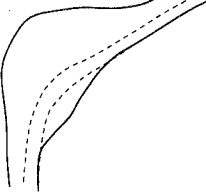
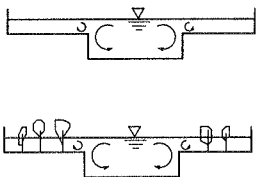
Flow structure		Comments
Single section 	Regular section 	Longitudinal deposition and erosion
	Curvature section 	Secondary flow Deposition near the inner river bank Erosion near the outer river bank
Compound section 		Two opposite large eddies in the interaction zone Dispersion and convection between the main channel and the flood plain Different river bed roughness for the main channel and the flood plains Large deposition on the flood plains during flood events

Figure 3.1: Open-channel flow

exist longitudinal momentum transfers from the main channel to the flood plain resulting in a decrease of the velocity in the main channel and an increase of that over the flood plains. The stream tube model can also be used to describe an overbank flow. In this case, a stream tube may include (Figure 3.3): a part of the main channel; a flood plain; a part of the main channel and a flood plain, including the interaction zone.

Configuration (a) can be thought of the same as the case of simple section.

For Configuration (b), the results of the stream tube model can simulate the real flow situation and the exchanges of mass and momentum between the main channel and the flood plains can be completely described.

Configuration (c) is quite common. Stream tube boundaries are unlikely to coincide with the interface between the main channel and the flood plain because of limitations inherent

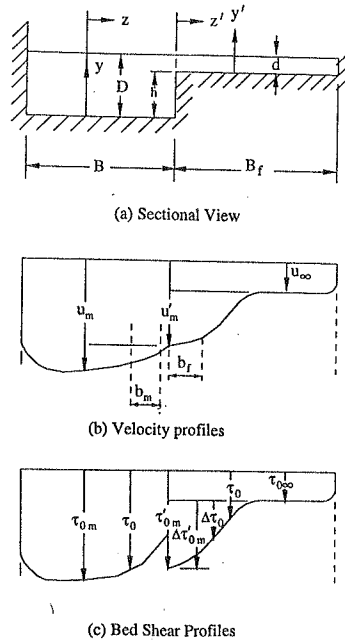


Figure 3.2: Compound channel flow configuration. After Rajaratnam and Ahmadi (1981) [118]

in dividing a river channel into a number of stream tubes. This Configuration differs from (a) and (b) in several ways:

- (1) Secondary currents at the interface of the main channel and the flood plain appear within one stream tube;
- (2) Exchange of mass and momentum are within one stream tube, the exchange and its influence does not appear explicitly in the flow calculation.
- (3) The calculated flow directions for the stream tube may deviate from that actually occurring.

Many previous stream tube models did not consider configuration (c), even though some of them were used to simulate sudden transverse expanding or secondary flow.

In order to describe the flow condition for configuration (c), two methods introduced in the model: one partially and the other wholly reflect the interaction and exchange of mass

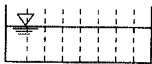
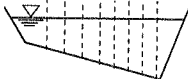
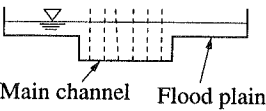

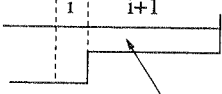
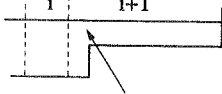
Section	Stream tube distribution	
Single section		
1. Prismatic section		
2. Curvature section		
Compound section		a.  Stream tube in the main channel
		b.  Stream tube including a flood plain
		c.  Stream tube including a part of the main channel and the flood plain

Figure 3.3: Stream tube distribution

and momentum at/near the interface between the main channel and the flood plains.

The effect of interaction between the main channel and the flood plain flow is greatest at the interface. It decreases gradually with the distance from the interface to the main channel and the flood plain. The partial interaction can be included in the calculation by determining a proportion of the interaction at the boundary between this stream tube and its neighboring one.

To reflect the interaction and exchange of mass and momentum, it is necessary for the interface to be a boundary of two neighboring calculating elements. This can be done by dividing this stream tube into two strips. One only includes the flood plain, and the other

contains only part of the main channel.

To describe the interaction and the exchange of mass and momentum, Evers (1983) [34] suggested the following equation for the diffusion coefficient and the shear stress of turbulent fluid, τ_{zx} , in the interaction zone:

$$\varepsilon = 2 \cdot \kappa \cdot (u_m - u_p) \cdot B, \quad (3.1.6)$$

$$\tau_{zxT} = \rho \varepsilon \frac{\Delta u}{\Delta z} = \rho \varepsilon \frac{\Delta u}{B} \quad (3.1.7)$$

where κ is a coefficient, u_m and u_p are flow velocities in the main channel and the flood plains, respectively and B is the width of the interaction zone. For practical application, Evers suggested κ equal to 0.01, while Kohane proposed κ to be 0.02.

In the eq. 3.1.6 B is defined as a mixing length and is given as an order of magnitude. The mixing length is relevant to the geometric parameters of compound sections. These parameters include the differences in elevation and the width between the main channel and the flood plain [2, 34, 118]. Considering that the widths of the main channel and the flood plain are large, the difference between the both widths does not have a large influence on the generation of the secondary flow. Consequently, the difference in bed elevation between the stream and the flood plain is the parameter used to describe the mixing length, expressed by the difference in water depths in the main channel and on the flood plain. According to experimental results [118], the relationship between the mixing length and the bed elevation difference is

$$B = 6 (h_m - h_p). \quad (3.1.8)$$

Thus, the dispersion coefficient due to differential convection in the interaction zone can be derived as:

$$\varepsilon_{mp} = \alpha (u_m - u_p) (h_m - h_p) \quad (3.1.9)$$

where α is taken as a coefficient to be calibrated, [171] suggested that $\alpha = 0.12 - 0.24$.

The total transverse diffusion at the interface of the main channel and the flood plain contains contributions of turbulent diffusion caused by bottom shear and dispersion due to differential convection. This can be expressed by

$$\varepsilon_{mpT} = \varepsilon_t + \varepsilon_{mp}. \quad (3.1.10)$$

From Figure 2.12 one can see that the maximum value of ε_{mp} occurs at the interface between the main channel and the flood plain, and that it is much larger than the pure transverse turbulent diffusion coefficient ε_t . At the interface, ε_{mp} increases with increasing in the ratio of the height of the flood plain and water depth on it. It decreases exponentially with increasing distance from the interface. The exponent should be mainly related to the geometric parameter of the compound cross section. Hence, the exponential function is assumed as:

$$\exp \left[-\frac{z (h_m - h_p)}{a h_p} \right] \quad (3.1.11)$$

where a is a coefficient and z is the distance from the interface to the calculated position in the main channel. Thus, the diffusion coefficient in the interaction zone can be written as:

$$\varepsilon_{mpz} = \alpha \cdot |u_m - u_p| \cdot |h_m - h_p| \exp \left[-\frac{z (h_m - h_p)}{a h_p} \right]. \quad (3.1.12)$$

The total transverse dispersion at the interaction zone contains contributions of turbulent diffusion and dispersion due to differential convection. It can be given by

$$\varepsilon_{mpzT} = \varepsilon_t + \varepsilon_{mpz}. \quad (3.1.13)$$

For suspended sediment diffusion, the diffusion coefficient in the interaction zone can be obtained using the turbulent-Schmidt number and the coefficient ε_{mpzT} :

$$\varepsilon_{sT} = \frac{\varepsilon_{mpzT}}{\sigma_t}. \quad (3.1.14)$$

$$\varepsilon_{sT} = \varepsilon_s + \varepsilon_{smpz}. \quad (3.1.15)$$

where σ_t is the turbulent-Schmidt number, $\sigma_t = 1$. In the interaction zone the particle diffusion coefficient is:

$$\varepsilon_{sT} = \varepsilon_s + \varepsilon_{smpz} = \varepsilon_s + (\alpha \cdot |u_m - u_p| \cdot |h_m - h_p|) \exp \left[-\frac{z (h_m - h_p)}{a h_p} \right] \quad (3.1.16)$$

At the interface the particle diffusion coefficient varies as:

$$\varepsilon_{smpT} = \varepsilon_s + \alpha \cdot |u_m - u_p| \cdot |h_m - h_p| \quad (3.1.17)$$

Using eq. 3.1.12, the calculated value of turbulent shear stress, τ_{zx} , can be considered partially for a stream tube as composed of a part of the main channel and a part of the flood plain (configuration (c)). The influence of τ_{zx} on sediment dispersion at/near the interface between the main channel and the flood plains can be included in the calculation. In order to reflect the influence of the interaction on the transverse particle diffusion, it is necessary to divide the stream tube into two strips (using eq. 3.1.17), especially when calculating deposition on the flood plains.

Application to a river channel with dead water zones (with groyne)

Figure 3.4 shows a river reach with dead water basins caused by groynes, in which three typical flow states exist:

- (a) water surface is lower than the top of groynes;
- (b) bankfull discharge with submerged groynes;
- (c) overbank flow with submerged groynes and flood plains.

For configuration (a), the amount of mass and momentum exchanged depends mainly on the velocity gradient and the groyne spacing, L_b [166, 170]. When $L_b \leq 30 \cdot h_m$, a mixing layer is assumed as a streamline along the groyne heads [151]. Here, h_m is the water depth in the main channel. The line along the groyne heads may be treated as a fictitious river bank. There is a little exchange of mass and momentum in dispersion method between the main stream and the groyne field. If $L_b > 30 \cdot h_m$, the main flow will penetrate into the dead water zone. This increases the mass and momentum exchange. The penetration depth, B_g , increases with L_b .

On the basis of results of breakwater experiments, Lean and Weare (1979) [75] stated that a large eddy is generated on the downstream side of the breakwater and is separated from the main flow by an expanding region of turbulence. There exists a lateral momentum transfer between the stream and the eddy within the mixing zone. This lateral momentum transfer results from turbulence and secondary flow due to the curvature of the streamlines.

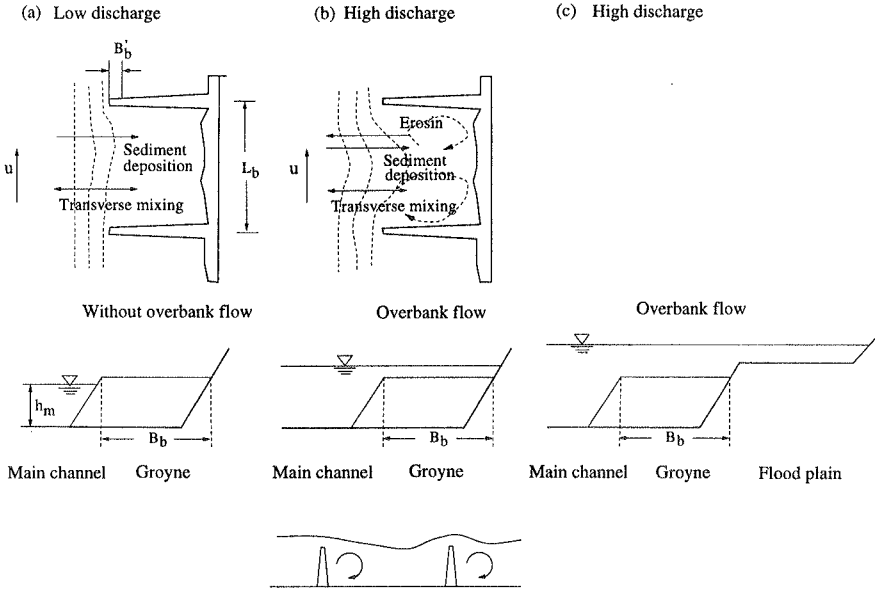


Figure 3.4: Mass exchange between the main stream and the groyne fields

The stream tube calculation is not difficult for configuration (a), under the assumption that B_g is small. The calculation domain consists of the main stream without the groyne fields, Figure 3.4 (a). The shear stress between the stream and dead water zones, τ_{xz} , is not considered in the flow calculation.

For configurations (b) and (c), the flow velocity in the groyne fields, u_{mb} , is smaller than one in the main stream, u_m . Spillage over the groynes results in strong mixing between flow in the main channel and water in groyne fields, Figure 3.4(b).

At the top of a groyne there is a point at which the flow separates. After this point a shear layer is generated and a large eddy exists behind the groyne. The mass exchange between the stream and groyne fields are caused not only by dispersion but also by convection.

When the water surface is over groynes, the stream tube nearest the shore includes a part of the main stream and the groyne field. When overbank flow occurs, the stream tube nearest the shore will consist of three parts: a part of the main stream, the groyne field and the flood plain. For these two configurations, the mass transfer coefficient is larger

than one in the case without submerged groynes, configuration (a). The particle lateral dispersion coefficient (eq. 3.1.16) is used to calculate the exchange of sediment between the main channel and the groyne field.

In order to determine hydraulic parameters in the groyne field, the following assumptions may be made:

- (1) The part of the stream involving the groyne is represented by a strip, whose width varies with the groyne length in the river direction;
- (2) The flow discharge in a section in the groyne field between two groynes is given by $Q_{B_{basin}} = Q_{Bi} + \frac{1}{2}qL$, $q_l = (Q_{Bi} - Q_{Bi+1})/L$ (the variables are defined in Figure 3.5);
- (3) The energy slope in the groyne field is approximately equal to that in the main stream.

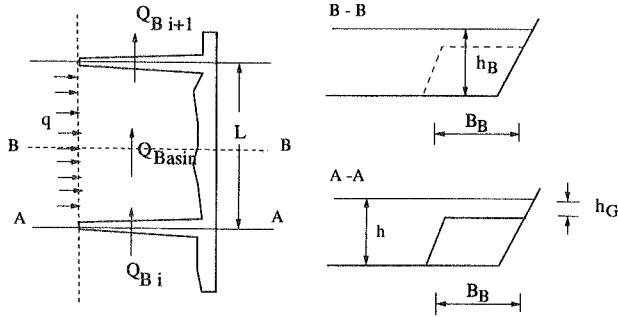


Figure 3.5: Definition of hydraulic variables

According to this assumption a reference bed roughness K_{stB} can be obtained:

$$k_{stB} = c_1 \cdot k_{st} \quad (3.1.18)$$

where c_1 is a coefficient related to $\left(\frac{B_B}{h}, \frac{h-h_B}{h}, \frac{L_B}{B_B}\right)$ and q , k_{st} is the roughness coefficient. If $h = h_B$, c_1 can be represented by

$$c_1 = \left(\frac{h-h_G}{h_B}\right)^{\frac{5}{3}} \left(\frac{B_B+h_B}{B_B+(h-h_G)}\right)^{\frac{2}{3}}.$$

When $B_B \gg h_B$ and $B_B \gg h - h_G$, c_1 is simplified as

$$c_1 \approx \left(\frac{h - h_G}{h_B} \right)^{\frac{5}{3}}. \quad (3.1.19)$$

The hydraulic parameters in the groyne field, such as velocity, u_B , can be estimated with the help of a reference bed roughness, K_{stB} .

The value of K_{stB} calculated according to the above assumption is different from the real roughness in the groyne field. The real roughness in the groyne field is smaller than that in the main channel. This is because its velocity is small and sediment deposited in the groyne field only contains soil or fine sand, which are carried by flow from upstream or are transferred from the suspended sediment of the main stream.

The energy loss is caused by turbulent eddies related to the groyne space, L_B , and the velocity gradient between the flow and dead water. The energy loss can be examined by increasing the bed roughness of the groyne field in the water surface calculation. Even though the decrease of a local water surface at the groyne cannot be described in detail, the influence of the turbulent eddy on energy loss can be considered to a certain extent.

The transfer coefficient for particles between the stream and the groyne field can be obtained according to the Schmidt number. It can be expressed by $\varepsilon_s = \frac{\varepsilon_t}{\sigma_t}$.

For configuration (a), the particles are transferred between the stream and the dead water zone due to turbulent diffusion and lateral differential convection. The particle transfer is considered by an additional term, Q^* , (Table 4.11) as a source term in the conservative equation of suspended sediment transport.

For configurations (b) and (c) the particle exchange also results from vertical differential convection and lateral differential convection. Sudden lateral and vertical expansion exist. In the calculation only the transfer due to lateral differential convection is considered. The transfer coefficient expressed by eq. 3.1.15 can be used. In eq. 3.1.15 h_p is replaced by h_G .

3.1.3 Governing equations in the flow calculation

For flow calculations in a river channel with a number of strips, the continuity and momentum equations are

$$\frac{dQ_T}{dx} = q_s, \quad (3.1.20)$$

$$\frac{d}{dx} \left(\frac{\beta Q_T^2}{A_T} \right) + g A_T \frac{dh}{dx} + g A_T J_T = 0. \quad (3.1.21)$$

where q_s is the lateral discharge. The total discharge and area of a flow are

$$Q_T = \sum_{i=1}^N Q_i, \quad A_T = \sum_{i=1}^N A_i$$

The energy slope is

$$J_T = \frac{Q_T |Q_T|}{K^2}. \quad (3.1.22)$$

The Boussinesq coefficient β caused by non-uniformity of the velocity profile is

$$\beta = \frac{\sum_{i=1}^N K_{st_i}^2 \cdot A_i \cdot R_{hy_i}^{\frac{4}{3}}}{K^2} \quad (3.1.23)$$

in which A_i and R_i are the area and the hydraulic radius for a strip, K_{st_i} is the roughness coefficient in the strip and K is the conveyance factor, represented by

$$K = \sum_{i=1}^N K_{st_i} \cdot A_i \cdot R_{hy_i}^{\frac{2}{3}}.$$

where the roughness coefficient, k_{st_i} , for i th section is represented by

$$\begin{aligned} k_{st_i} &= C && \text{(de Chezy),} \\ k_{st_i} &= k_{st} \cdot R_{hy}^{\frac{1}{6}} && \text{(Manning-Strickler),} \\ k_{st_i} &= \sqrt{\frac{8 \cdot g}{\lambda}} && \text{(Darcy-Weisbach),} \end{aligned} \quad (3.1.24)$$

The numerical solution of the equations above can be obtained using the Preismann's finite difference approximation. The flow equations in 3.1.20 and 3.1.21 are completed using a constant water surface elevation as the downstream boundary condition. It is assumed that the flow always remains subcritical, as is the case in most naturally occurring river systems. The detailed calculation procedure is given by Kohane (1991) [67]. The calculation method for stream tubes is given in the next section.

3.1.4 Stream tube computation

The stream tube computation is made by the flow modulus method. It is based on the assumption that each subsection in the considered cross-section has the same energy gradient which is equal to the total energy gradient for the whole cross-section. According to

eq. 3.1.22 the subsections with equal conveyance (flow modulus) have the same discharge. The conveyance is a function of the bed roughness and the geometric parameters of the cross section. The calculation of the locations of stream tubes can be accomplished by giving each subsection equal conveyance values while moving the boundaries of strips.

The procedure to calculate stream tubes is as follows (Figure 3.6):

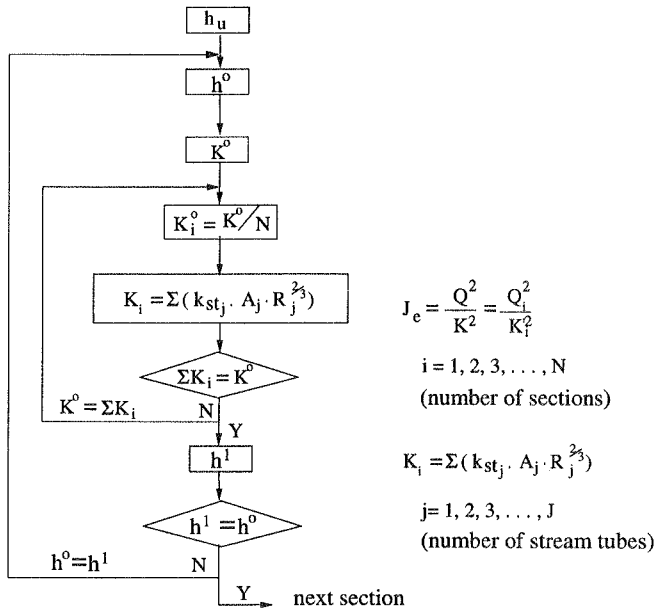


Figure 3.6: Flow chart showing the steps for calculation of stream tube locations

1. Divide each cross-section of a river channel into a constant number of strips.
2. Calculate the water surface by using the one dimensional flow model.
3. Determine the conveyance for each strip according to the given discharge distribution.
4. Make each strip meet with the given value of the conveyance by moving the boundaries of strips from the left bank to the right one.
5. Compare the value of conveyance of the last strip with the previous distributed value. If they are not equal, return to Step 3. This calculation is carried out section by section from downstream to upstream.

6. Calculate the water surface using the new location of each stream tube. If the difference between the calculated upstream water surface values in this new step and in old step 2 is smaller than a given value, finish the calculation, otherwise return to Step 3.

In principle, the total discharge can be distributed to stream tubes with equal or different sub-discharge values along the lateral direction defined at the first downstream cross-section.

3.2 Suspended sediment transport model for uniform sediments

In this section, a two dimensional depth averaged suspended sediment transport model using a natural orthogonal curvilinear coordinate system for river channels is developed. The semi-empirical formula describing the strong dispersion at the interface between the main channel and the flood plains derived in the last section is introduced in the model. The flow fields calculated by the stream tube flow model are used for simulation of sediment transport processes. A natural orthogonal curvilinear coordinate system is automatically built in flow calculation. Compared with a rectangular Cartesian coordinate system it is less complicated to deal with moving boundaries and simplifies the convection-dispersion equation because there is no lateral flow ($v=0$).

The discretized convection-dispersion equations of suspended sediment transport are solved by Finite-Volume Method which provides full mass conservation for each control volume.

3.2.1 Natural orthogonal curvilinear coordinate system

Generally speaking, in order to describe a two dimensional phenomena of solute or sediment transport in a river, the flow velocities in transverse and longitudinal directions should be known. However, the computation of a two dimensional flow field for a river is very complicated due to limitations of computation algorithms, computer techniques and difficult in calculation of moving wetted boundaries and energy losses which result from complicated river channel geometries and relatively narrow computation domains. A simplified method for calculating the flow field was suggested by Fischer (1966) [37], in which the transverse velocity was eliminated in the continuity and convection-dispersion equations. The main idea of this method is that the longitudinal coordinate can be chosen as closely as possible to the direction of the depth-averaged local velocity vectors so

that the longitudinal coordinates coincide with the boundaries of stream tubes. Later on, this method was improved by introducing the natural coordinate system for the much more restrictive case of steady state uniform flow in straight prismatic channels by Chang (1971) and Sayre and Yeh (1973) [24, 126] and by introducing the concept of accumulative discharge for a river channel with curved alignment and width variation by Yotsukura (1972, 1976) [183, 184].

In the present work, a modification of the Fischer method with a natural coordinate system is suggested to describe a river channel with curved alignment, variable width and compound cross-sections. The longitudinal coordinates are perfectly aligned along streamlines. The transverse coordinates are located in the cross-sections. These cross-sections are preferably selected at positions with major changes in width, lateral shifts in the location of a river and the positions having detailed measured information in order to obtain more accurate simulation results.

Metric coefficients In order to obtain a natural orthogonal curvilinear coordinate system, two important coefficients, m_x and m_y , are introduced. As shown in Figure 3.7, if the x axis of the coordinates is defined along the center of a river channel and the z axis is located at the first cross section upstream in the domain, the x axis does not always run parallel to the longitudinal coordinates due to the variation in width and the curvature in channel. Therefore, a difference occurs between measured distances along the x axis and along the longitudinal coordinates. A similar case is also found in the measured distances along the z axis and along the transverse coordinates.

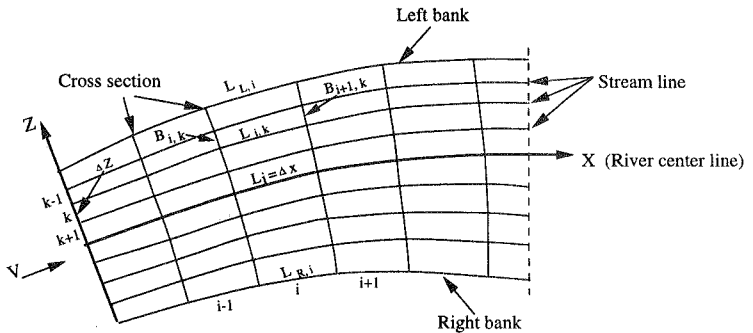


Figure 3.7: Definition of metric coefficients

To correct such differences, $L_{i,k}$ and $B_{i,k}$ is defined by the expressions:

$$L_{i,k} = \int_{x_i}^{x_{i+1}} m_x dx \quad \text{and} \quad B_{i,k} = \int_{z_k}^{z_{k+1}} m_z dz. \quad (3.2.25)$$

The average values of m_x and m_z in the distance of Δx and Δz can be simplified by:

$$\overline{m}_{x_{i,k}} \simeq \frac{L_{i,k}}{\Delta x} \quad \text{and} \quad \overline{m}_{z_{i,k}} \simeq \frac{B_{i,k}}{\Delta z} \quad (3.2.26)$$

where Δx and Δz are the distances along the axes x and z , respectively. $L_{i,k}$ is the distance between the k th and $(k-1)$ th cross-sections along the i th streamline. $B_{i,k}$ is the width of the i th stream tube at the k th cross-section. $B_{i,k}$ is already determined in the flow calculation and may be directly used in sediment transport calculations, i.e., $m_{z_{i,k}} = 1$. $B_{T,k}$ is the total water surface width of k th cross-section. $L_{L,k}$ and $L_{R,k}$ are the distance between the k th and the $(k-1)$ th cross-sections along the longitudinal coordinates which are coincided with the left and the right river banks. $L_{L,k}$ and $L_{R,k}$ are curved or straight lines. $L_{i,k}$ can be estimated with sufficient accuracy by interpolating between $L_{L,k}$ and $L_{R,k}$ as the expression:

$$L_{i,k} = L_{L,k} + \frac{1}{2} (L_{R,k} - L_{L,k}) \left[\frac{B_{i,k}}{B_{T,k}} + \frac{B_{i,k+1}}{B_{T,k+1}} \right]. \quad (3.2.27)$$

If the x axis is a circular arc with the radius of the curvature, r_c , and all of the longitudinal coordinates are circular cylinders concentric with the x axis, the metric coefficient is

$$m_{x_{i,k}} = 1 \pm \frac{z}{r_c}.$$

The sign of $\frac{z}{r_c}$ is positive for bends curving to the left looking downstream and negative curving to the right. It is clear that for a natural river the value of m_x may vary for the different specific status of river reaches. For the River Neckar from 125.2 to 135.7 km, the value of m_x varies between 0.5 and 1.7.

In some cases, where the streamline curvature is small and the width of the river does not vary greatly, the expressions $m_x=1$, and $m_z=1$ can be used as useful approximations. If $m_x=1$ and $m_z=1$ holds true everywhere, the coordinate system simplifies as a rectangular Cartesian system.

3.2.2 Governing equations for suspended sediment transport

Depth-averaged convection-dispersion equation

Taking into account the metric coefficient, m_x and m_z , an unsteady, two dimensional depth-averaged convection-dispersion equation for suspended sediment transport can be written in an orthogonal curved coordinate system as follows:

$$\begin{aligned} & \frac{\partial(m_x m_z h C)}{\partial t} + \frac{\partial(m_z h u C)}{\partial x} + \frac{\partial(m_x h v C)}{\partial z} \\ &= \frac{\partial}{\partial x} \left(\frac{m_z}{m_x} h D_x \frac{\partial C}{\partial x} \right) + \frac{\partial}{\partial z} \left(\frac{m_x}{m_z} h D_z \frac{\partial C}{\partial z} \right) + \dot{E} - \dot{S} \end{aligned} \quad (3.2.28)$$

where C denotes the depth-averaged local concentration, u and v are local depth-averaged velocities in longitudinal (streamline) and lateral directions, x and z , respectively, h is the average water depth, D_x and D_z are the dispersion coefficients in x and z directions, and \dot{S} and \dot{E} are deposition and erosion rates. For a river channel with moderate curvature and a gradually varying width, the expressions $m_x \simeq 1$ and $m_z \simeq 1$ can be used. The above equation can then be rewritten as follows:

$$\frac{\partial h C}{\partial t} + \frac{\partial u h C}{\partial x} + \frac{\partial v h C}{\partial z} = \frac{\partial}{\partial x} (h D_x \frac{\partial C}{\partial x}) + \frac{\partial}{\partial z} (h D_z \frac{\partial C}{\partial z}) + \dot{E} - \dot{S}. \quad (3.2.29)$$

It is evident that the equation in this case is the same as that in the general Cartesian coordinate system.

Considering a steady transport process, i.e., $\frac{\partial C}{\partial t} = 0$, the convection-dispersion equation can be represented by

$$\frac{\partial(m_z h u C)}{\partial x} + \frac{\partial(m_x h v C)}{\partial z} = \frac{\partial}{\partial x} \left(\frac{m_z}{m_x} h D_x \frac{\partial C}{\partial x} \right) + \frac{\partial}{\partial z} \left(\frac{m_x}{m_z} h D_z \frac{\partial C}{\partial z} \right) + \dot{E} - \dot{S}. \quad (3.2.30)$$

In the stream line coordinate system with $v = 0$, eq. 3.2.30 become:

$$\frac{\partial(m_z h u C)}{\partial x} = \frac{\partial}{\partial x} \left(\frac{m_z}{m_x} h D_x \frac{\partial C}{\partial x} \right) + \frac{\partial}{\partial z} \left(\frac{m_x}{m_z} h D_z \frac{\partial C}{\partial z} \right) + \dot{E} - \dot{S}. \quad (3.2.31)$$

Erosion rate

The expression (2.1.17) for the erosion rate is used in the model

$$\dot{E} = \begin{cases} M(\frac{\tau}{\tau_{c,E}} - 1) & \tau > \tau_{c,E} \\ 0 & \tau \leq \tau_{c,E} \end{cases}$$

where M is an erosion coefficient to be calibrated. The critical shear stress is calculated by the expression [154] (Figure 2.9)

$$\tau_{c,E} = (\rho_s - \rho)g dF_c^* \quad (3.2.32)$$

with

$$F_{rc}^* = f(D^*). \quad (3.2.33)$$

where $D^* = D_{50} \left[\frac{\rho_s - \rho}{\rho} \frac{g}{\nu^2} \right]$ is the particle parameter.

Sedimentation rate

The sedimentation rate is determined by (eq. 2.1.18)

$$\dot{S} = \begin{cases} w_s C_a (1 - \frac{\tau}{\tau_{c,S}}) & \tau < \tau_{c,S} \\ 0 & \tau \geq \tau_{c,S} \end{cases} \quad (3.2.34)$$

The critical shear stress $\tau_{c,S}$ calculated by the expression of 2.1.19. The values of C_a are given by Rouse's vertical distribution of suspended sediment (eq. 2.1.13).

Dispersion coefficients

The depth averaged longitudinal and transverse dispersion coefficients of suspended particles are given by

$$D_x = \beta_x u_* h \quad \text{and} \quad D_z = \beta_z u_* h \quad (3.2.35)$$

in which u_* and h are the bottom shear velocity and the water depth, β_x and β_z are coefficients. Considering the pure turbulent diffusion and vertical differential convection a value of $\beta_x=5.93$ is suggested by Elder [31].

β_z is equal to 0.23 in a straight channel without secondary currents according to Elder [31]. In a river reach with compound sections there exists particle exchange in the interaction zone between the main channel and the flood plains due to turbulent diffusion and differential convection. According to the eq. 3.1.15 the particle dispersion at the interface between the main channel and the flood plain is:

$$D_z = \varepsilon_{sT} = \beta u_{*mp} h + \alpha \cdot |u_m - u_p| \cdot |h_m - h_p|. \quad (3.2.36)$$

In the interaction zone, according to eq. 3.1.16, the particle dispersion coefficient varies with the distance from the interface:

$$D_z = \beta u_{*mp} h + \alpha \cdot |u_m - u_p| \cdot |h_m - h_p| \exp \left[-\frac{z}{a} \frac{(h_m - h_p)}{h_p} \right] \quad (3.2.37)$$

According to Rajaratnam and Ahmadi (1981) [118] (Figure 3.2), the values of u_{*mp} are experimentally given by

$$u_{*mp} = u_{*p} \left(1 + 0.24 \left(\frac{h_m}{h_p} - 1 \right) \right) \quad (3.2.38)$$

where $\tau_p = u_{*mp}^2 \rho$ is the undisturbed bottom shear stress on the flood plain ($\tau_p = \tau_{0\infty}$, see Figure 3.2).

Using eq. 3.2.36 and 3.2.37 the lateral exchange of sediments between the main channel and the flood plains can be determined. The deposition rate and deposition volume on the flood plain during the flood events can then be evaluated.

Bed elevation change

The calculation of river bed changes is based on the mass conservation equation. It is given by

$$dy = \frac{\dot{S} - \dot{E}}{\rho_p} dt \quad (3.2.39)$$

where ρ_p is the density of sediment.

The river bed elevation Y_b can be calculated by

$$Y_{bt+\Delta t} = Y_{bt} + \frac{\dot{S} - \dot{E}}{\rho_p} \Delta t. \quad (3.2.40)$$

This is a one layer, one grain size model which cannot account for the effect of consolidation of fine cohesive sediments and the non-uniformity of sediments. To simulate suspended sediment transport with the effect of consolidation of cohesive sediments a multiple-layer model is needed. In order to calculate the change of bed elevation at the Lauffen Reservoir in the River Neckar, where the bed material contains fine cohesive clay with strong consolidation and non-cohesive clay, sand and gravel, a simple two layer model is adopted, the details of which are given in Chapter 4.

3.2.3 Numerical method

Discretization of the equation system

In the present work, the Finite-Volume Method (FVM) is used as the numerical method to solve the convection-dispersion equation of the sediment transport. The Finite-Volume Method is based on the mass-balance over a finite number of control volumes.

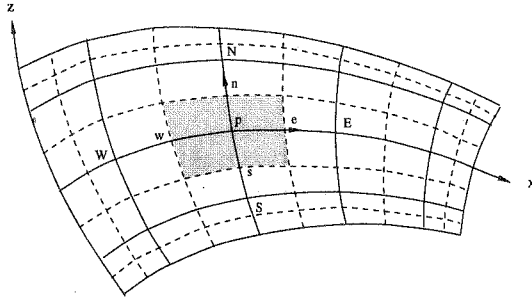


Figure 3.8: Control volume with the center point P

In the FVM, the dependent variable is placed at the center of the control volume, called a grid point P, which has the grid points N, S, E, W as its neighbors (Figure 3.8 and 3.9). The variation of the dependent variable between two grid points, for example E and P,

is assumed to have a linear distribution. Linear interpolation functions are used between the grid points. The dashed lines in Figure 3.8 show the faces of the control volume which is denoted by n, s, e, w.

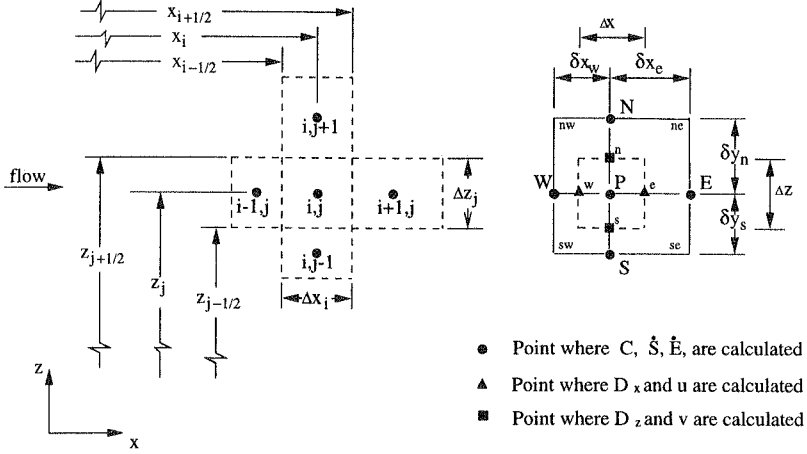


Figure 3.9: Schematic element and node arrangement used to evaluate the sediment concentration variables

If Eq. 3.2.30 is written in tensor notation, we have:

$$\text{div } J + S = 0 \quad (3.2.41)$$

with

$$J = \vec{v}hC - hD \nabla C \quad (3.2.42)$$

where J is the total flux of C through each of the four boundaries of the control volume related to point P, and S is the rate of sediment concentration generation per unit volume. The integration of the above equation yields:

$$\iiint_V \text{div } J dV + \iiint_V S dV = 0 \quad (3.2.43)$$

Applying the Gauss theorem to eq. 3.2.43 with the normal vector \vec{n} on the boundary of the calculation element (Figure 3.10), we obtain

$$\oint_{\Omega} (\vec{v} h C - h D \nabla C) \cdot \vec{n} d\Omega + \iiint_V S dV = 0. \quad (3.2.44)$$

where Ω is integration surface.

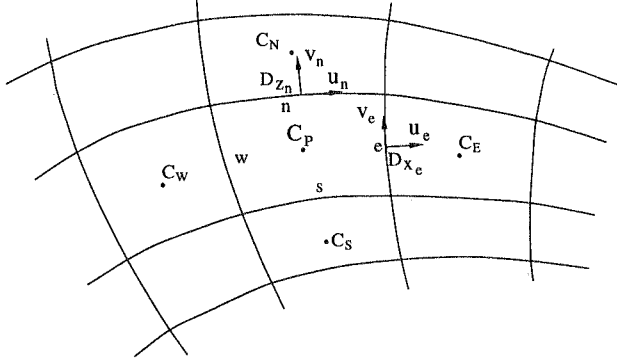


Figure 3.10: Schematic convection and diffusion terms

Before integrating eq.3.2.44, we defined the expressions as:

$$F_e = (hu)_e \Delta z, \quad D_e = (hD_x)_e \frac{\Delta z}{\delta_{xe}}. \quad (3.2.45)$$

in which F_e and D_e are the mass flow rates due to convection and dispersion through the east face of a control volume, respectively (Figure 3.10). Similarly, we can write for the west, north and south face of the control volume.

In order to obtain the steady solution, the dispersion term is represented by the central-difference scheme and the convection term is represented by the upwind scheme in deriving the discretization equation. The upwind scheme assumes that the value of the dependent variable at the interface is equal to that at the grid point on the upwind side of the face. Therefore, for the convection term at the east interface of the control volume, we have

$$F_e C_e = [F_e, 0] C_P - [-F_e, 0] C_E \quad (3.2.46)$$

where $[]$ denotes the largest of the quantities contained within.

In an orthogonal curvilinear coordinate system, the discretization equation obtained by integration of Eq. 3.2.44 can be written as:

$$\{[F_e, 0] + [-F_w, 0] + [F_n, 0] + [-F_n, 0]\} C_P - \quad (3.2.47)$$

$$[-F_e, 0] C_e - [F_w, 0] C_w - [-F_n, 0] C_n + [F_s, 0] C_s$$

$$= -(D_e + D_w + D_n + D_s)C_p + D_e C_e + D_w C_w + D_n C_n + D_s C_s + (S_c + S_p)\Delta x \Delta z$$

where the source term S is linearized by $S = S_c + S_p C_p$. S_p must be negative so that instabilities and physically unrealistic solutions do not occur [109].

To arrange the equation more compactly, the equation are rewritten in the form:

$$a_p C_p = a_e C_e + a_w C_w + a_n C_n + a_s C_s + b, \quad (3.2.48)$$

where

$$a_e = D_e + [-F_e, 0], \quad a_w = D_w + [F_w, 0],$$

$$a_n = D_n + [-F_n, 0], \quad a_s = D_s + [F_s, 0],$$

$$a_p = D_e + D_w + D_n + D_s + [F_e, 0] + [-F_w, 0] + [F_n, 0] + [-F_s, 0] - S_p \Delta x \Delta z,$$

$$b = S_c \Delta x \Delta z.$$

Patankar (1980) [109] suggested several discretization schemes, in which the ratio of convection to diffusion is represented by the Peclet number,

$$P \equiv \frac{uL}{D}.$$

The Peclet number, P , shows the ratio of the intensities of the convection and the diffusion processes. A high value of P means that the convection process dominates over the diffusion process; and a low value shows the diffusion dominates over the convection.

The hybrid scheme of Spalding (1972) [136] is a combination of the upwind scheme and central difference scheme, separately for approximating dispersion and convection terms. For convection terms, the upwind scheme is used when convection dominates ($Pe > 2$). Compared to the convection, diffusion is negligible and is set to be equal to zero. If $Pe < 2$, the central difference scheme is used.

The power scheme of Patankar (1979) [108] gives a better approximation of the exact solution. In the power scheme, the upwind scheme is used only for $P_e > 10$. If $P_e < 10$, a power-law expression is used to generate the discretization equation. This scheme is used in the present work.

Patankar introduced a dimensionless coefficient, which is a function of the Peclet number, $A(|P|)$. The coefficients, $A(|P|)$, for different schemes are given in the follows.

Scheme	$A(P)$
central-difference scheme	$1 - 0.5 P $
upwind scheme	1
Hybrid scheme	$[0, 1 - 0.5 P]$
Power-law scheme	$[0, (1 - 0.1 P)^5]$
Exponential scheme	$ P / [\exp(P) - 1]$

Using the coefficient $A(|P|)$, the coefficient of discretization equation, for example at the east boundary of the control volume, can be rewritten as

$$a_e = D_e A(|P_e|) + [[-F_e, 0]] = a_E + F_e.$$

Thus, the two dimensional discretization equation can be given as follows:

$$A_P C_P = \sum_{nb} a_{nb} C_{nb} + b, \quad nb = W, E, S, N \quad (3.2.49)$$

where

$$a_E = D_e A(|P_e|) + [[-F_e, 0]], \quad (3.2.50)$$

$$a_W = D_w A(|P_w|) + [[F_w, 0]], \quad (3.2.51)$$

$$a_N = D_n A(|P_n|) + [[-F_n, 0]], \quad (3.2.52)$$

$$a_S = D_s A(|P_s|) + [[F_s, 0]], \quad (3.2.53)$$

$$A_P = \sum_{nb} A_{nb} - S_P \Delta x \Delta y, \quad (3.2.54)$$

$$b = S_c \Delta x \Delta y. \quad (3.2.55)$$

Boundary conditions

Upstream boundary For suspended sediment transport simulation, the upstream boundary conditions are suspended sediment inflow and discharge.

For a two dimensional problem in the horizontal plain, it is necessary to have the transverse distribution of concentrations. This nonuniform lateral distribution of suspended sediment concentrations may exist downstream of the confluence of two rivers with different sediment concentrations or downstream of a hydro project with a dam, navigation lock or power plant.

Downstream boundary The boundary condition downstream has almost no influence on the upstream domain. For large Peclet numbers, convection dominates the sediment transport process. Hence, some simple boundary conditions can be introduced into the numerical solution scheme. The dependent variation at the boundary can be determined by linear extrapolation

$$C_D = \frac{3}{2}C_i - \frac{1}{2}C_{i-1},$$

or by quadratic interpolation

$$C_D = \frac{3}{8}C_{i+1} + \frac{3}{4}C_i - \frac{1}{8}C_{i-1}.$$

Assuming that $C_{i+1} = C_i$, we obtain

$$C_D = \frac{9}{8}C_i - \frac{18}{C_{i-1}}.$$

A zero concentration gradient can also be used as the downstream boundary condition. It is given by

$$C_D = C_i \quad \text{or} \quad \frac{\partial C_B}{\partial x} = 0$$

At the bank boundary At the bank boundary, there is no inflow or outflow of suspended sediment and no dispersion of sediment.

Solving the algebraic equation system

Sediment transport in a river is an unsteady problem. Here a quasi-steady solution is used. The velocity of the river bed change due to sediment transport is very low and

has only a small influence on water depth and flow velocity. Each individual time step of an unsteady problem is treated as a steady one, which eliminates the stability problem of computation. The accuracy of results given by quasi-steady solution is acceptable for engineering practice.

An algebraic equation system is obtained through the discretization of the convection-dispersion equation of suspended sediment transport. The difference scheme is the five-point formula, which has a truncation error of $O[(\Delta x)^2, (\Delta z)^2]$. As the dependent variable of the grid point is related to its four neighbors, we have a five-diagonal matrix of coefficients.

The coefficients of the algebraic equations are functions of the dependent variable. Hence, the iterative method is used. The algebraic equation system is solved by the elimination method in an overall iterative procedure. The iterative procedure is finished when the convergence criterion is satisfied. The convergence criterion is that the normalized sum of the absolute residual over all grid points or the largest value of $|R_n|$ is less than a given small number ε . The residual at a grid point after n iterations is represented as follows

$$R_{cp}^n = \left(\sum_{nb} A_{nb} C_{nb} + b - A_P C_P \right)^2. \quad (3.2.56)$$

The convergence criterion can then be given by

$$\left(\frac{\sqrt{\sum_N R_{cp}^n}}{RNORM} \right) \leq \varepsilon \quad (3.2.57)$$

where N is total number of computation nodes, $RNORM$ is a reference value used for normalization and ε is a convergence criterion.

Generating grids

When using FVM to simulate the suspended sediment transport process in a natural river, the numerical generation of an orthogonal curvilinear coordinate system is essential. The problem-oriented grid helps to increase the convergence rate and decrease the demand for the storage of the computation in order to obtain a satisfactory accuracy. Refining the grid in the region of large gradients in the main variables increases the accuracy, but it is not necessary to refine the grid in the entire domain.

In this work, the grid for sediment transport simulation in the calculation domain is built with the help of the stream tube flow model. The boundaries of the stream tubes and the cross sections determine control volumes. The sizes and the locations of the control volumes vary with discharges, since determination of stream tubes are related to discharges.

The grid points are placed at the centers of the control volumes after the locations of the control volumes are determined. Thus, the concentration at a center of a control volume is a good representative value for the control volume in the determination of the source, sedimentation and erosion rates. The calculation domain is completely filled by control volumes and the boundary grid is placed at the boundary face. The boundary control volume has a zero thickness. Due to the fact that the boundaries of the stream tube near the two banks happen to be the boundaries of the calculation domain for a given discharge there are no special considerations of dry and wet boundaries to consider

3.3 Suspended sediment transport model for nonuniform sediment mixtures

The above discussion and calculation of suspended sediment transport are for uniform sediment transport in a river channel. In simulating sediment transport processes, the composition of river bed material is held continually in time and space. A representative grain diameter is used for both suspended and bed material in the modeling. However, the transported sediment and bed material are in fact composed of nonuniform sediments. The transport of nonuniform sediments is different from that of uniform sediments. Fractional deposition and erosion of nonuniform sediment transport are related to the grain size distributions of suspended sediment, bed material and flow conditions. Suspended particles and bed material usually have different grain size distributions and mixtures.

In the erosion process, the sediment transport capacity of flow for smaller particles is larger than that for larger particles, hence, smaller particles are more likely to be in suspension and transported. This gradually results in coarser bed material on the bed surface. Owing to increases in the critical shear stress with coarsening of the bed material, the sediment transport approaches an upper limit. This variation develops from upstream to downstream. In the deposition process, the flow strength decreases along the river course. Thus, the median grain size of sediments in suspension is reduced along river channels and the fall velocities for initial deposition of suspended sediment particles decrease along the river course (Figure 3.11). The effects of selective erosion and deposition, selective transport, result in downstream fining and play an important role in changes in river

morphology.

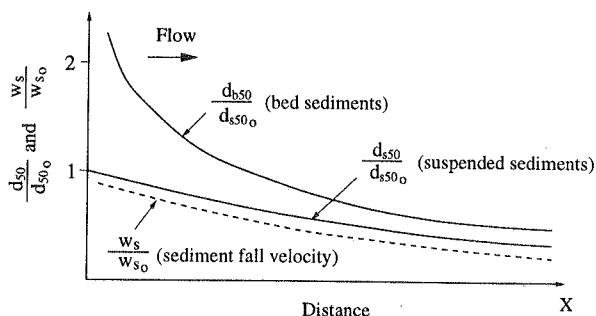


Figure 3.11: Selective transport: particle size sorting and critical velocity for particle sedimentation along a river course

The entrainment of sediment particles of a given size fraction along an alluvial bed is stochastic. It depends on the instantaneous strength of turbulence, on the supply of particles of the given size fraction in the bed material, on their location on the bed form, ripple or dune, and on suspended sediment concentration in the water body. These dependent factors can be described separately by probabilities of mobility and availability.

In this section, the concepts of mobility and availability are introduced to simulate the suspended sediment transport process for nonuniform sediment in a river channel. A new approach to estimate the percentage of size fractions of transported material is derived according to probability analysis. To verify the new method, a comparison of predicted and measured values of grain size distributions of the suspended load and the bed material will be made by flume and physical model data (Chapter 4 Section 1). The effect of selective transport on changes in river morphology will be studied in the Lauffen Reservoir on the River Neckar (Chapter 4 Section 2).

3.3.1 Probabilistic approach to nonuniform suspended sediment transport

Mobility of size fraction for prevailing hydraulic conditions

The bed instability is stochastic and can be described by the probability method. Grass (1970) [48] indicated that the turbulence near the boundary region is relevant to initial instability and the entrainment is mainly dependent on the difference between instantaneous bed shear stress and critical shear stress.

Instantaneous bed shear stress, τ , is assumed to have a Gaussian distribution with a mean bed shear stress, $\bar{\tau}$, and a standard deviation, σ_τ . Instantaneous bed shear stress can be represented as the sum of the mean of bed shear stress and the fluctuation of the shear stress

$$\tau = \bar{\tau} + \tau' \quad (3.3.58)$$

For uniform sediments the criterion of erosion is described by the critical shear stress, τ_c . For nonuniform sediments, the criterion of the particle incipient motion of size fraction n is represented by the value of critical shear stress over the range of sediment sizes considered, τ_{cn} . In practice, an average value of the distribution of the critical shear stresses for a given size range of particles is selected as the criterion for bed instability. Similarly, the value of $\frac{\tau}{\tau_{cn}}$ can also be assumed to have a Gaussian distribution with a mean of $\frac{\bar{\tau}}{\tau_{cn}}$ and a standard deviation, σ_n . We have

$$\frac{\tau}{\tau_{cn}} = \frac{\bar{\tau}}{\tau_{cn}} + \frac{\tau'}{\tau_{cn}} \quad (3.3.59)$$

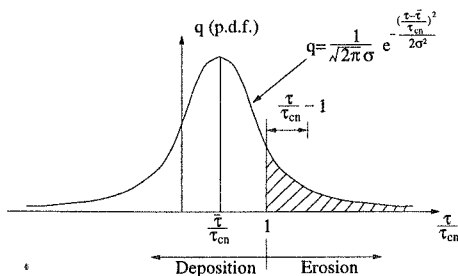


Figure 3.12: Gaussian distribution of instantaneous bottom shear stress and critical shear stress.

When the value of $\frac{\tau}{\tau_{cn}}$ is larger than 1, erosion occurs. Assuming that the shear stress fluctuation is statistically described by a Gaussian distribution the probability of the local shear stress acting on an individual grain smaller than the critical shear stress of that grain under a given flow condition is (Figure 3.12)

$$P_n = \int_{-\infty}^1 \frac{1}{\sqrt{2\pi}\sigma} e^{-\frac{(\frac{\tau}{\tau_{cn}} - \frac{\bar{\tau}}{\tau_{cn}})^2}{2\sigma_n^2}} d\left(\frac{\tau}{\tau_{cn}}\right) \quad (3.3.60)$$

Replacing the variation $\frac{\tau}{\tau_{cn}}$ by $\frac{\tau'}{\tau_{cn}}$ in eq. 3.3.59, the expression 3.3.60 can be rewritten as:

$$P_n = \int_{-\infty}^{1 - \frac{\bar{\tau}}{\tau_{cn}}} \frac{1}{\sqrt{2\pi}\sigma} e^{-\frac{(\frac{\tau'}{\tau_{cn}})^2}{2\sigma_n^2}} d(\frac{\tau'}{\tau_{cn}}) \quad (3.3.61)$$

The critical shear stress is obtained from a graph of dimensionless critical shear stress and dimensionless particle parameter, D_* , versus critical mobility parameters. For fine material, the standard deviation is taken to be $\sigma = 0.4$ according to an experimental approximate relationship [48].

New approach to evaluate the percentage of the size fraction of transported material

To describe the particle erosion and deposition the zone near the bed surface are vertically divided into following horizontal zones: water zone, bottom, mobile and immobile layers (Figure 2.10). The mobile layer is further divided into two sub-layers, active and parent (deactivated) layers. It is defined that only in the active layer the exchange between suspended sediment and bed material occurs on the given flow condition. Sediment in the parent layer is at rest on this given flow condition but part of it may be added into the active layer and eroded as the flow condition changes. Sediment particles are entrained directly from the bed surface (in the active layer) or from material transported as bed-load (in the bottom layer). Since here only suspended sediment transport is considered, it is assumed that the sediments are resuspended directly from the bed surface (in the active layer). The flow condition and grain size distributions of bed material in the active layer dominate the erosion processes. Selective erosion and sedimentation vary the grain-size distribution of bed material in the active layer, as a result, the grain size distribution of bed sediment gradually becomes finer along the river course. The downstream fining in turn affects the suspended sediment transport process by changing conditions of particle incipient motion and availability of bed material in the active layer. In order to correctly describe the effects of the selective transport and downstream fining on the sediment transport process, a new formula is derived to calculate the grain size distribution of erosion particles.

Suspended sediment transport can be classified as equilibrium and non-equilibrium transports. The equilibrium transport has three cases:

- (1) There is no deposition and erosion. There is no change in concentration;

- (2) There is an exchange between the bed material and suspended particles, but the deposition and erosion rates for each size fraction of sediment mixture are equal;
- (3) There is exchange between the bed material and suspended particles, but the deposition and erosion for each size fraction of the sediment mixture are not equal. This means that the total concentration does not change, but the fractional concentrations vary.

All other sediment transport processes are non-equilibrium ones. The new formula is derived assuming equilibrium transport condition.

The deposition rate of size fraction n of nonuniform sediments depends on the reference concentration, C_a , the particle fall velocity, w_s , and the deposition stage parameter, $1 - \frac{\tau}{\tau_{cn}}$. The vertical velocity of particles is defined as the mean value of effective particle fall velocity, which is equal to the difference of particle fall velocity and downward fluctuation flow velocity, which is shown later. The value of $\frac{\tau}{\tau_{cn}}$ follows a Gaussian distribution. Only where $\frac{\tau}{\tau_{cn}} < 1$ (region out shaded in Figure 3.12) does relate this value to the particle deposition.

Considering a given value of $\frac{\tau}{\tau_{cn}} < 1$, the normalized Gaussian probability density function can be described by

$$q_n = \frac{1}{\sqrt{2\pi}\sigma} e^{-\frac{(\frac{\tau}{\tau_{cn}} - \frac{\bar{\tau}}{\tau_{cn}})^2}{2\sigma^2}} d\left(\frac{\tau}{\tau_{cn}}\right). \quad (3.3.62)$$

Corresponding to this probability the deposition rate for size fraction n can be represented by

$$C_{an} \bar{V}_{sn} \left(1 - \frac{\tau}{\tau_{cn}}\right) \frac{1}{\sqrt{2\pi}\sigma} e^{-\frac{(\frac{\tau}{\tau_{cn}} - \frac{\bar{\tau}}{\tau_{cn}})^2}{2\sigma^2}}. \quad (3.3.63)$$

The sediment deposition rate of size fraction n for $\frac{\tau}{\tau_{cn}} < 1$, in a time, Δt , per square meter is the integral of the above expression from negative infinity to 1

$$\dot{m}_{dn} = \int_{-\infty}^1 \left[C_{an} \bar{V}_{sn} \left(1 - \frac{\tau}{\tau_{cn}}\right) \frac{1}{\sqrt{2\pi}\sigma} e^{-\frac{(\frac{\tau}{\tau_{cn}} - \frac{\bar{\tau}}{\tau_{cn}})^2}{2\sigma^2}} \right] d\left(\frac{\tau}{\tau_{cn}}\right). \quad (3.3.64)$$

where C_{an} denotes the reference concentration of grain size fraction n near the bed surface, \bar{V}_{sn} denotes the averaged particle fall velocity for grain size fraction n , σ denotes the standard deviation of the distribution of bottom shear stress.

Considering

$$\frac{\tau'}{\tau_{cn}} = \frac{\tau}{\tau_{cn}} - \frac{\bar{\tau}}{\tau_{cn}} \quad (3.3.65)$$

and

$$d\left(\frac{\tau}{\tau_{cn}}\right) = d\left(\frac{\tau'}{\tau_{cn}}\right), \quad (3.3.66)$$

substituting these values in eq. 3.3.64 and changing the integration limit, we have

$$\dot{m}_{dn} = \int_{-\infty}^{1 - \frac{\bar{\tau}}{\tau_{cn}}} \frac{1}{\sqrt{2\pi\sigma}} \left\{ C_{an} \bar{V}_{sn} \left[\left(1 - \frac{\bar{\tau}}{\tau_{cn}}\right) - \frac{\tau'}{\tau_{cn}} \right] e^{-\frac{(\frac{\tau'}{\tau_{cn}})^2}{2\sigma^2}} \right\} d\left(\frac{\tau'}{\tau_{cn}}\right) \quad (3.3.67)$$

In the same time interval, the amount of eroded sediment of grain size fraction n per square meter is related to the grain size distribution in the active layer, upward fluctuation in flow velocity and the erosion stage parameter, $\frac{\tau}{\tau_{cn}} - 1$. Erosion occurs, only when $\frac{\tau}{\tau_{cn}} > 1$ is satisfied. The right part of the area in Figure 3.12 contributes to erosion. Corresponding to the probability expressed by the shaded area in Figure 3.12 the erosion rate for size fraction n can be represented by

$$V_{bn} \bar{V}_{rsn} \left(\frac{\tau}{\tau_{cn}} - 1 \right) \frac{1}{\sqrt{2\pi\sigma}} e^{-\frac{(\frac{\tau}{\tau_{cn}})^2}{2\sigma^2}}. \quad (3.3.68)$$

Similar to the calculation of the deposition rate, the erosion rate of size fraction n for $\frac{\tau}{\tau_{cn}} > 1$ in the time interval per square meter is the integral of the above expression from 1 to infinity, given by

$$\dot{m}_{en} = \int_1^{\infty} \frac{1}{\sqrt{2\pi\sigma}} \left[V_{bn} \bar{V}_{rsn} \left(\frac{\tau}{\tau_{cn}} - 1 \right) e^{-\frac{(\frac{\tau}{\tau_{cn}})^2}{2\sigma^2}} \right] d\left(\frac{\tau}{\tau_{cn}}\right). \quad (3.3.69)$$

where \bar{V}_{bn} denotes the volume in the active layer for grain size fraction n and where \bar{V}_{rsn} denotes averaged particle resuspension velocity for grain size fraction n ,

Substituting eq. 3.3.65 in eq. 3.3.69 and also changing the integration limit, we achieve

$$m_{en} = \int_{1 - \frac{\bar{\tau}}{\tau_{cn}}}^{\infty} \frac{1}{\sqrt{2\pi\sigma}} \left\{ V_{bn} \bar{V}_{rsn} \left[\frac{\tau'}{\tau_{cn}} - \left(1 - \frac{\bar{\tau}}{\tau_{cn}}\right) \right] e^{-\frac{(\frac{\tau'}{\tau_{cn}})^2}{2\sigma^2}} \right\} d\left(\frac{\tau'}{\tau_{cn}}\right) \quad (3.3.70)$$

Under equilibrium transport conditions, assuming that the deposition rate equals the erosion rate, i.e.,

$$\dot{m}_{dn} = \dot{m}_{en} \quad (3.3.71)$$

With the help of

$$T_n = 1 - \frac{\bar{\tau}}{\tau_{cn}} \quad (3.3.72)$$

and

$$x = \frac{\tau'}{\tau_{cn}} \quad (3.3.73)$$

and substituting eq. 3.3.67, 3.3.70 in eq. 3.3.71, we have

$$\begin{aligned} & \int_{-\infty}^{T_n} \frac{1}{\sqrt{2\pi}\sigma} [C_{an} \bar{V}_{sn} (T_n - x) e^{-\frac{x^2}{2\sigma^2}}] dx \\ &= \int_{T_n}^{\infty} \frac{1}{\sqrt{2\pi}\sigma} [V_{bn} \bar{V}_{rsn} (x - T_n) e^{-\frac{x^2}{2\sigma^2}}] dx \end{aligned}$$

Simplifying the formula above, we obtain

$$\begin{aligned} \frac{C_{an}}{V_{bn}} &= \frac{\int_{T_n}^{\infty} \frac{1}{\sqrt{2\pi}\sigma} [\bar{V}_{rsn} (x - T_n) e^{-\frac{x^2}{2\sigma^2}}] dx}{\int_{-\infty}^{T_n} \frac{1}{\sqrt{2\pi}\sigma} [\bar{V}_{sn} (T_n - x) e^{-\frac{x^2}{2\sigma^2}}] dx} \quad (3.3.74) \\ &= \frac{\bar{V}_{rsn} \int_{T_n}^{\infty} \frac{x}{\sqrt{2\pi}\sigma} e^{-\frac{x^2}{2\sigma^2}} dx - T_n \int_{T_n}^{\infty} \frac{1}{\sqrt{2\pi}\sigma} e^{-\frac{x^2}{2\sigma^2}} dx}{\bar{V}_{sn} \left[\int_{-\infty}^{T_n} -\frac{x}{\sqrt{2\pi}\sigma} e^{-\frac{x^2}{2\sigma^2}} dx + T_n \int_{-\infty}^{T_n} \frac{1}{\sqrt{2\pi}\sigma} e^{-\frac{x^2}{2\sigma^2}} dx \right]} \end{aligned}$$

Let χ and ϕ represent the following functions

$$\chi_n\left(\frac{T_n}{\sigma}\right) = \int_{-\infty}^{T_n} \frac{1}{\sqrt{2\pi}\sigma} e^{-\frac{x^2}{2\sigma^2}} dx, \quad (3.3.75)$$

$$\phi_n = \frac{1}{\frac{\sigma}{\sqrt{2\pi}} e^{-\frac{T_n^2}{2\sigma^2}} + T_n \chi\left(\frac{T_n}{\sigma}\right)} \quad (3.3.76)$$

Thus eq. 3.3.77 can be simplified as

$$\frac{C_{an}}{V_{bn}} = \frac{\bar{V}_{rsn}}{\bar{V}_{sn}} (1 - T_n \phi_n) = \alpha_n (1 - T_n \phi_n). \quad (3.3.77)$$

where the parameter of particle velocity, α_n is defined by

$$\alpha_n = \frac{\bar{V}_{rsn}}{\bar{V}_{sn}}. \quad (3.3.78)$$

Considering the total amount of sediment in the active layer to be V_b and the percentage of sediments for size fraction n to be p_{bn} , the value of V_{bn} is equal to $p_{bn} V_b$. The fractional reference concentration can then be expressed by

$$C_{an} = p_{bn} V_b \cdot \alpha_n (1 - T_n \phi_n). \quad (3.3.79)$$

C_{an} implies that the reference concentration of size fraction n is related to the flow condition and the percentage of bed material of size fraction n in the active layer, p_{bn} . p_{bn} is usually defined as the availability of grain size fraction n in the active layer.

The total reference concentration in the bottom layer can be obtained by the sum of reference concentrations of all grain size fractions

$$C_a = \sum_{n=1}^N C_{an} = V_b \sum_{n=1}^N p_{bn} \alpha_n (1 - T_n \phi_n). \quad (3.3.80)$$

Dividing eq. 3.3.79 by eq. 3.3.80, the percentage of size fraction n of particles in the bottom layer can be obtained

$$p_{an} = \frac{C_{an}}{C_a} = \frac{p_{bn} \alpha_n (1 - T_n \phi_n)}{\sum_{n=1}^N p_{bn} \alpha_n (1 - T_n \phi_n)}. \quad (3.3.81)$$

Eq. 3.3.81 represents the relationship of the percentage of size fraction in the bottom and active layer under a given flow condition. It determines the grain-size distribution

of the transported material in the bottom layer. Under equilibrium transport conditions the grain size distribution will be the same as the grain size distribution of the eroded material from the active layer.

From this relation we can see that

- p_{an} is affected by p_{bn} and flow conditions.
- The grain size distribution of eroded material is finer than one in the active layer.
- For a given p_{bn} , the distribution of p_{an} becomes coarser with increasing in flow velocity.

Based on the grain size distribution of eroded material, one can determine the median diameter and the corresponding critical shear stress for eroded material, as well as the fractional and total erosion rates. The detailed calculations are given in section 3.3.4.

Mean effective fall and resuspension velocity of particles Considering the fluctuation in velocity near the bed surface, the effective fall velocity of a particle is defined as the difference of the fall velocity and instantaneous velocity. It can be expressed by

$$w_s - w'.$$

Assuming that the fluctuation velocity can be described by Gaussian distribution:

$$\frac{1}{\sqrt{2\pi}\sigma_w} e^{-\frac{w'^2}{2\sigma_w^2}},$$

the probability of the particle fall velocity larger than the flow fluctuation velocity for a given particle can be expressed by the integral of the two expressions above from negative infinity to w_{sn} :

$$P(w' < w_{sn}) = \int_{-\infty}^{w_{sn}} (w_{sn} - w') \frac{1}{\sqrt{2\pi}\sigma_w} e^{-\frac{w'^2}{2\sigma_w^2}}.$$

The mean effective fall velocity is given by:

$$\bar{V}_{sn} = \frac{\int_{-\infty}^{w_{sn}} (w_{sn} - w') \frac{1}{\sqrt{2\pi}\sigma_w} e^{-\frac{w'^2}{2\sigma_w^2}} d(w')}{\int_{-\infty}^{w_{sn}} \frac{1}{\sqrt{2\pi}\sigma_w} e^{-\frac{w'^2}{2\sigma_w^2}} d(w')} \quad (3.3.82)$$

The effective resuspension velocity of particles is the difference between the upward fluctuation velocity and the particle fall velocity, $w' - w_s$. When $w' > w_s$, sediments begin to resuspend. The probability of the upward velocity exceeding the particle fall velocity for a given size fraction is

$$P(w' > w_{sn}) = \int_{-\infty}^{w_{sn}} (w' - w_{sn}) \frac{1}{\sqrt{2\pi}\sigma_w} e^{-\frac{w'^2}{2\sigma_w^2}} d(w')$$

The mean effective resuspension velocity of particles for the given size fraction:

$$\bar{V}_{rsn} = \frac{\int_{w_{sn}}^{\infty} (w' - w_{sn}) \frac{1}{\sqrt{2\pi}\sigma_w} e^{-\frac{w'^2}{2\sigma_w^2}} d(w')}{\int_{w_{sn}}^{\infty} \frac{1}{\sqrt{2\pi}\sigma_w} e^{-\frac{w'^2}{2\sigma_w^2}} d(w')} \quad (3.3.83)$$

After simplifying Eq. 3.3.82 and 3.3.83, we have

$$\bar{V}_{sn} = \frac{\frac{\sigma_w}{\sqrt{2\pi}} e^{-\frac{w_{sn}^2}{2\sigma_w^2}} + w_{sn} \chi\left(\frac{w_{sn}}{\sigma_w}\right)}{\Phi\left(\frac{w_{sn}}{\sigma_w}\right)} \quad (3.3.84)$$

$$\bar{V}_{rsn} = \frac{\frac{\sigma_w}{\sqrt{2\pi}} e^{-\frac{w'^2}{2\sigma_w^2}} - w_{sn} \left[1 - \chi\left(\frac{w_{sn}}{\sigma_w}\right)\right]}{1 - \chi\left(\frac{w_{sn}}{\sigma_w}\right)} \quad (3.3.85)$$

where σ_w denotes the standard deviation of the distribution of w' and $\sigma_w = u_*$ [52]. The parameter of α_n can then be determined as

$$\alpha_n = \frac{\bar{V}_{rsn}}{\bar{V}_{sn}} = \left[1 - \frac{w_{sn}}{\frac{\sigma_w}{\sqrt{2\pi}} e^{-\frac{w_{sn}^2}{2\sigma_w^2}} + w_{sn} \chi\left(\frac{w_{sn}}{\sigma_w}\right)} \right] \frac{\chi\left(\frac{w_{sn}}{\sigma_w}\right)}{1 - \chi\left(\frac{w_{sn}}{\sigma_w}\right)}. \quad (3.3.86)$$

When the ratio of $\frac{w_{sn}}{\sigma_w}$ is smaller, the value of α_n is approximated as 1. In this case, eq. 3.3.81 can be simplified as

$$p_{an} = \frac{p_{bn}(1 - T_n \phi_n)}{\sum_{n=1}^N p_{bn}(1 - T_n \phi_n)} \quad (3.3.87)$$

Non-equilibrium transport The above derivation is based on equilibrium transport conditions. In practice, non-equilibrium transport of sediment usually occurs. The grain size distribution of erodible material for non-equilibrium transport is difficult to determine, because the phenomena of non-equilibrium transport is more complicated than equilibrium transport. For weakly non-equilibrium transport conditions, the expression of 3.3.81 or 3.3.87 can be used as a useful approximation.

3.3.2 Governing equations of suspended sediment transport for nonuniform sediment mixtures

Depth-averaged convection-dispersion equation

For simulating suspended sediment transport of nonuniform sediment mixtures, the bed material is divided into a number of size fractions. It is assumed that the particles in different size fractions do not interact with each other. The suspended sediment concentration of size fraction n can be determined by the unsteady, depth-averaged convection-dispersion equation of suspended sediment transport for each size fraction. The flow parameters used here are calculated by the stream tube flow model.

For grain size fraction n , the depth-averaged convection-dispersion equation of suspended sediment transport can be represented by

$$\begin{aligned} & \frac{\partial m_z h v C_n}{\partial x} + \frac{\partial m_x h v C_n}{\partial z} \\ &= \frac{\partial}{\partial x} \left(\frac{m_z}{m_x} h D_x \frac{\partial C_n}{\partial x} \right) + \frac{\partial}{\partial z} \left(\frac{m_x}{m_z} h D_z \frac{\partial C_n}{\partial z} \right) + \dot{E}_n - \dot{S}_n \end{aligned} \quad (3.3.88)$$

where C_n is suspended sediment concentration of size fraction n . \dot{S}_n and \dot{E}_n denote the rates of the deposition and the erosion of size fraction n , respectively. The other variations are the same in eq. 3.2.28.

Deposition of sediments of the size fraction n occurs when the bottom shear stress is smaller than the critical shear stress for the initial deposition of suspended sediments in the same size fraction n . The deposition rate of size fraction n is given by

$$\dot{S}_n = \alpha_{s,n} w_{s,n} C_n \left(1 - \frac{\tau}{\tau_{c,s,n}}\right), \quad \tau < \tau_{c,s,n} \quad (3.3.89)$$

where $w_{s,n}$ and $\tau_{c,s,n}$ denote the particle fall velocity and the critical shear stress of size fraction n , $\alpha_{s,n}$ is a coefficient of the concentration distribution of size fraction n . The values of $\tau_{c,s,n}$ and $\alpha_{s,n}$ are given separately by eq. 2.1.19 and 2.1.13.

The total sedimentation rate is

$$\dot{S} = \sum_{n=1}^N \dot{S}_n. \quad (3.3.90)$$

Erosion rates for nonuniform sediment mixture

The representation of bed material of size fraction n in the active layer is defined as the availability of that size fraction in the active layer. The amount of eroded material of that size fraction from the active layer relates to the flow condition and the availability of size fraction n . This relationship is described by the percentage of size fraction n , p_{an} , which is represented by Eq. 3.3.81 and rewritten here

$$p_{an} = \frac{p_{bn} \alpha_n (1 - T_n \phi_n)}{\sum_{n=1}^N p_{bn} \alpha_n (1 - T_n \phi_n)}.$$

Based on the grain size distribution of erodible sediments, the median diameter of eroded bed material and the corresponding critical shear stress can be determined. The total erosion rate and the fractional erosion rates can then be calculated.

Assuming that the critical shear stress of eroded sediments corresponding to the median diameter is $\tau_{c,E}$, the total erosion rate can be determined by

$$\dot{E} = M \left(\frac{\tau}{\tau_{c,E}} - 1 \right), \quad \tau \geq \tau_{c,E} \quad (3.3.91)$$

The erosion rate of size fraction n is then

$$\dot{E}_n = p_{an} \dot{E}. \quad (3.3.92)$$

Evaluation of changes in grain size distribution of bed material and bed elevation

The river bed is divided into mobile and immobile layers to calculate changes in the river bed level. The mobile layer includes the active and parent (deactivated) layers. It is assumed that the exchange of sediment particles between the suspended sediment and bed material exists only in the active layer, and bed material in the parent layer remain still on the current flow condition. Sediment in the parent layer may be eroded as flow condition changes. In the immobile layer bed material is not erodible.

The active layer thickness, T_a , varies with hydraulic conditions and bed formations. It is defined as a proportional height of bedform, or $2d_{50}$ according to Einstein assumption or equal to $2d_{50} \frac{\tau}{\tau_{c50}}$. The active layer and the parent layer are further divided into more layers, which may be used to represent the difference in grain size distribution, mineral density, for different deposition situations.

Sorting equation and bed level changes In the active layer, there is a multiple grain-size distribution. It represents the availability of grain size fraction n in the active layer, is defined as

$$p_{bn} = \frac{z_{bn}}{T_a} = \frac{\sum_{l=1}^L z_{bnl}}{\sum_{n=1}^N \sum_{l=1}^L z_{bnl}}$$

where z_{bnl} is the thickness of size fraction n in the layer l . The subscripts of b, n, l denote bed, particular size fraction of nonuniform sediments and layer in the active layer, respectively. Here, layer l is used for the effect of the different mineral densities or different degrees of compaction related to the deposition environment.

Near the bed surface continuous exchange of sediment particles takes place. It is assumed that this particle exchange only occurs between the bottom and the active mixing layer during each time step. If erosion occurs, sediments are entrained at depths anywhere from the first to the last sublayer within the active mixing layer. The grain-size distribution of each layer in the active layer changes depending on the amount of erosion and deposition in the layer. If net deposition occurs within a time step, a new layer will be developed with the same grain-size distribution as the original deposition in that step. For a new time step with different hydraulic and bed conditions there is a new T_a . This new active layer may include the new layer, if net deposition occurs at the last time step or a few layers from the underlying parent bed.

Sorting equations based on the principle motion of volume conservation in the active layer are applied to each size fraction n and each layer l :

$$\frac{\partial}{\partial t}(y_{bnl}) = \frac{1}{\rho_p}(\dot{S}_{nl} - \dot{E}_{nl}) \quad (3.3.93)$$

where y_{bnl} is the sediment thickness of layer l of size fraction n . The sum of this equation over all size fractions gives the continuity equation of the complete sediment mixture for layer l . The total change in the height of layer l is

$$\frac{\partial}{\partial t}(y_{bl}) = \sum_{n=1}^N \frac{\partial}{\partial t}(y_{bnl}). \quad (3.3.94)$$

The change in bed elevation is equal to:

$$\frac{\partial y_b}{\partial t} = \sum_{l=1}^L \frac{\partial y_{bl}}{\partial t} = \frac{1}{\rho'} \sum_{l=1}^L \sum_{n=1}^N (\dot{E}_{nl} - \dot{S}_{nl}), \quad n = 1, 2, \dots, N; \quad l = 1, 2, \dots, L. \quad (3.3.95)$$

The percentage of size fraction n for each layer l in the active layer is determined by

$$p_{bnl} = \frac{y_{bnl}}{\sum_{l=1}^L y_{bnl}}. \quad (3.3.96)$$

After the time step it is updated by

$$\frac{\partial p_{bnl}}{\partial t} = \frac{y_{bnl}^{new}}{\sum_{l=1}^L y_{bnl}^{new}}, \quad \text{or} \quad p_{bnl}^n = \frac{p_{bnl} y_l + \Delta y_{nl}}{y_l + \Delta y_{nl}}. \quad (3.3.97)$$

Finally, the change in bed elevation Y is then calculated by

$$\frac{\partial Y}{\partial t} = \frac{1}{\rho'} \sum_{n=1}^N \sum_{l=1}^L (\dot{E}_{nl} - \dot{S}_{nl}), \quad n = 1, 2, \dots, N; \quad l = 1, 2, \dots, L. \quad (3.3.98)$$

In this section a new method to determine the grain size distribution of eroded material on the bed surface is derived taking into consideration:

- mobility of the grain size fraction of bed material;
- availability of the grain size fraction of bed material;
- Suspended sediment concentration

In comparison with other methods this method is simple and can be used without any modifications. It takes into account three important factors in determining the fractional eroded material, (a) particle incipient condition (probability of erosion occurring) which is dominated by the effective bottom shear stress, (b) particle supply controlled by the availability of size fraction n on the bed surface and (c) the influence of suspended sediment concentration on the erosion rate. The effects of selective transport and downstream fining on sediment transport processes and changes in river geometry can be described more realistically and reasonably than in previous methods.

Chapter 4

Model test and application

In this chapter, model tests were carried out in order to verify that the two formulae derived and three models developed in Chapter 3 can really and accurately reproduce the following physical model data (Section 4.1):

- Exchange of particles between the main channel and the flood plains from James' flume study;
- Fractional deposition and entrainment from Samaga's flume study;
- Reservoir deposition over 76-year operation using the physical model of Tsinghua University.

Secondly, the three models are used for a field study at the Lauffen Reservoir (Section 4.2):

- Calibration of the flow model and uniform suspended sediment transport model;
- Prediction of river morphology change;
- Calculation of deposition on the flood plain.
- Study of the effects of selective transport and downstream fining using the transport model for nonuniform sediment mixtures.

Finally, the dispersion between the stream and the dead water zone (groyne field) and the deposition and erosion in the dead water zone are calculated as an application example of the sediment transport model (Section 4.3).

4.1 Model test by physical model studies

The goal of this section is to test whether the suspended sediment transport models can realistically and accurately simulate suspended sediment transport processes in river

channels. Measured physical data from James, Samaga and Tsinghua University are used to test the suspended sediment transport models.

Sediment dispersion at the interface between the main channel and the flood plains in a river reach with compound sections was studied using the data of the James' flume experiment.

The experimental data of Samaga and Tsinghua University were used to test the sediment transport model for nonuniform sediment mixtures. The model calculates the temporal and spatial variations in the grain size distributions of eroded material and bed material and simulates the sediment deposition and erosion processes focusing on the selective transport of grains. The computational results show good agreement with the measured data from the model tests. This implies that the present numerical models can be used for predicting changes in river morphology and the reservoir sedimentation and investigating the effect of selective transport on nonuniform suspended sediment transport processes.

4.1.1 Sediment transfer from main channel to flood plains

James [58] used flume experiments to investigate the transfer of suspended sediment from a main channel to an adjacent flood plain under the conditions of steady, uniform flow. To verify the derived formula to describe the lateral dispersion of sediments at the interface between the main channel and the flood plains, the numerical results are compared with the laboratory data measured by James.

Method		Q l/s	H cm	u_m m/s	u_p m/s	k_{stm} $m^{\frac{1}{2}}/s$	k_{stp} $m^{\frac{1}{2}}/s$
Experiment	3	9.9	12.0	0.90	0.40		
	4	9.5	10.0	0.75	0.30		
Calculation	3	14.7	12.0	0.77	0.23	50.0	50.0
	4	12.0	10.0	0.68	0.30	50.0	49.0

Table 4.1: Flow variables used in the simulations of James' flume study (1985).

The compound channel section used in the experiment is shown in Figure 4.1. The model was 38cm wide and 10m long with a bed slope of 0.004. Sediments were classified into four groups, $d < 75\mu m$, $75 - 150\mu m$, $150 - 300\mu m$ and $> 300\mu m$. Two different flood plain surfaces, a completely absorbing surface and a non-absorbing surface, were used to describe the deposition probability. The completely absorbing surface was a 15cm long

sediment particle trap, in which particles can settle rapidly and be collected after each experiment. Two such traps were separately placed at 1.8m and 4.6m from the end of the flume. Before each experiment, sediment particles were placed on the main channel with a thickness determined by the flow depth required in the main channel.

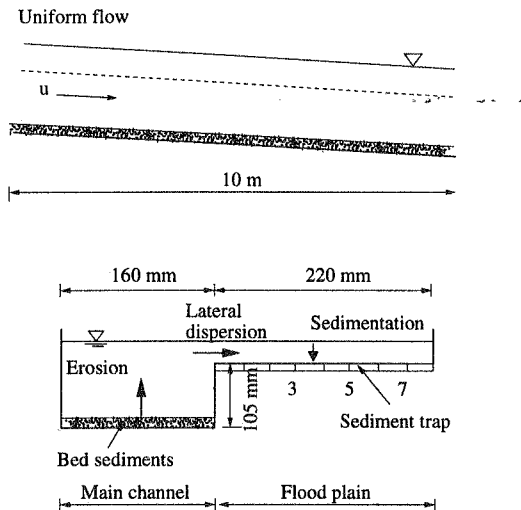


Figure 4.1: Sketch of flume experiment set-up of James.

For numerical modeling, the flume is divided into 21 sections and 19 strips. Since flow is uniform and the lateral velocity is zero, the strip is coincident with the stream tube. The relative distribution is predicted as the uniform sediment for diameter $d = 75, 75 - 150, 150 - 300, 300 \mu\text{m}$ and median diameter $200 \mu\text{m}$ by the sediment transport model for uniform sediments. The influences of different sized grains on each other cannot be taken into account. The flow parameters used in the computation and the experiment are given in Table 4.1. The computed and the measured relative deposition distribution on the flood plain for the tests 3 and 4 are shown in Figure 4.2. It can be seen that the relative deposition distributions at upstream and downstream sections agree well with the results of James' experiments. The largest deposition rate is near the interface between the main channel and the flood plains. The smaller the particles are, the wider is the range of deposition. The deposition masses compare well at the upstream sampling section. The model test using James' experiment results implies that the lateral dispersion formula to describe the sediment transfer from the main channel to the flood plain works well. The quasi two-dimensional transport model can predicted the sedimentation on the flood

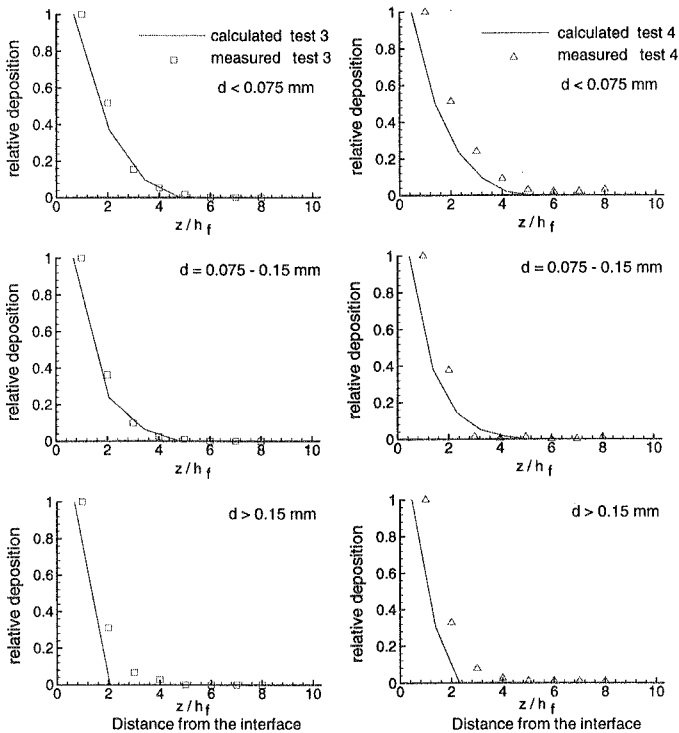


Figure 4.2: Comparison of deposition distribution on the flood plain calculated and measured by James [58].

plain.

4.1.2 Transport model of nonuniform sediment mixtures

Flume study of Samaga et al. (1986)

Samaga et al. (1986) [125] used flume experiments to investigate suspended sediment transport (Figure 4.3). The model was 30m long and 0.2m wide. The flume slope was adjusted to obtain uniform flow over the flume.

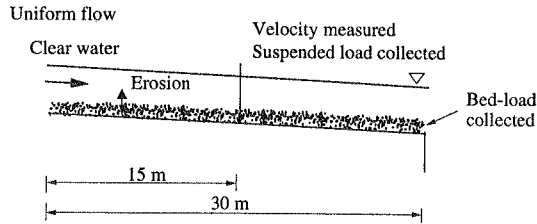


Figure 4.3: Sketch of flume experiment set-up of Samaga et al. (1986).

The flume bed surface was covered with 15 cm of nonuniform sediments. The particle diameter ranged from 0.007 to 2 mm with a density of 2650 kg/m^3 . Four mixtures with different median diameters and standard deviations were adopted in the experiments, shown in Figure 4.4. Each mixture of sediments was divided into 10 size fractions.

In the experiment, the vertical velocity distribution was measured at different elevations in the center of the flume at a distance of 15 m from the entrance of the flume. At the same locations, the sediment was collected and dried, and the concentration was calculated for each grain size fraction. According to the Einstein's assumption that the boundary between the suspended load and bed load is at the height of 2 diameters of grain size over the bed surface, the suspended loads of each grain size fraction were calculated by integrating the product of concentration and velocity profiles from the height of 2 diameters over the bed surface to the water surface.

The total transport load in the experiments was also calculated by collecting the sediments over the whole width of the flume at the downstream end of the flume. The bed load was determined by the total load minus the suspended load. The hydraulic parameter of the experimental set up used for the calibration are listed in the Table 4.2.

Run	Discharge l/s	Water depth cm	Velocity m/s	Bed slope $S * 10^3$	Temp. $^{\circ}C$
M12	10.400	7.690	0.675	5.760	23.0
M32	12.920	8.657	0.746	6.926	23.0
M44	13.180	8.733	0.755	5.268	26.0

Table 4.2: Hydraulic parameters of the flume experiment of Samaga et. al. (1986)

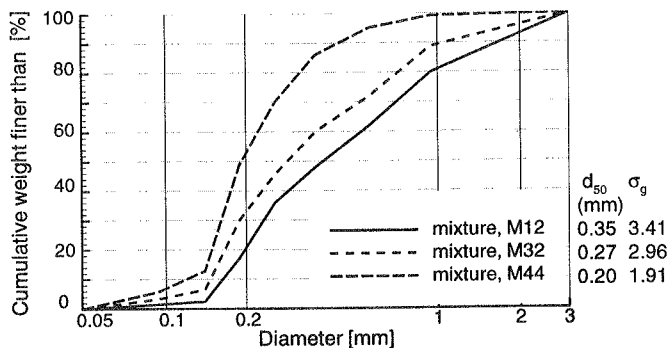


Figure 4.4: Cumulative grain size distribution of original bed material used for flume experiments by Samaga et al. (1986).

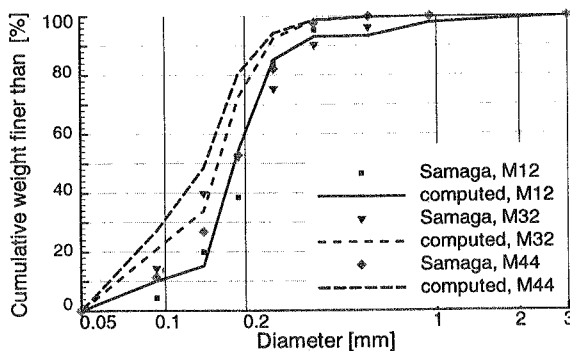


Figure 4.5: Comparison between computed and measured grain-size distributions of suspended load in flume experiments of Samaga et al. (1986).

In the numerical model, the length of the flume was divided into 60 sections and 12 stream tubes. The flow conditions were simulated by adjusting the bed roughness. Under a steady, uniform flow, the suspended sediment concentrations were predicted and the grain-size distributions of suspended load were calculated. Three experiments from 33 experiments

carried out by Samaga et al. were selected for the calibration. A comparison of predicted and measured results are given in Figure 4.5.

Three runs (M12, M32 and M44) with different slopes, discharges and initial bed material were selected. The initial grain size distributions of bed material was divided into 8 size fractions ($d=0.073-2.36$ mm). Computed and measured grain size distributions of the suspended-load (Figure 4.5) agree well for runs M12 and M32. The median grain diameters are close (M12: 0.183 mm computed and 0.203 mm measured; M32: 0.16 mm and 0.177 mm). Nevertheless, for run M44, the computed and the measured curves differ by more than 20%. The median diameters for computed and measured runs are 0.142 and 0.182 mm, respectively. However, within the coarsest 80%, the median diameter are nearly equal. The computed distributions were finer than the measured distributions for runs M32 and M44.

Comparing the figures of 4.4 and 4.5, we can see that: 1. the grain size distribution of

d[mm]	TEST-M12				TEST-M32				TEST-M44			
	measured		predicted		measured		predicted		measured		predicted	
	p	$\sum p$	p	$\sum p$	p	$\sum p$	p	$\sum p$	p	$\sum p$	p	$\sum p$
0.073	.0428	0.0000	.1000	0.0000	.143	0.0000	.2008	0.0000	.113	0.0000	.2700	0.0000
		0.0428		0.1000		0.1436		0.2080		0.1130		0.2700
0.116	.1557	.0506		0.1510	.154	.3980	.1382	.3390	.155	.2676	.2144	.4850
		0.1985		0.1510		0.3980		0.3390		0.2676		0.4850
0.164	.1857	.3935		0.5440	.225	.5232	.3853	.7240	.260	.5279	.3193	.8040
		0.3842		0.5440		0.5232		0.7240		0.5279		0.8040
0.212	.4571	.3081		0.8520	.230	.7534	.2009	.9250	.294	.8221	.1383	.9420
		0.8413		0.8520		0.7534		0.9250		0.8221		0.9420
0.295	.1114	.0790		0.9310	.149	.9024	.0695	.9850	.155	.9771	.0447	.9870
		0.9527		0.9310		0.9024		0.9850		0.9771		0.9870
0.421	.0471	.0017		0.9330	.059	.9619	.0126	.9970	.022	1.0000	.0111	.9980
		1.0000		0.9330		0.9619		0.9970		1.0000		0.9980
0.707	.0000	.0452		0.9780	.000	1.0000	.0026	1.0000	.000	1.0000	.0014	0.9999
		1.0000		0.9780		1.0000		1.0000		1.0000		0.9999
1.180	.0000	.0022		1.0000	.000	1.0000	.0000	1.0000	.000	.0006	.0006	1.0000
		1.0000		1.0000		1.0000		1.0000		1.0000		1.0000

Table 4.3: Comparison between measured and computed grain size distribution of suspended sediment load in the flume study by Samaga et. al (1986)

suspended sediments is finer than that of the bed sediments, which means that finer particles tend to be eroded more easily than larger particles; 2. the grain size distribution of eroded material is not equal to that of bed material. These demonstrate that the concept of selective transport used in this model is correct. It gives reasonable prediction of the selective transport processes.

Physical model study of the Three Gorges Project (1994)

The Three Gorges Project (TGP) currently is the world's largest hydraulic engineering project. The Three Gorges Reservoir drains an area of $10 \cdot 10^6 \text{ km}^2$. The Reservoir is on the Yangtze River in Yicang, Hubei Province, China. It is a multipurpose project for flood control, power supply and navigation. The spillway dam is located at the center of the river and two power-houses are arranged on either side of the spillway dam with an installed capacity of 17680 MW. The navigation lock and ship lift are found at the left river bank.

Sediment deposition within the reservoir is one of the key issues of the Three Gorges Project, since it influences the navigation and the effective storage. Three physical models to predict sediment transport have been developed. The model built at the Tsinghua University simulates deposition and erosion in the reservoir during and after impoundment. It covers a river reach 17.5 km upstream of the dam with the water surface width of 500 - 3000 m (Figure 4.6).

The transported sediment in the study reach is mainly composed of suspended sediment with a median diameter of 0.033 mm. The percentage of sediments with a diameter smaller than 0.1 mm is 88% of the annual suspended sediment transport. There is a small portion of bed-load in the total sediment load transport.

During the first 10 years of operation, the normal water level of the reservoir will be 156.0 m. In flood seasons the water level will be lowered from 156 m to 135 m. After 10 years of operation, the normal water level of the reservoir will be 175.0 m and the flood control level will be 145.0 m (FCL). In flood seasons, the sediment amount is 88-90 % of the annual sediment amount and the runoff amount is 61 % of the annual runoff amount. Sediment deposition in the TGP occurs mainly during flood seasons. In low-water seasons, sediment concentrations are small. Therefore, sediment transport was calculated only over flood periods in the modeling.

For modeling purposes, the research reach was divided into 30 sections and 8 stream tubes. Suspended sediment was divided into 4 size fractions, 5, 17.5, 37.5, and 85 μm . The original percentage of size fractions of the bed material was equally set for each size

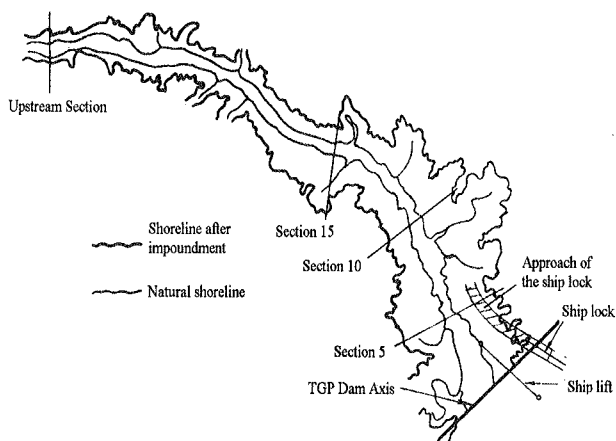


Figure 4.6: Sketch of the TGP Reservoir showing the calculation domain in present work. After Zhou (1995) [185].

fraction. The discharge and sediment concentration variations with time at the upstream boundary were given by a one-dimensional mathematical model. A minimum discharge value of $15200 \text{ m}^3/\text{s}$ and a maximum value of $55900 \text{ m}^3/\text{s}$ were used in the computation. The concentration of suspended sediment inflow varied from 0.022 to 4.25 mg/l . The median diameter of suspended sediments varies from 0.007 mm to 0.038 mm (Figure 4.7) [185].

The focus of the present study is to see how the reservoir bed elevations and cross section areas will change after 76 years of reservoir operation. The accumulated deposition over this 76-year period is shown in Figure 4.8.

From this figure it can be seen that during the first $45 \sim 50$ years of impoundment, the reservoir traps a large amount of sediment. After that the deposition volume curve reaches a plateau indicating that a balance of sediment inflow and outflow exist at this point. This can also be seen in Figure 4.9, which shows the changes in cross sectional areas. The flow cross-sectional areas decrease rapidly in the first 32 years of operation. After 76 years of operation, the Reservoir will have trapped a large amount of sediment and the flow cross-sections areas along the river will not vary much in the study reach. The predicted results agree well with the data measured in the river model for both deposition volumes and cross section area changes below the elevation of 145 m (Flood Control Level).

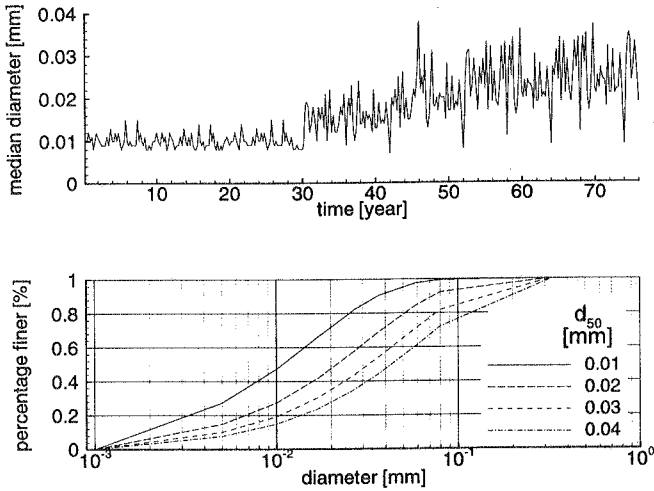


Figure 4.7: Median diameter and grain size distribution of suspended sediment inflow used for present work.

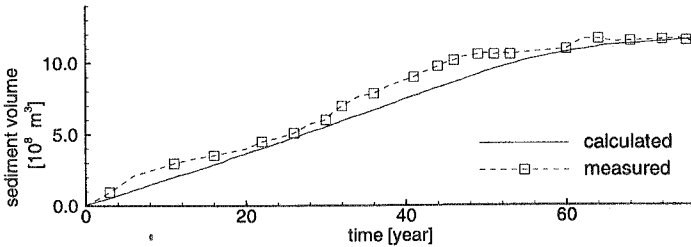


Figure 4.8: Comparison of accumulated deposition volumes over the 76-year period of calculation predicted and measured in the river model.

The measured and simulated changes of several cross sections due to deposition are given in Figure 4.10. After 32-years of operation, the bed elevation will rise from the original level, which is near the sea level, to above 60 m. The measured and simulated bed elevation changes are in good agreement. These test results imply that the present nonuniform sediment transport model can describe the fractional deposition and erosion processes well within reservoirs under unsteady flow conditions.

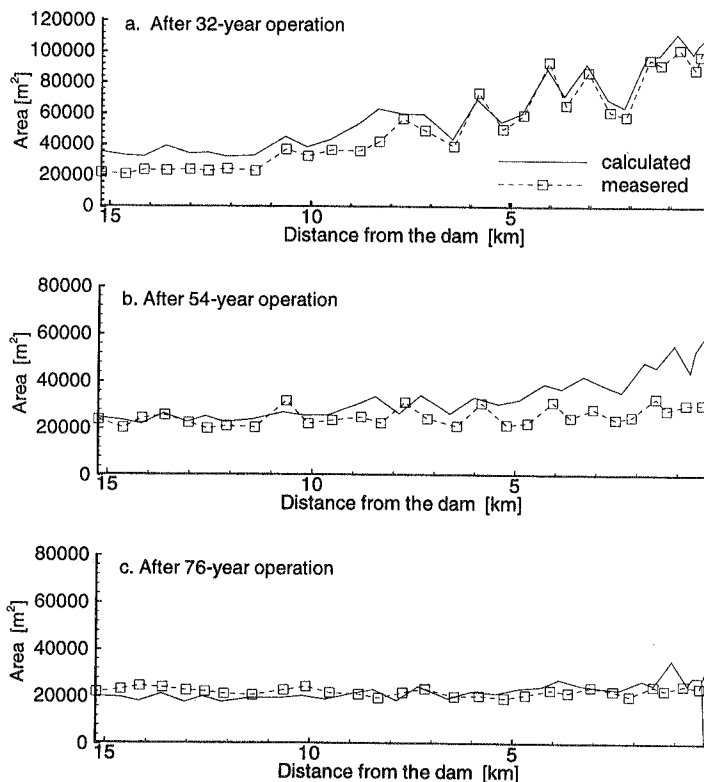


Figure 4.9: Changes in cross sectional areas along the river course below 145 m (FCL) during operation.

4.2 Field study in the Lauffen Reservoir on the River Neckar

In this section the numerical model of suspended sediment transport for uniform sediment is applied to the Lauffen Reservoir on the River Neckar. After calibration of the model using field data, predictive calculations over a period of 50 years were carried out to assess possible changes in river morphology during the next decades. The nonuniform sediment transport model is also applied to the Lauffen Reservoir to study the effect of selective

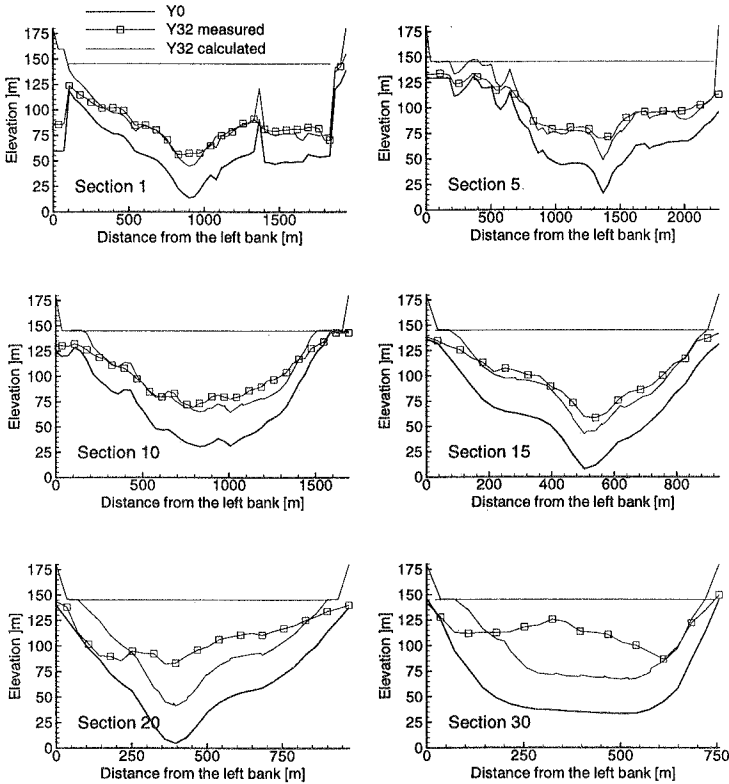


Figure 4.10: Changes in the cross sectional areas below 145 m (FCL) during operation.

transport in rivers.

4.2.1 Description of study reach

The Lauffen Reservoir is located between Stuttgart and Heilbronn, on the middle reach of the River Neckar, in Germany (Figure 4.11). It stretches from Besigheim (km 136.8) to Lauffen (km 125.2). The maximum discharge measured at the gauging station at Lauffen is $1650 \text{ m}^3/\text{s}$, the minimum discharge $14.1 \text{ m}^3/\text{s}$ and mean discharge $88.5 \text{ m}^3/\text{s}$. The water surface elevation at the Lauffen Reservoir is 169.79m. The mean suspended sediment con-

centration measured at Lauffen is 33 mg/l . The annual erosion of the 7916 km^2 drainage basin varies from 7.4 t/km^2 to 70.9 t/km^2 with an average value of 33 t/km^2 [41]. The Enz River discharges into the River Neckar, downstream of the Besigheim Power Station. The mean discharge of the Enz River is $20.8 \text{ m}^3/\text{s}$.

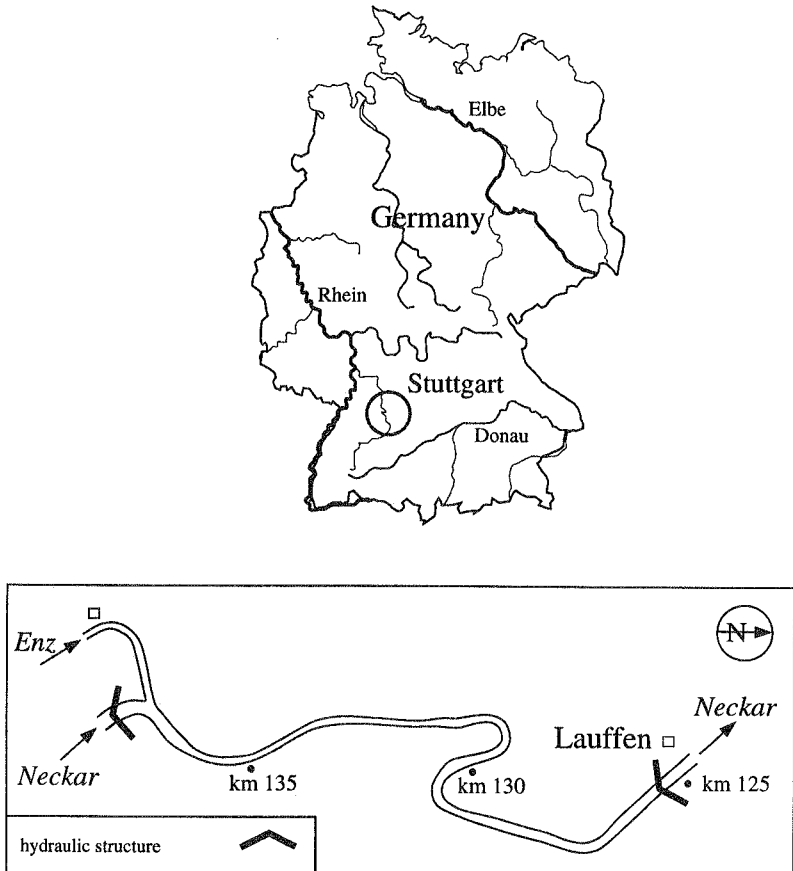


Figure 4.11: Plan of the Lauffen Reservoir from Besigheim to Lauffen.

The Lauffen Reservoir was built in 1938. Since 1950 the suspended sediment inflow decreased considerably due to the construction of 13 cascade dams upstream. The river bed profiles in the Lauffen Reservoir were measured by the Water and Navigation Authority in

1950, 1972 and 1974, and in 3/1981, 3/1984, 8/1989, 6/1991, 8/1992, 3/1994 and 10/1994.

According to the measured data the changes in mean river bed elevations varied along the river course with the maximum changes occurring between 125.2 and 126.0 km. Over the period of 1950 to 1973, sediment was deposited to a height of about 2 m in the region near the dam between 125.2 km and 130.0 km. However, after 1973 erosion occurred often in this region during flood events and sediment deposition only occurred between 3/1984 - 8/1989. The volume of material deposited or eroded in the reach from 125.2 to 130.0 km varied from time interval to time interval. (Figure 4.12). The difference between the sediment and erosion results in the peak discharge during flood events.

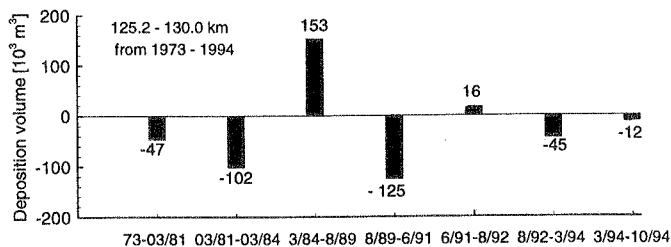


Figure 4.12: Measured deposition volumes (from 125.2 to 130.0 km) during the period of 1973 - 1994. After Kern (1997) [62].

The suspended sediment transport model was calibrated for the period between 1973 and 10/1994, in which many flood events occurred. This period was selected because flood events produce changes in river morphology, determine sediment dynamics and have a considerable influence on the sediment budget. Mean and low discharges control the processes of deposition and should also be considered in the computation.

4.2.2 Calibration of the flow model

The flow model was calibrated using the floods in 05/1978, 02/1990, 12/1993 and 04/1994 at Lauffen Reservoir, in which the maximum discharges were 1630, 1644, 1335 and $1382 \text{ m}^3/\text{s}$, respectively. The flow model was calibrated by adjusting the Strickler-coefficient, k_{st} . The Strickler-coefficient, k_{st} , is necessary to account for the difference in hydraulic resistance, and the additional energy loss during overbank flow. The Strickler-coefficient k_{st} was set as $32 \text{ m}^{1/3}/\text{s}$ in the upstream reaches and increased to $42.2 \text{ m}^{1/3}/\text{s}$ in the downstream

reaches [70]. It was set as $15.4 \text{ m}^{1/3}/\text{s}$ on the flood plains.

The calculated water surface profiles are compared with the measured stages in Figure 4.13 and 4.14. These Figures show that satisfactory reproductions of the water surface elevations are obtained using the flow model.

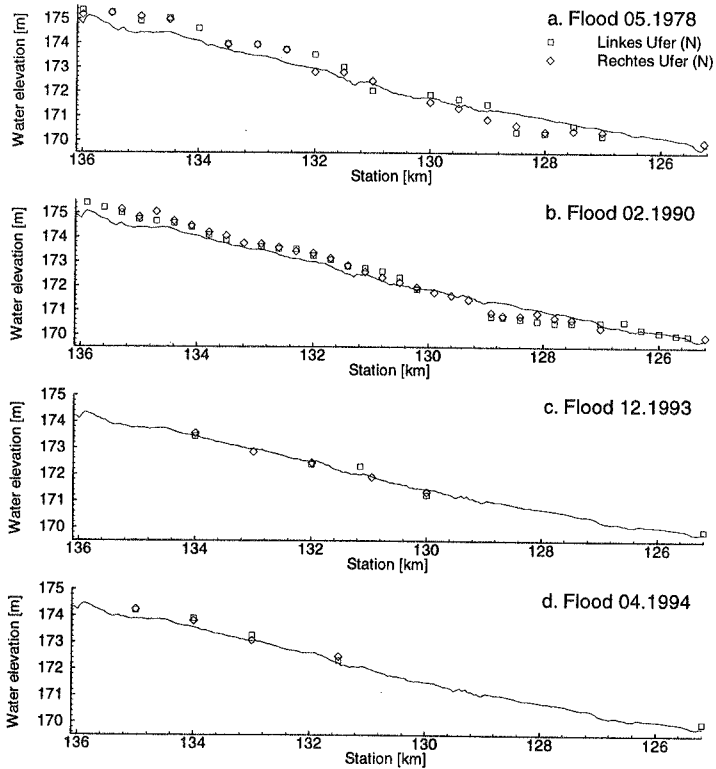


Figure 4.13: Reproduction of water surface profiles for the greatest discharges over the floods of 1978, 1990, 1993 and 1994. Solid line: model calculation, open squares: field measurement.

Accuracy of the flow model was determined by comparing the measured and predicted water surface elevation. The mean value of the relative error is defined:

$$\epsilon_{\Delta h} = \frac{1}{N} \sum_{I=1}^N \frac{|h_{pred.} - h_{meas.}|}{h_{meas.}}. \quad (4.2.1)$$

Table 4.4 shows that the absolute deviations of the value calculated from those measured for discharges during the floods 1978, 1990, 1993, 1994 are very small. The calibration of water surface profiles was not carried out for lower and mean discharge, because there is little measured data available.

Flood events	left bank	right bank
	$\overline{\Delta h}$	$\overline{\Delta h}$
	m	m
05/1978	-.019	-.006
02/1990	-.007	-.014
12/1993	-.001	.004
04/1994	-.027	-.027

Table 4.4: Mean deviation of the water surface elevations calibrated from measured.

4.2.3 Calibration and application of transport model for uniform sediments

Description of input data

Sediment inflow Only a few measurements of the suspended sediment concentration have been carried out at Besigheim over the 22-year calibration period. The sediment inflow will be given by the following functions for the station of Lauffen on the River Neckar [63]

$$C_{s, LN} = 0.005226 \cdot 10^{-3} \cdot Q_{LN}^{1.78024} \quad r = 0.976 \quad n = 350;$$

and for the station of Besigheim on the River Neckar

$$C_{s, BN} = 0.005 \cdot 10^{-3} \cdot Q_{BN}^{1.73} \quad r = 0.944 \quad n = 369;$$

and for the station of Besigheim on the Enz River

$$C_{s, BE} = 0.005226 \cdot 10^{-3} \cdot Q_{BE}^{1.78024} \quad r = 0.849 \quad n = 375.$$

LN, BN and BE represent Lauffen and Besigheim on the River Neckar and Besigheim on the Enz River, respectively. r is the correlation coefficient and n is the number of samples.

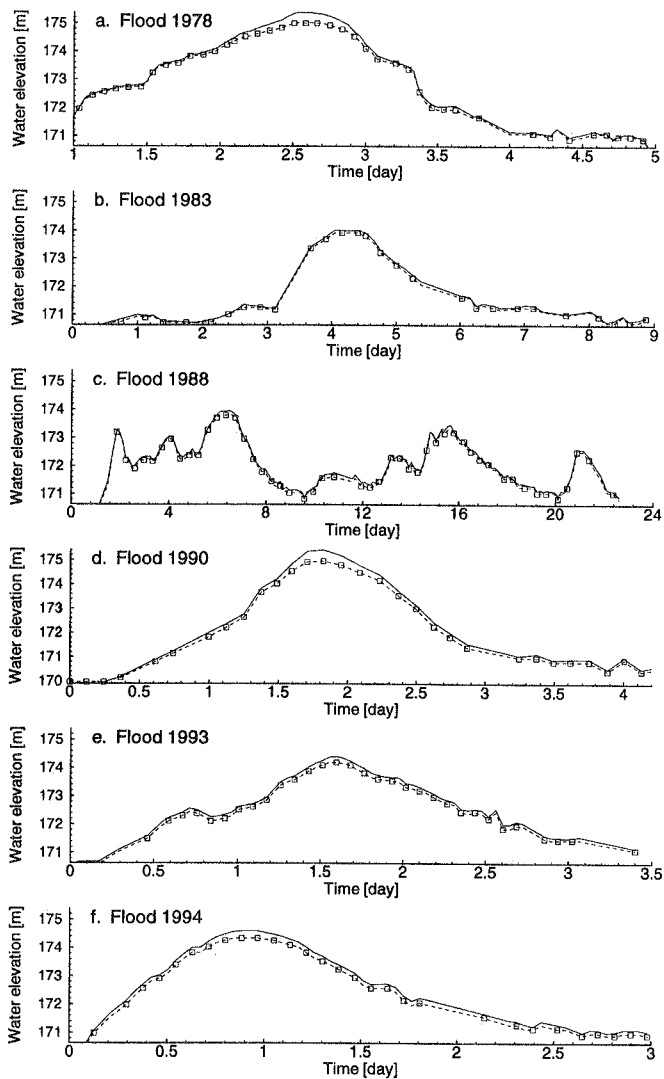


Figure 4.14: Reproductions of water surface elevation at the gauge of Besigheim during the flood events from 1978 to 1994.

The functions were obtained according to data measured during the 1993 flood using the least square method. The discharge and the suspended sediment concentration calculated by the equations above are shown in Figure 4.15 and Table 4.5

Period	at Besigheim Neckar + Enz	at Lauffen
1973 - 03.1981	2298.217	2331.058
03.1981 - 03.1984	1473.956	1591.465
03.1984 - 08.1989	1935.733	2039.389
08.1989 - 06.1991	385.619	441.046
06.1991 - 08.1992	153.430	98.932
08.1992 - 03.1993		
03.1993 - 10.1994	677.828	753.155

Table 4.5: Transported suspended sediment volume (in $10^6 m^3$) over the calibration period

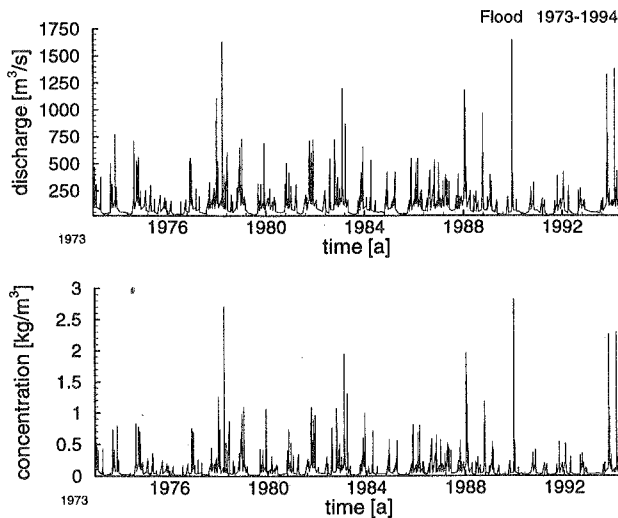


Figure 4.15: Hydrograph and suspended sediment concentration at Besigheim over the calibration period, from 1973 to 1994 [62].

Characteristics of flow parameters Several representative velocity and bottom shear stress profiles along the river are shown in Figure 4.16 b. and c. The velocity varies in the range of 0.1 - 3.8 m/s. Bottom shear stress varies from 0.12 to 65.5 N/m² corresponding to a discharge range from 14 to 1650 m³/s. In the area between 125.2 and 130.0 km, defined here as the lower reach, the bottom shear stress is much smaller than in the area between 130.0 and 136.3 km, defined here as the upper reach. The river bed level changes from 165 to 168 m within the study reach. (Figure 4.16 a.).

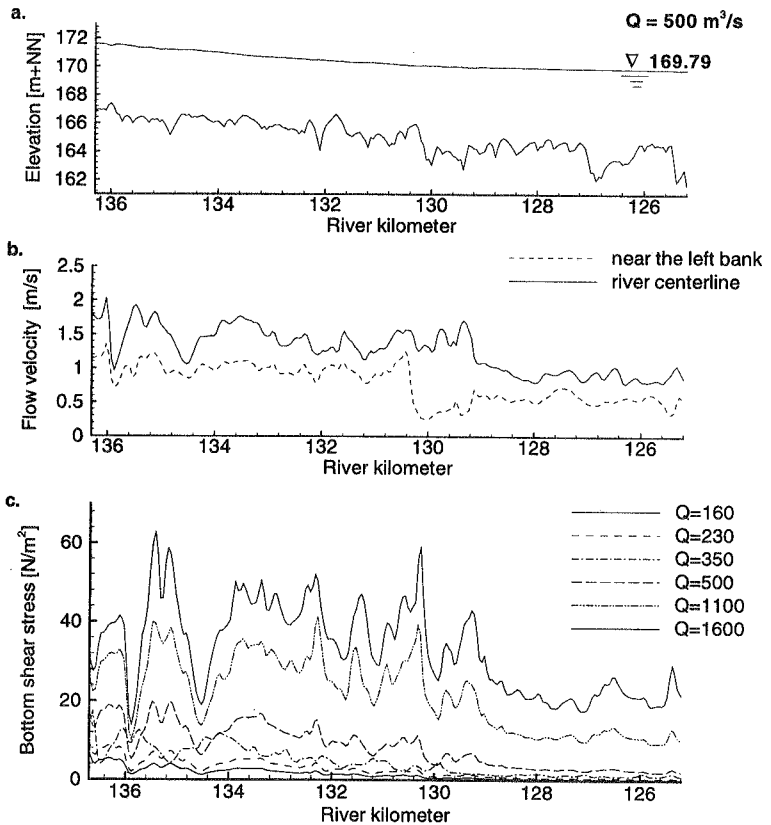


Figure 4.16: Characteristics of flow variables: a. Water surface and river bed profiles in the study reach, b. Velocity distribution along the river ($Q = 500 \text{ m}^3/\text{s}$); c. Bottom shear stress increasing with discharge.

Profiles The profiles measured in 1972, 1974, 1981, 1988, 1989, 1991, 1993, 1994 are used for the calibration of the sediment transport model. The profile of 1973 (combination of the profiles of 1972 and 1974) is used for the initial river geometry in the calibration. The whole calculation domain of 11 km from the station of Besigheim to the Lauffen Reservoir is divided into 12 stream tubes and a number of cross sections with a constant spacing of 50 m.

The sediment mass balance resulting from bed profiles measured over the calibration period, from 1973 to 1994 are given in the Table 4.6.

Period	Deposition volume (125.2 - 130.0 km)	Deposition volume (130.0 - 136.3 km)
	$10^3 m^3$	$10^3 m^3$
1973 - 03.1981	-47	-12.8
03.1981 - 03.1984	-102	-43.00
03.1984 - 08.1989	153	-32.61
08.1989 - 06.1991	-125	-4.07
06.1991 - 08.1992	16	
08.1992 - 03.1993	-45	10.64
03.1993 - 10.1994	-12	-21.47

Table 4.6: Balance of sediment volume based on the measured profiles

Calibrated parameters

The following model parameters were adjusted to fit the simulated volume of deposited sediment to the profile data:

- Erosion coefficient M ,
- Sedimentation coefficient T_k , used to determine the initial condition for deposition,
- Critical shear stress for erosion, $\tau_{c,E}$

All other parameters used were determined directly from the field and laboratory data, as shown in the Table 4.7

parameter	symbol	unit	value
density of fluid	ρ	ML^{-3}	1000
kinematic viscosity	ν	MLT	0.0000101
sediment density	ρ_s	ML^{-3}	2650
sediment bulk density	ρ_p	ML^{-3}	1800
grain diameter	d	L	0.02
sediment fall velocity	w_s	LT^{-1}	0.000345
critical shear stress of erosion, freshly deposited sediments	τ_{cf}	$ML^{-1}T^{-1}$	0.5
critical shear stress of erosion, old deposited sediments	τ_{co}	$ML^{-1}T^{-1}$	3 - 20
longitudinal dispersion coefficient	β_x		0.8
lateral dispersion coefficient	β_z		0.8
coefficient (eq. 3.2.36)	α		0.6-0.24
erosion parameter	M	$ML^{-2}T^{-1}$	0.00075
sedimentation coefficient	T_k		0.005

Table 4.7: Parameters used for the model calibration

According to the model calibration, an erosion coefficient of

$$M = 0.00075$$

and a sedimentation coefficient of

$$T_k = 0.005$$

yield the best results.

In the Lauffen Reservoir the river bed material is composed of cohesive and non-cohesive fine sediments, sand and gravel (with the diameters of $10 - 80\mu m$, $80 - 200\mu m$, $600 - 2000\mu m$ and $2 - 20mm$). Cohesiveness of the very fine particles causes deposited sediment consolidation and compaction with depth and time. It has been observed that only a finite amount of material can be eroded from a fine-grained cohesive sediment bed under a given bottom shear stress [50, 42, 187, 188]. This bottom shear stress is much greater than the

critical erosion shear stress of non-cohesive particles with the same size. The critical shear stress of cohesive fine sediments is related to the time elapsed since deposition and appears as time-dependent compaction. Experiments show that within the first 7 days of deposition the critical shear stress for erosion increases. After 7 days this critical shear stress reaches a maximum value, then remains constant [148] (Figure 4.17). This process is referred to as bed armoring and has been observed and quantified in flume and field experiments by Parchure and Mehta (1985) [104], Tsai and Lick (1991) [148], Graham et al. (1992) [47], Hawley (1991) [50].

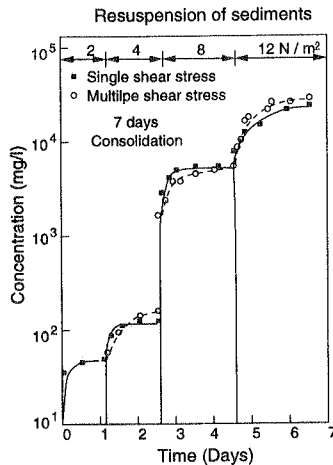


Figure 4.17: Critical shear stress of cohesive sediment. After Tsai and Lick (1987) [148].

In order to compute the suspended sediment transport in the Lauffen Reservoir, the inclusion of both the cohesive and non-cohesive sediment particles in simulation is necessary because 80% of suspended sediment is cohesive, and the remaining part is composed of non-cohesive silt, sand and gravel.

To consider the effect of consolidation of cohesive sediments, a two-layer model is applied. The state of consolidation and the compaction in each layer varies with time. The river bed is divided into two layers (Figure 4.18). The top layer contains the sediments deposited within the last 7 days, the lower one sediment older than 7 days. The former is named the top layer and the latter is called the low layer. The sediments under the bed surface of the original 1973 profiles are considered as older deposition and are included in the under layer.

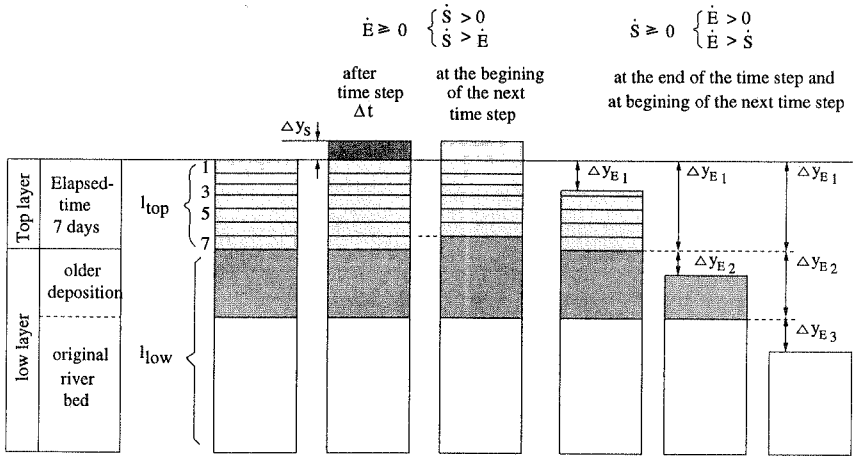


Figure 4.18: Scheme of the two layer sediment model.

The top-layer of material is composed of cohesive and non-cohesive fine sediments. The critical shear stress is determined as the mean value of critical shear stress in the first 7 days after it was deposited. The critical shear stress was studied experimentally by Kern [62]. The top layer of sediments has a density that varies from 1347 to 1422 kg/m^3 and a critical shear stress within the range of 0.5 - 1.3 N/m^2 . Values between 0.5 and 1.25 N/m^2 are used for the top layer in the calibration. If the variation of the critical shear stresses with time is represented by a parabolic line, the corresponding maximum value of the critical shear stress is about 1.5 -3.75 N/m^2 .

The lower deposition layer includes consolidated fine cohesive sediments, non-cohesive fine sediments, sand and gravel. Its critical shear stress is determined as a value that takes into consideration the consolidation effect of cohesive fine sediments and armoring effects caused by sand and gravel. For the lower deposition layer the best model calibration was obtained using a critical shear stress in the range of 3 - 25 N/m^2 . In the upper reach of the study region the larger values for critical shear stress were used because of a large amount of sand, gravel on the river bed surface.

It should be pointed out that the calibrated critical shear stress along the river course nearly coincides with that of the bottom shear stress corresponding to a discharge of about 500 – 600 m^3/s . The bankfull discharge has a recurrence interval 1.5 years [80]. In the study river reach the occurrence frequency of overbank discharge is 700 m^3/s [62]. The bankfull discharge is the 'channel-forming discharge' [5], which occurs and forms the

channel.

Results of calibration and analysis

Distributions of suspended sediment concentration The concentration distributions in longitudinal and transverse directions in the study reach were measured on 23/11/1992 and 02 - 08/03/1994. The calculated concentration profiles are compared with the measured data shown in Figure 4.19 - 4.20. Figure 4.19 shows the concentration profiles calculated and measured on 23/11/1992 along the river centerline at a discharge of $274 \text{ m}^3/\text{s}$. Because the Enz River enters at the left bank of the River Neckar at Besigheim, the concentrations of suspended sediment at this cross section in the two rivers are different and a larger lateral concentration gradient exists. In this area a large amount of lateral dispersion of sediments occurs in a certain distance. The concentration in the river center decreases from 220 mg/l to 160 mg/l within the distance of 1 km downstream of the confluence. It increases from 40 mg/l to 150 mg/l within the reach of 3-4 km along the left bank. This can also be seen in Figure 4.21.

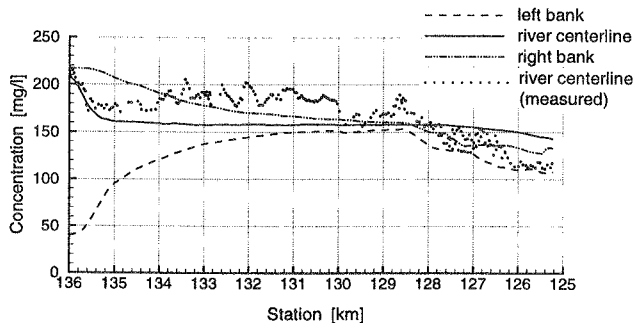


Figure 4.19: Comparison of calculated concentration profiles of suspended sediment with the data measured at 23/11/1992.

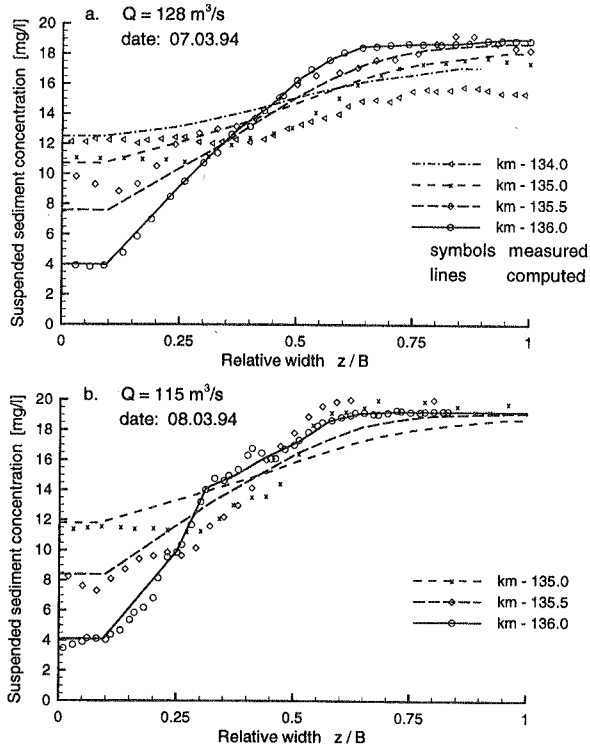


Figure 4.20: Comparison of calculated lateral concentration distribution of suspended sediment with the data measured at 07/03/1994 and 08/03/1994.

The calculated lateral concentration distribution is compared with the distribution measured on 07-08/03/1998 in Figure 4.20. In the area between 135.0 and 136.3 km, the model reproduced the changes in lateral dispersion of suspended sediment concentrations measured in the river. At the station at 134.0 km, the computed concentration is a little larger than the data measured on 07/03/94/. At this section the lateral distribution of concentration is approximately uniform.

Figure 4.21 a. shows the two dimensional distribution of suspended sediment concentrations for a discharge of $274 \text{ m}^3/\text{s}$. The sediment concentrations coming from the Enz River and the River Neckar are very different, the lateral distribution of the concentration at the Besigheim is non-uniform. The larger lateral dispersion of sediment due to the differential

concentration occurs. Figure 4.21 b. illustrates the grid for computation, in which the element boundaries in the longitudinal direction coincide with the boundaries of stream tubes.

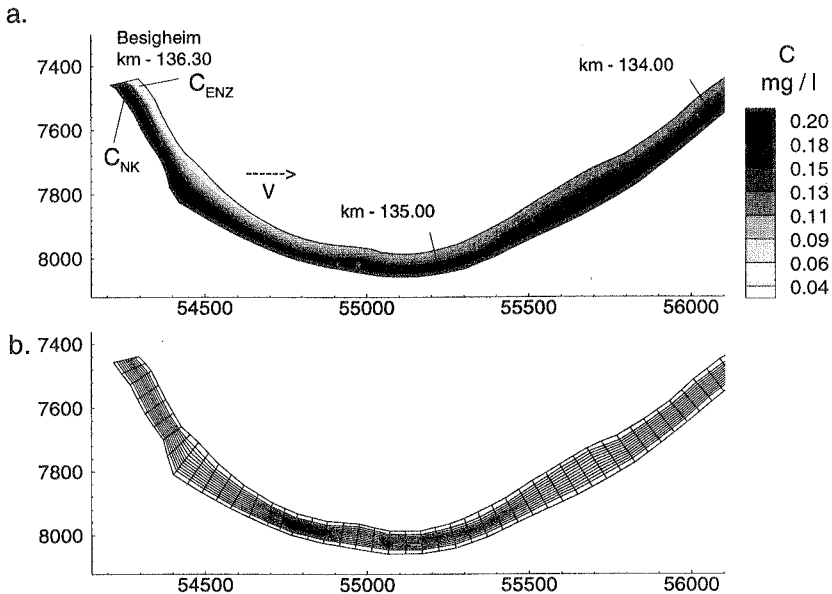


Figure 4.21: a. Concentration distribution of suspended sediment calculated, b. Grid for computation.

Mass balance of suspended sediment transport Over the 22-year period used for calibration, many flood events occurred. During these floods a large amount of sediment, as both bed-load and suspended load, was transported into the study reach. Some of this sediment was deposited in the sand and gravel trap near Besigheim between 135.7 and 136.3 km, while the rest was transported further downstream. During the floods, flow in the upper reach between 130.00 and 136.3 km can carry a larger sediments as suspended sediments. For example, sand with a diameter of 2 mm is expected to be carried in suspension when the discharge is beyond 300 m³/s because the parameter of $\frac{w_s}{\kappa U_*}$ is smaller than 2.0. Therefore, in this reach the deposited sediments contain larger particles.

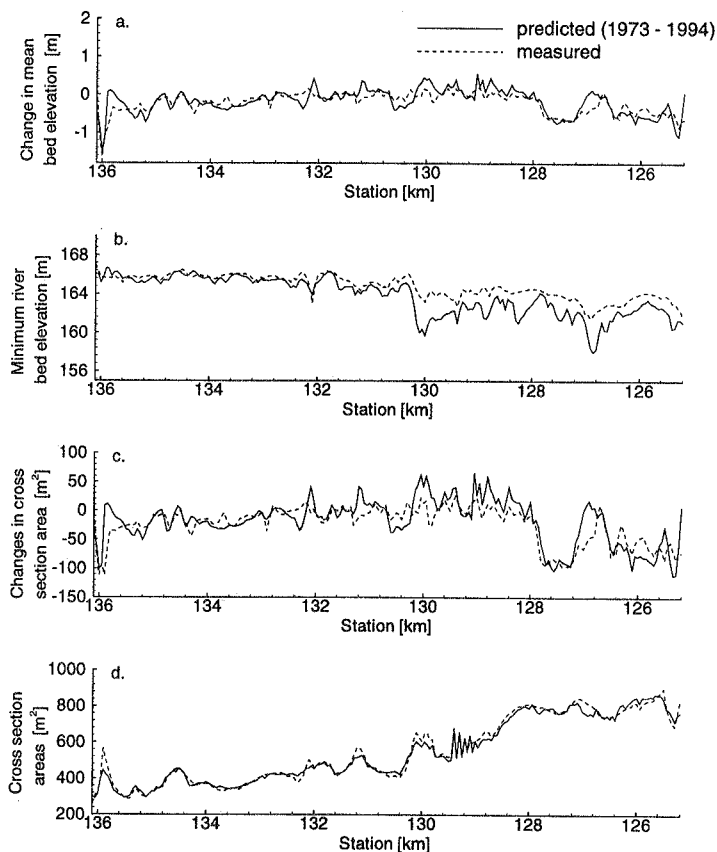


Figure 4.22: Comparison of the calculated and measured data: a. Changes in average river bed elevation; b. Changes in the minimum river bed elevation; c. Changes in cross-sectional area; d. Changes in bankfull cross-sectional area over the calibration period, from 1973 to 1994.

During the calibration period, from 1973 to 1994, the sediment inflow was evaluated as $6.78 \cdot 10^6 \text{ m}^3$ and outflow as $4.03 \cdot 10^6 \text{ m}^3$. According to the profile data measured in 1973 and 1994, $166 \cdot 10^3 \text{ m}^3$ of sediment was eroded between 125.2 and 130.0 km and $88 \cdot 10^3 \text{ m}^3$ between 130.0 - 136.3 km.

The comparisons of the calculated sediment volume with measured data have been carried out. The total mass balance calculated is in good agreement with the data measured according to the measured bed profiles between 1973 and 1994. The erosion volumes account to 167.16 and 166.74 m^3 in the reach from 125.2 to 130.0 km , and 90.51 and 88.63 m^3 in the reach 130.0 to 136.3 km . Over the 22-year period calibrated, the model predicted that $255 \cdot 10^3 m^3$ of bed material would be eroded from the Lauffen Reservoir.

Figure 4.22 shows a comparison of calculated results with measured data, including changes in average bed elevation, bankfull cross-sectional areas and the minimum of the river bed elevation. Agreement between observation and simulation was found to be good. The results in Table 4.9 and 4.8 were quite satisfactory.

Station	1973	Changes in average river bed elevation, m			
		1994 (meas.)	1994(cal.)	$\Delta Y[m](meas.)$	$\Delta Y[m](cal.)$
133.000	165.730	165.659	165.560	-.170	-.071
132.000	165.747	165.639	165.870	.123	-.108
131.000	165.250	165.272	165.220	-.030	.022
130.000	163.070	162.754	163.200	.130	-.316
129.000	164.050	164.406	164.020	-.030	.356
128.500	164.470	164.317	164.410	-.060	-.153
128.000	164.170	164.081	164.540	.370	-.089
127.000	162.600	162.579	161.920	-.680	-.021
126.000	164.160	163.809	164.040	-.120	-.351
125.500	164.540	164.180	163.850	-.690	-.360
125.200	161.640	161.602	161.550	-.090	-.038

Table 4.8: Change in average river bed elevation in the Lauffen Reservoir from 1973 to 1994.

The figures above indicate that the model can predict the net erosion and net sediment amounts with reasonable accuracy. The accuracy of the sediment transport model was quantified using the absolute value of relative error (eq. 4.2.1) of river bed changes. The average relative error of the changes in the cross section areas for all of the study domain was 4% with a range from 0.1% to 15%.

Analysis

station	changes in bankfull cross section area		bankfull cross section area
	1994(measured)	1994(calculated)	1973(measured)
133.000	1.75	-2.77	401.9
132.000	3.82	-9.26	447.5
131.000	12.75	-3.64	478.4
130.000	32.57	13.90	620.6
129.000	47.78	23.42	634.4
128.500	13.28	-16.83	701.0
128.000	17.42	-8.16	806.6
127.000	21.26	-64.94	774.7
126.000	-23.63	-47.49	772.2
125.500	-3.56	-85.16	813.8
125.200	13.68	-72.88	770.1

Table 4.9: Changes in bankfull cross-sectional areas (in m^2) in the Lauffen Reservoir from 1973 to 1994.

Relationship of discharge, bottom shear stress and deposition and erosion rates

When discharge is greater than a certain value, the bottom shear stress is larger than the critical shear stress of erosion, and erosion takes place. In the calculation domain this value was about 500 - 600 m^3/s . The probability of a discharge larger than 550 m^3/s is about 1.4% according to data measured from 1950 to 1994 at the study field. This means that over one year erosion will only occur for about 4.5 days. The relationship between discharges, erosion and sedimentation rates are shown in Figure 4.23 a. and b.

The deposition rate depends on the concentration of suspended sediment and the relationship of bottom shear stress and the initial condition of deposition. According to the calculation, the deposition takes place rapidly at all flow rates at the downstream reach. The deposition rate first increases up to a maximum value with increasing discharge and then decreases with increasing discharge (Figure 4.23 b.). The reason for the decrease in the sedimentation rate may be that the discharge is large enough to keep sediments in suspension.

Erosion coefficient and deposition parameter The erosion rate is sensitive to the erosion coefficient, M , and critical shear stress, $\tau_{c,E}$, (eq. 3.2.32). The erosion rate increases with increases in the coefficient M and decreases with increasing critical erosion shear

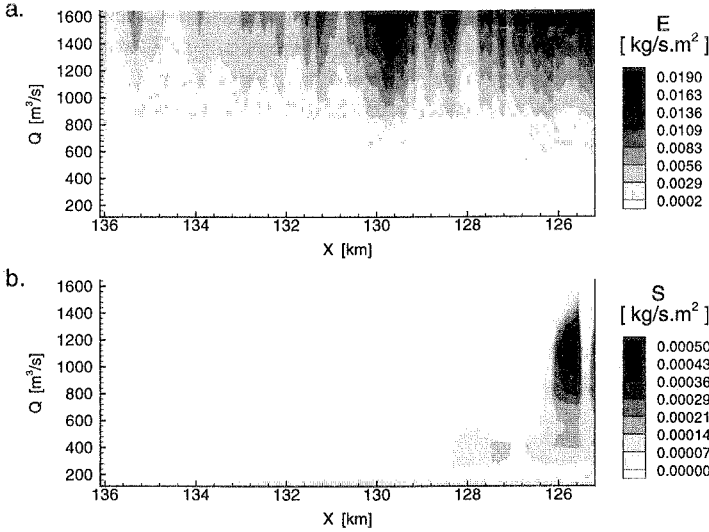


Figure 4.23: Relationship of discharges, deposition and erosion rates along the river centerline.

stress. The comparison showed that as M increased from 0.0014 to 0.0015, the calculated erosion volume increased from $110 \cdot 10^3 \text{ m}^3$ to $139 \cdot 10^3 \text{ m}^3$ (by 26%) for the 22-year calibration period. In principle, critical shear stress can be determined by the sediment type of the river bed. The erosion coefficient is often difficult to determine and it should be determined by experiments or calibration calculations.

The sedimentation rate is related to concentrations, particle fall velocity and the critical shear stress required to initial deposition of suspended sediments. The critical shear stress is sensitive to the parameter T_k ,

$$\frac{1}{\tau_{c,S}} \frac{\rho_s - \rho}{\rho} \frac{ghw_s C}{U}.$$

As T_k increases, the sediment transport capacity of flow increases and deposition decreases. The influence of T_k on the change of river bed elevation is considerable. A good calibration should be detailed for these parameters. Our calibration here is limited to the original field data and more detailed analysis have not yet been done.

Number of stream tubes The selection of the number of stream tubes is related to the research problem and the geometry of the study region. Since at Besigheim a large non-uniform lateral concentration and two sharp river bends exist in the research reach, 12 stream tubes are used for simulating lateral mixing, non-uniform lateral distribution of the concentrations and sedimentation and erosion. In order to investigate the influence of the stream tube number on the calculation results, a computation with 4 stream tubes was made. Comparison of results for 12 stream tubes (case 1) with that for 4 stream tubes (case 2) shows that the calculated deposition volume in case 1 is larger than that in case 2 during the 209-day period (1994), that included one flood event. The reason may be that the calculated water surfaces have a large difference in the large discharge stage for these two cases. The computation results are given in Table 4.10. The calibration of water surface elevations for case 2 has been done. After calibration the difference of the results for case 1 and 2 decreases considerably. However a large difference in deposition volume still exists between these cases.

number of stream tubes	Water surface elevations (136.3 km [$m + NN$])						Deposition volume [m^3]
	183*	630	1052	1382	1008	283	
12	170.31	172.20	173.68	174.64	173.53	170.76	39 090
4	170.32	172.27	173.97	175.07	173.73	170.75	10 620
4**	170.25	172.05	173.66	174.76	173.46	170.65	25 040

* Discharge in [m^3/s]

** Corrected water surface

Table 4.10: Influence of the number of stream tubes selected on the calculated total sediment volume and the calculated water surface level for different discharges varying with time.

Prediction of the bed change in the Reservoir Lauffen in 50 years

The stream tube flow model and the suspended sediment transport model were calibrated using the field data in the Lauffen Reservoir, between 125.2 and 136.3 km. The 22-year simulation of suspended sediment transport in the Lauffen Reservoir indicated that the suspended sediment transport model can reproduce the lateral dispersion and distribution of suspended sediment concentration, and simulate the changes in river bed elevation, and the net erosion and net sedimentation areas with reasonable accuracy. These results prove

that the suspended sediment transport model can be used to confidently predict future changes in river bed elevations due to erosion and deposition.

Prediction of hydrograph in 50 years, from 1995-2045 A long term prediction of suspended sediment transport is an important objective in numerical modeling of the evolution of river morphology. River morphology changes are dominated by discharges. A long time series of discharge is necessary for prediction.

The hydrologic variable, discharge, is recorded as a time series. For example, a daily series of discharge is often considered as a realization of a stochastic process. With the help of models of the time series, one can obtain the future values of the series. These predicted values will have a similar stochastic profile as the original measured series.

For the prediction of changes in river bed elevation in the Lauffen Reservoir, the discharge for the next 50 years is predicted by the stochastic method (TIPS-structure, Yevjevich, 1984, 1987). In the method of TIPS, the daily precipitation and daily runoff series has four basic structural characteristics: tendency, intermittency, periodicity and stochasticity. A prediction value is generated by a sum of the effects of the four terms.

In the present work the model of GENESIS (Generation of Simultaneous Stream Flows; Kron, 1996 [69]) is used to predict daily discharge for long-term simulation of suspended sediment transport in the Lauffen Reservoir.

The time series of discharge between 11/1949 and 10/1994 measured at the gauging station at Lauffen was used to generate the daily discharge for the following 50 years. 10 daily discharge series were generated by Kern [62]. Among these 10 generated daily discharge time series, the one with the second largest peak discharge during the 50-year period was selected for the prediction modeling.

Prediction results The total deposited sedimentation volume in the study reach during the predicted period, from 1995 to 2045 is shown in Figure 4.24. The sedimentation volume increases during low discharge and rapidly decreases during the flood events. Over this period about $1.1 \cdot 10^6 \text{ m}^3$ sediment is eroded from the study reach. It is much larger than the value evaluated according to the eroded volume over the calibrated period. However, it is reasonable, since the maximum daily discharge used ($1745 \text{ m}^3/\text{s}$) was larger than the maximum daily discharge ($1490 \text{ m}^3/\text{s}$) during the calibration period. The predicted results are sensitive to the peak discharge of the generated daily discharge series but not to the total discharge runoff [62]. This indicates that the model works realistically and accurately. Figure 4.24 gives two curves corresponding to the river reach from 125.2 to

130.0 km and from 125.2 to 136.3 km. The difference between two curves shows the volume deposited in the reach from 130.0 km to 136.3 km.

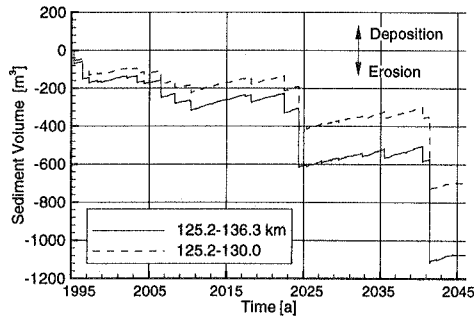


Figure 4.24: Deposition volume versus time during the prediction period.

Changes in river bed elevations and water flowing areas are given in Figure 4.25. The average decrease in the river bed level over the whole research region is about 1 m and the average increase of the cross section area is 110 m². The cross section area increased by a mean value of 23 m² according to the measured profile data of 1973 and 1994. The predicted average change in cross section area for 1995 - 2045 is 4 times as large as the measured data for 1973 - 1994.

Prediction of the deposition volume on the flood plains

When overbank flow occurs, there exists a transfer of momentum between the deep, faster flow of the main channel and the shallow, slow flow of the flood plain. The energy transfer is accompanied by suspended sediment flux from the channel to the flood plains. Here rapid settling occurs as flow velocity and transport capacity diminish.

The proportion of the length of flood plains to the active channel varies with river type and planform. Within the 11 km long study domain of the Lauffen Reservoir, there is a river reach of 5 km with flood plains. A large flood plain area exists in the reach from 133 km to 130 km with two bends. A calculation of sedimentation volume deposited on the left and the right flood plains over a 5-year period including 3 floods events has been made. The dispersion coefficient obtained by flume study of James were used. The other parameters are the same as those used in the model calibration.

Figure 4.26 shows that sedimentation on the flood plain occurs only when the discharge

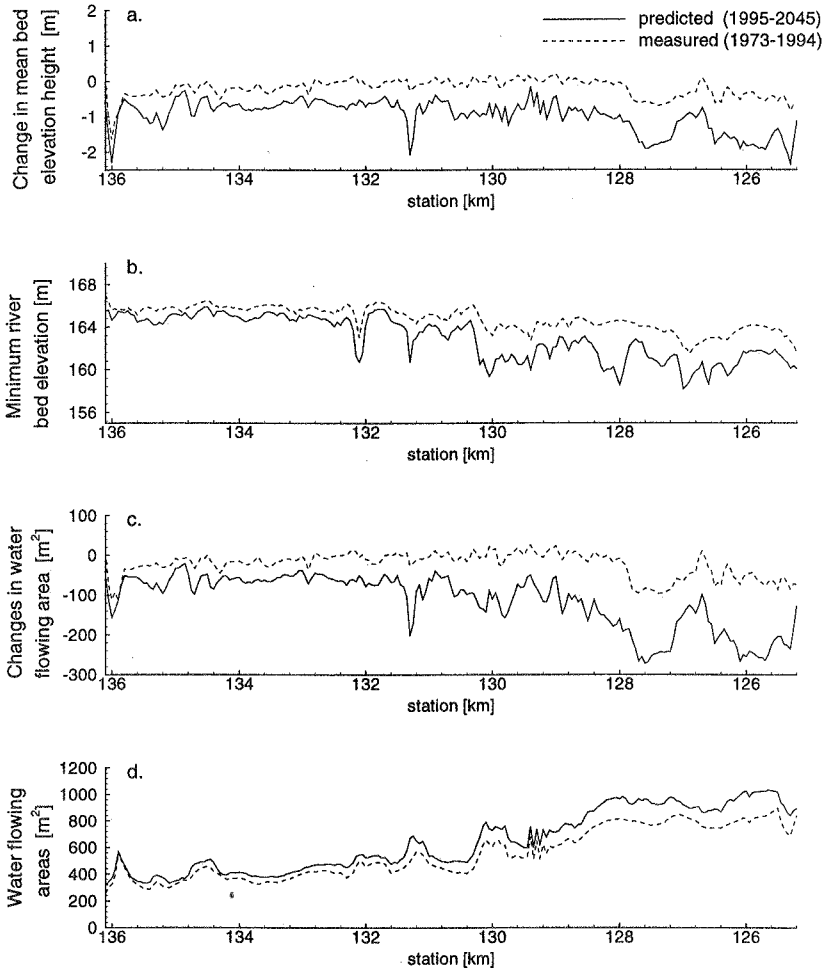


Figure 4.25: Comparing the calculated and measured data: a. Changes in the average river bed elevation; b. Changes in the minimum river bed elevations; c. Changes in cross-sectional area; d. Changes in the bankfull cross-sectional area over the prediction period, from 1995 to 2045.

exceeds $600 \text{ m}^3/\text{s}$. This discharge has a frequency of 1.45 years. The predicted value is nearly the same as the value of the discharge observed on the field [80, 120].

Since there is few measured data on deposition on the flood plains in the River Neckar, a comparison of calculated with measured results has not been made. However, the deposition tendency on the flood plain can be clearly seen. According to the calculation over the study period the deposition volume on the left and the right flood plains was estimated at about 2800 and 6100 m^3 , respectively. The total sediment inflow at the upstream boundary during three flood events is $0.57 \cdot 10^6 m^3$, about 47.1% of the total sediment inflow over the predicted 5 years, being $1.2 \cdot 10^6 m^3$. 1.6% of sediment inflow during the flood events was deposited on the flood plains.

A maximum volume of 52 m^3 is predicted to be deposited on the right flood plain within a spacing of 50 m near the station of 130.4 km (Figure 4.26). At this cross section the water surface width of the right flood plain is 70 m and the corresponding average deposition height is 15 cm. The maximum total sediment height over the 5-year period is about 15 cm and the average accumulation rate is about 3 cm per year. The maximum deposition height appears at the station at 129.8 km during the flood of 1989. The maximum sedimentation rate is about 0.003 kg/m^2s at the station at 132.22 km with a discharge of 1300 m^3/s during the flood of 1994.

Figure 4.26 shows that erosion rarely takes place on the flood plain with the exception of the station at 130 km on the left flood plain. This may be because the flow strength, the criterion for erosion, is too low to erode sediments from the river bed on the flood plains.

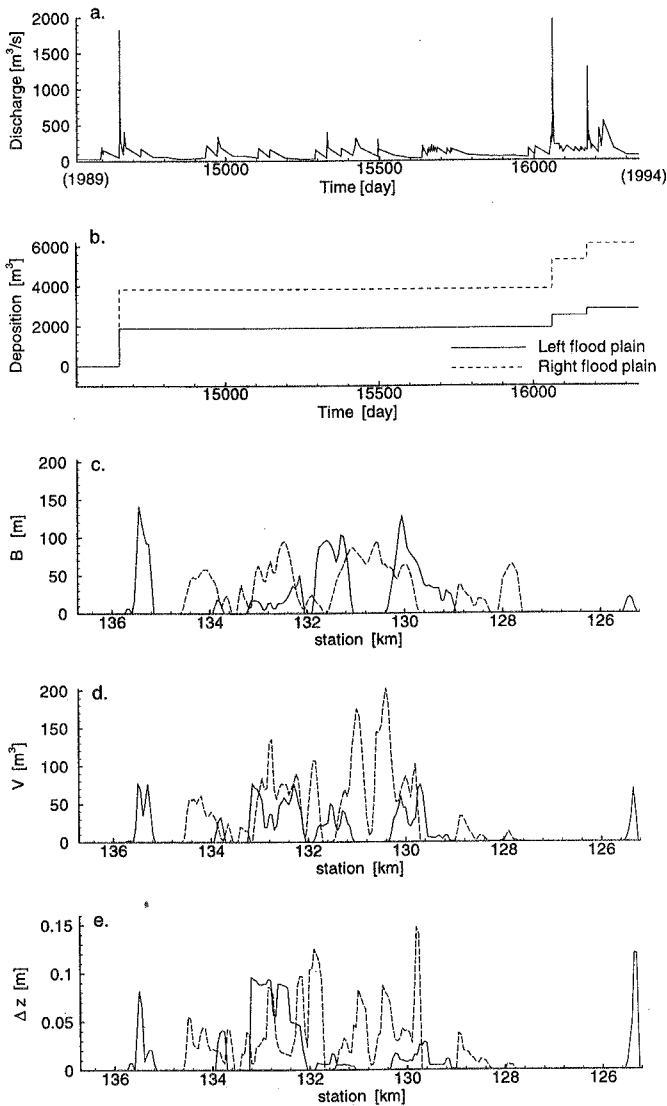


Figure 4.26: Characteristics of overbank flow and calculation of sediment deposition on the flood plains from 1989 to 1994: a. Hydrograph over the calculated period; b. Total deposition volume on the flood plains; c. Maximum water surface width of overbank flow; d. Maximum deposition volume on the flood plains; e. Maximum deposition height from 1989 to 1994.

4.2.4 Investigation of selective transport of nonuniform sediment mixtures

The Lauffen Reservoir on the River Neckar is used here to prove the capability of the numerical model for simulating transport, sedimentation and erosion of nonuniform sediment mixtures accounting for the sorting effect in river channels. Since bed material in the area between 125.2 and 130.0 at the Lauffen Reservoir contains a large amount of cohesive silt, it is not appropriate for the calibration of the nonuniform suspended sediment transport model. However, in the reach between 130.0 and 136.3 the bed materials contains no fine cohesive sediments and therefore can be used for the model study. Here the study focuses on the property of fractional suspended sediment transport without consideration of fine cohesive grains. The trend of grain size distributions on the bed surface and in the transported material are predicted for the whole Lauffen Reservoir. The results for the reach from 130.0 to 125.2 km can only be taken as an approximation. Nevertheless, it is worth understanding the selected transport process for sediment mixtures.

Description of input data

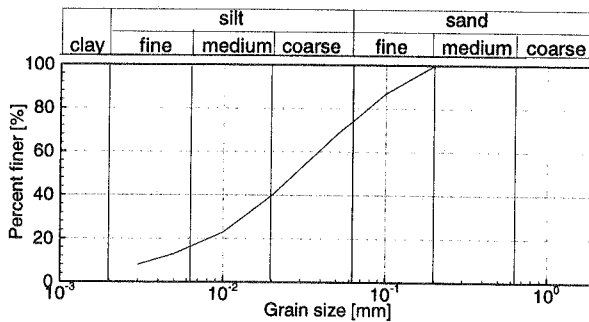


Figure 4.27: Measured grain size distribution of bed material in the Lauffen Reservoir.

The data of the Lauffen Reservoir have already been given in Section 4.2.1. The grain size distribution of the bed material is given in Figure 4.27 [64, 89, 88]. Grain size distributions of suspended sediments were collected by U. Kern [64] for lower discharge stages. The median diameter measured for suspended sediment is 0.02 mm for discharges ranging from 43 - 264 m³/s. There is a lognormal grain size distribution of suspended sediments for normal discharges (Figure 4.28).

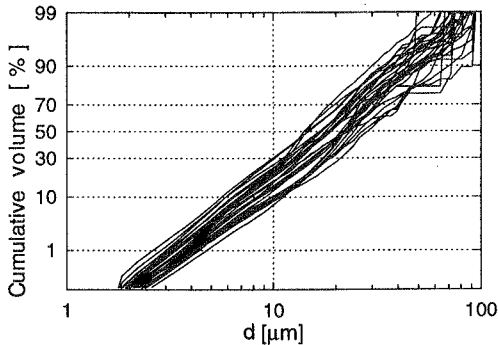


Figure 4.28: Measured grain size distribution of suspended sediment load in the Lauffen Reservoir. After Kern [64].

The grain size distribution of sediment inflow for the low discharge stage is determined according to the field data. It is extended to large discharges based on the assumption that the grain size distribution is lognormal for high discharge stages. The largest particle in suspension during flood periods is taken as the upper limit of the grain size distribution. The median diameter of sediment inflow for the large discharge of $1350 \text{ m}^3/\text{s}$ is 0.08 mm and for low discharges of $350 \text{ m}^3/\text{s}$ is 0.02 mm . For discharges smaller than $350 \text{ m}^3/\text{s}$ the same median diameter of 0.002 cm is used in the computations (Figure 4.29 and 4.30). The values of σ_g for discharges of $1350, 1000, 700, 350 \text{ m}^3/\text{s}$ are $1.1, 1.0, 0.83$ and 0.71 , respectively.

Since only a few samples of the bed material were analyzed, the original grain size distribution of the bed material was assumed for the entire study reach. The grain sizes vary from 0.001 to 3.5 mm , as shown in Figure 4.31 and were divided into 7 size fractions.

Suspended sediment transport is calculated for the 12/1993 flood event. The largest discharge was $1335 \text{ m}^3/\text{s}$. The hydrograph is shown in Figure 4.32.

Calculation results

Grain size distributions in eroded and active-layer material Figure 4.33 describes the relationship of discharges and grain size distributions in eroded and active-layer material. In Figure 4.33, p_{an} and p_{bn} are the percentage of eroded and bed material for grain size fraction n . The difference of grain size distributions between the eroded

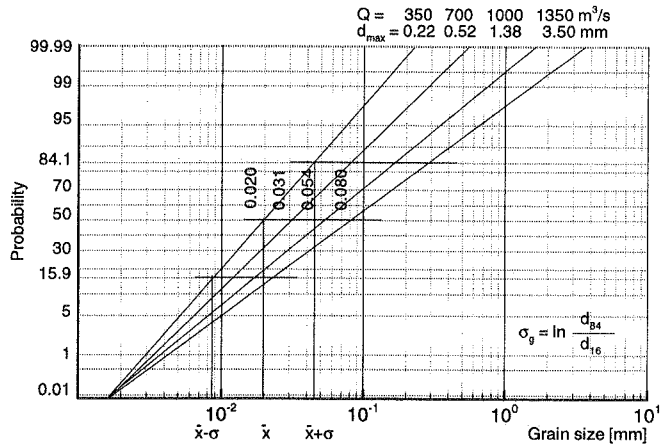


Figure 4.29: Evaluation of the grain size distribution of suspended sediment inflow according to measured data.

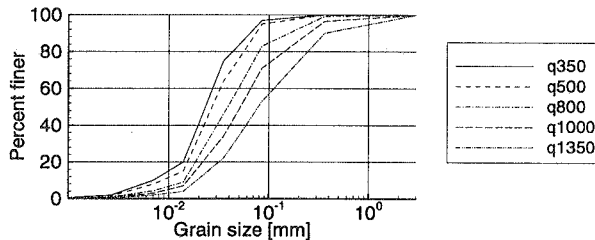


Figure 4.30: Grain size distributions of suspended sediment inflow used for computation.

material and the bed material clearly decreases with increasing discharge. The former is always finer than the latter. Another factor affecting this difference is the sediment supply of the grain size fractions in the active layer.

Since finer particles are more easy to erode than coarser ones, the composition of bed material gradually coarsens and fine sediments are transported downstream where they may be deposited there. The result of this is that the composition of material in the active layer along the river course gradually becomes finer downstream. This evolution of

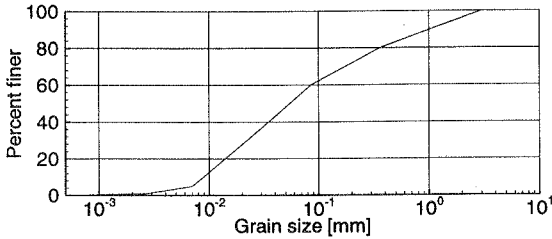


Figure 4.31: Original grain size distribution of bed material assumed for computation.

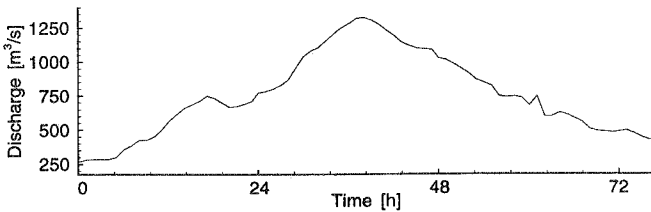


Figure 4.32: Hydrograph of the flood 1993.

the sediment composition in the active layer becomes more and more evident with time (Figure 4.34 and 4.35). The median diameter of bed material decreases from upstream to downstream reaches due to sorting (Figure 4.36).

The variations in the transverse grain size distributions of bed material are small. The cause may be that the transverse velocity distribution is relatively uniform. The larger difference of lateral grain size distributions is only found in the section of the river reach with curves. The distribution of bed sediment in the river center and near the river bank at 130.0 km and the corresponding cross section profile are given in Figure 4.37. One can see that the water depth near the right bank is smaller than at the river center. The median diameter of bed material is 0.045 mm in the river center and 0.03 mm near the left bank.

Deposition and Erosion Volume To investigate the effects of selective transport on the river morphology, grain size distributions of bed material are predicted for three subsequent flood events (with each flood lasting 81h). The results show that the grain size distributions of bed material vary considerably. The composition of active-layer sediment

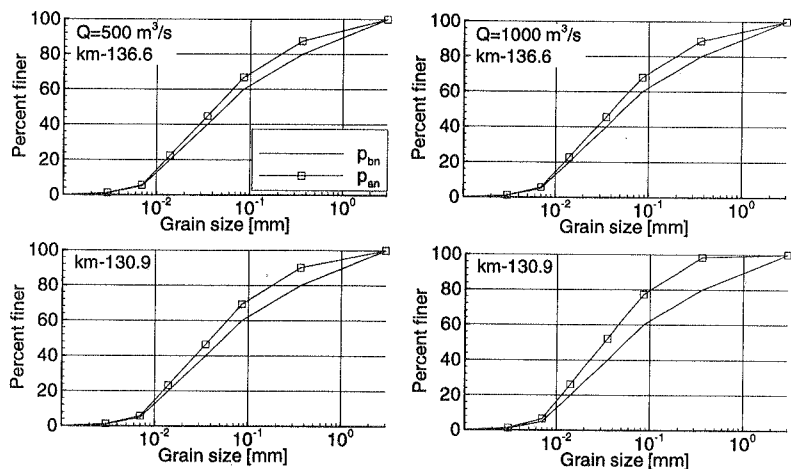


Figure 4.33: Influence of discharges on the grain size distributions of active layer material and eroded material.

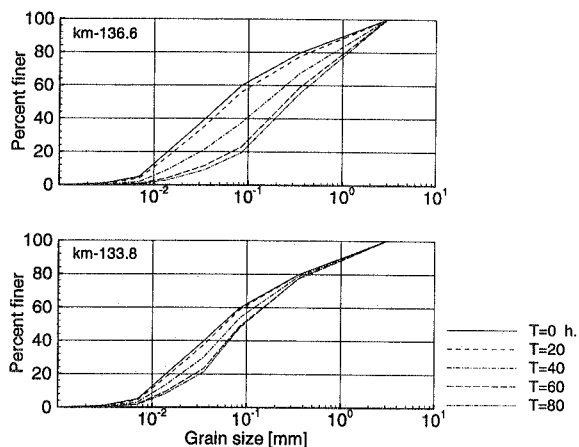


Figure 4.34: Grain size distributions of the active-layer material along the river varying with time.

becomes coarser with time. It lowers the mobility and the availability of sediment and

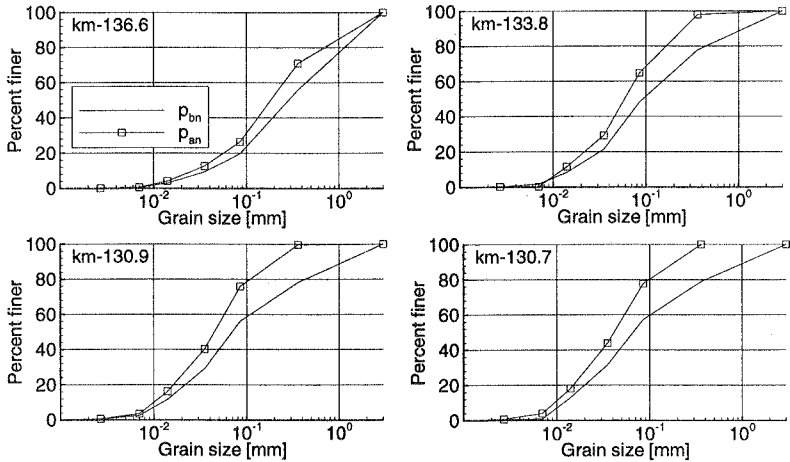


Figure 4.35: Grain size distributions of eroded and active-layer material at selected locations.

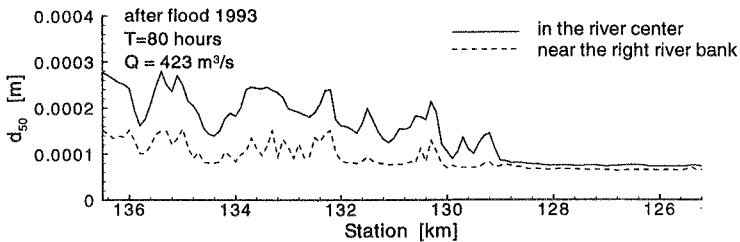


Figure 4.36: Longitudinal distribution of the median diameter of the active sediment layer after the flood 1989.

results in decreases in erosion volumes (Figure 4.38). The erosion volumes during each flood period decrease with time, e.g. $111 \cdot 10^3 \text{ m}^3$, $42 \cdot 10^3 \text{ m}^3$ and $10 \cdot 10^3 \text{ m}^3$ after 1st, 2nd, 3rd simulation flood, respectively. For a given discharge the erosion rate is considerably decreased at the end of the computation comparing with the data at the beginning (by 47% for $Q = 420 \text{ m}^3/\text{s}$ during the first-flood simulation) due to grain size sorting in the active-layer material.

Grain size distribution of suspended sediment load To verify the predicting capability of the nonuniform sediment transport model, the comparison of measured and

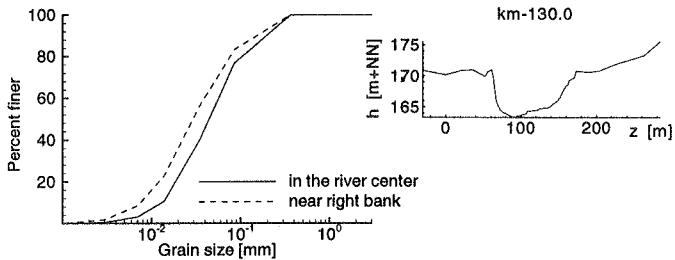


Figure 4.37: Lateral grain size distribution of bed material after the 81-hours calculation.

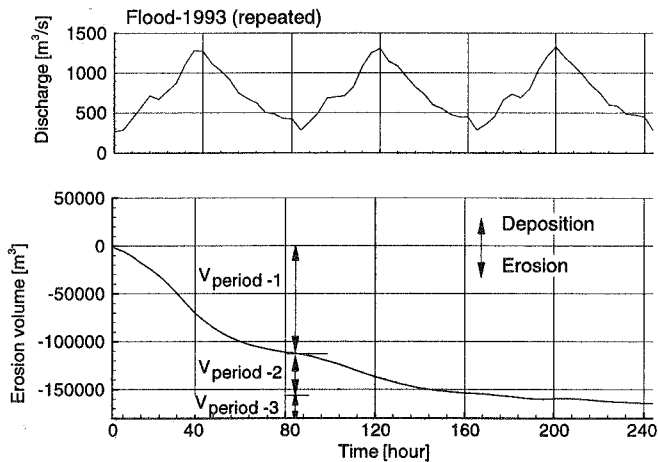


Figure 4.38: Effect of selective transport on the erosion volume.

predicted grain-size distributions of the suspended load have been made (Figure 4.39). The field data were measured during low water stages ($Q = 43\text{--}264\text{ m}^3/\text{s}$) at the station of 125.2 km. The simulations showed that the computed distribution curve of the suspended-load is within the bounds of the measured curves. The computed and measured median grain diameters compare well (0.02 mm computed and 0.022 mm measured). However, for the fraction finer than 0.010 mm , the computed percentages of 25% of suspended-load differs from the measured quantity of 15%. The computed distribution is slightly finer than the mean measured distribution in the field. The reason may be that the high degree

of consolidation of bed material at this position was not in consideration.

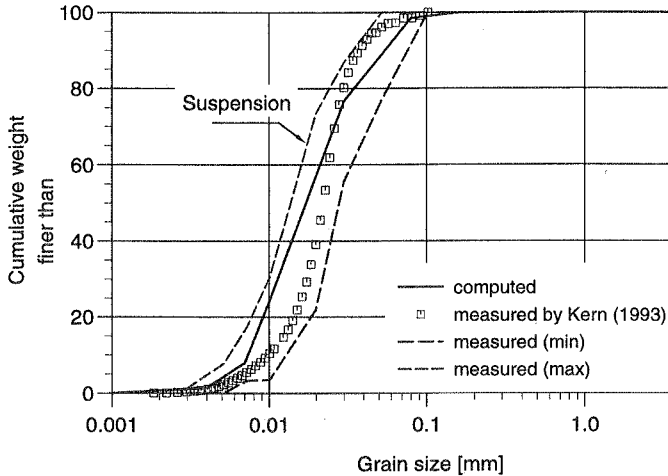


Figure 4.39: Grain size distribution of suspended sediment load at the station 125.2 km on the River Neckar.

The calculation results above indicates that selective transport plays an important role in nonuniform sediment transport processes. It affects the river morphology by changing the compositions of bed material and suspended sediment. Selective sedimentation results in that fine sediment is accumulated on the flood plains and in the reservoirs which will affects the effective storage of reservoir and environmental problems may arise when pollutants are bound to sediments which may be resuspended and transported during future flood events. Selective erosion results in gradually coarsening of sediment particles on river bed surfaces, which protects the under-laying material from movement and decrease erosion at depth. Resistance to flow and water depth vary with changes in friction resistance, as a result of changes in bed material compositions. The present model has an ability for predicting selective transport processes under unsteady flow condition. It can give reasonable prediction and can describe the effect of selective transport on river morphology.

4.3 Sediment exchange between the stream and the dead water zones

4.3.1 Lateral exchange

A two dimensional convection-dispersion equation of suspended sediment transport considering the effects of a dead water zone can be represented as:

$$\frac{\partial hC}{\partial t} + \frac{\partial uhC}{\partial x} + \frac{\partial vhC}{\partial y} = \frac{\partial}{\partial x} (hD_x \frac{\partial C}{\partial x}) + \frac{\partial}{\partial y} (hD_y \frac{\partial C}{\partial y}) + \dot{E} - \dot{S} + Q^* \quad (4.3.2)$$

where Q^* is mass exchange rate between the main stream and the dead water zones. A negative value of Q^* denotes particle transfer from the stream to the dead water zone. A positive value describes the flux in the opposite direction. The other variables are the same as ones in eq. 3.2.29. The variable, Q^* , is related to changes in concentration, sediment and erosion. The formulae used to determine Q^* and the other flow variables for the two cases, with and without submerged groynes, are given in Table 4.11.

variable	low discharge without submerged groynes case a	high discharge with submerged groynes case b and c
U_g	0	> 0
\dot{S}_g	$\zeta U_{\bar{V}}^O C_g$	$\omega_s C_{fg} (1 - \frac{\tau_{fg}}{\tau_{c, Sfg}})$
\dot{E}_g	0	$M(\frac{\tau_{fg}}{\tau_{c, Sfg}} - 1)$
Q^*	$\epsilon U_{\bar{V}}^A (C - C_g)$	$D_{zfg} (C - C_{fg})$
$\frac{dC_a}{dt}$ or $\frac{dC_{fg}}{dt}$	$\epsilon U_{\bar{V}}^A (C - C_g) + \zeta U_{\bar{V}}^O C_g$	$D_{zfg} (C - C_{fg}) + \zeta U_{\bar{V}}^O C_{fg} - M(\frac{\tau_{fg}}{\tau_{c, Sfg}} - 1)$

Table 4.11: Formulae to describe flow, particle exchange, deposition and erosion within groyne fields.

In Table 4.11, U is the velocity, V is the water volume in the dead water zone, A is the interface area through which sediments transfer from the stream to groyne fields or otherwise, O is the horizontal area of the dead water zone, ζ is the sedimentation parameter in groyne fields, ϵ is the transfer coefficient between the stream and the dead water zone, w_s is the sediment fall velocity, and $\tau_{c, Sfg}$ and $\tau_{c, Efg}$ are critical shear stresses for sedimentation and erosion in the groyne field and on the flood plains. The subscript g denotes the groyne field and f denotes the flood plain.

The transfer of mass and momentum occurs at/near the interface between the stream and the groyne fields. Westrich (1977, 1990) [166, 168] suggested that the transfer coefficient of pollution between the stream and the dead water zone be 0.0005 - 0.003. The Alarm model [137] suggested that the coefficient ε be equal to 0.001. Van Mazijk (1996) suggested that the value of ε be related to flow and pollution velocities and a lag coefficient, which was defined as a ratio of cross section areas of the main stream and the dead water zone. For Peclet numbers larger than 10, he suggested values of 0.01 - 0.0001 for ε .

4.3.2 Case study

Case a.

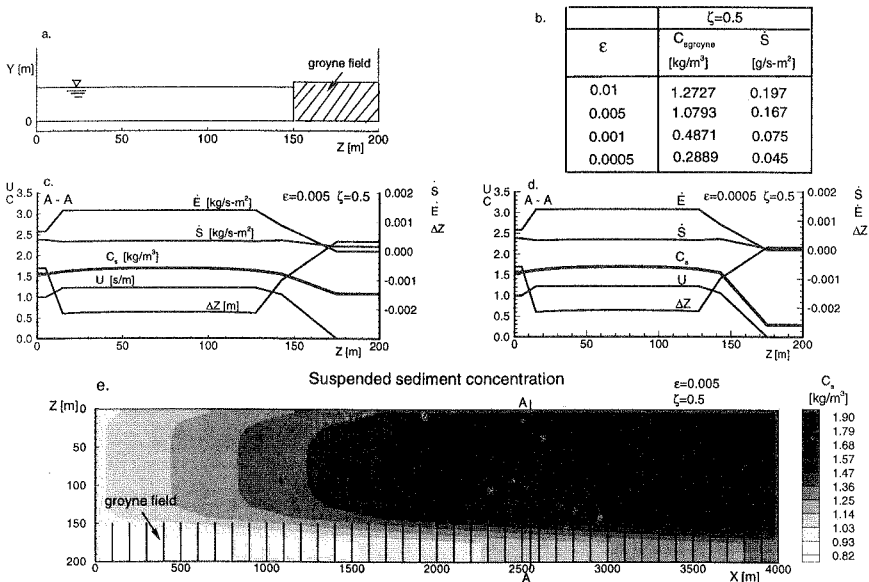


Figure 4.40: Influence of mass exchange coefficients between the stream and dead water zone on the sediment concentration distribution.

The sediment exchange between the main stream and the groyne fields near the bank, as well as deposition and erosion in the groyne fields are calculated for non-submerged and submerged groynes (case a. and case b.). A channel with a rectangular cross section and groynes located along the right bank (Figure 4.40) was considered. The study reach is

4000 m long and 200 m wide. Groynes are 50 m long and 2 m high. The stream without groyne fields is divided into 41 sections and 12 stream tubes. A concentration of 1 kg/m^3 with a uniform lateral distribution was used at the upstream boundary

Several calculations with different mass transfer coefficients, ε , for case a. have been made, as shown in Figure 4.40. The results indicate that the concentrations and sedimentation rates in the groyne field increase with transfer coefficients under a given deposition parameter, ζ . The larger the transfer coefficient is, the larger the concentration in the dead water zone and the larger the sediment volume transferred from the main stream to the groyne fields. The concentration in the main stream increases due to erosion along the flow direction and thus the concentration in dead water zones also increases.

Case b.

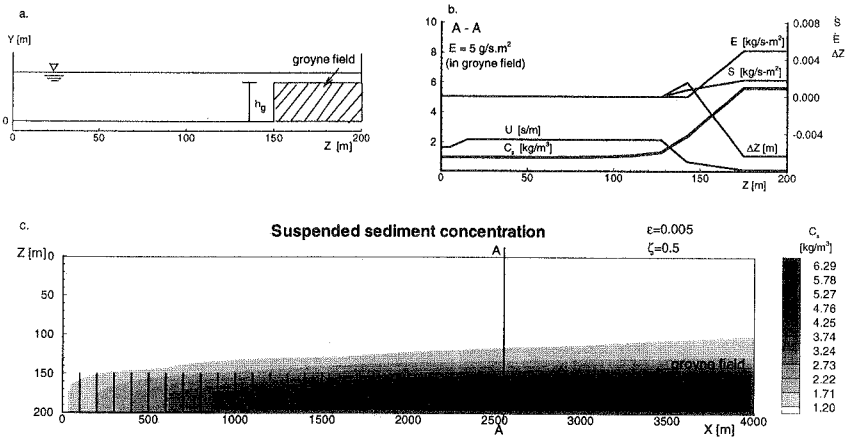


Figure 4.41: Sediment concentration distribution under the condition of a high erosion rate in the groyne field.

Figure 4.41 shows the calculation results for case b. In this case, the groynes are submerged and erosion in the groyne field takes place. Since sediment is eroded from the bed within the groyne field, the concentration in this zone is larger than that in the stream and sediment is transferred from the groyne field into the stream. Lateral dispersion of concentration in the stream can be seen in Figure 4.41c.

Chapter 5

Conclusions and proposals

5.1 Conclusions

River sediment transport processes are often disturbed by natural and human activities, which interferes the natural equilibrium of river channels. During restoration of equilibrium, sediment deposition and erosion often occur. To describe changes in river morphology many numerical models have been developed. The present work investigated the sedimentation and erosion processes in rivers and developed quasi two-dimensional suspended sediment transport models for uniform sediment and nonuniform sediment mixtures. The validations and limitations of the models were studied using data from the physical model tests of James, Samaga and Tsinghua University and by application to the River Neckar. The main conclusions can be summarized as follows:

1. The quasi two-dimensional numerical models for uniform and nonuniform sediment are useful tools for simulating suspended sediment transport processes in rivers. The computation grid and the natural orthogonal curvilinear coordinate system can be automatically generated during the flow calculation with fixed or moving boundaries as discharge changes. This coordinate system avoids the difficulties in dealing with wet-dry boundary problems found when Cartesian coordinate is used to represent a two-dimensional model. It was shown that hydraulic variations calculated by the stream tube model are generally acceptable in simulating river morphological changes for engineering purposes. The mass balance is almost certainly satisfied on each control volume, since the FVM was used for solving the convection-dispersion equation for sediment transport.
2. The uniform sediment transport model was applied to an 11-km reach of the Lauffen Reservoir on the River Neckar. A two-layer model was developed to deal with the complicated composition of bed material, which includes cohesive and non-cohesive soil and coarser bed material. The transport model was calibrated using field data and was then used for predicting river bed changes over a 50-year period, from 1995 to 2045. The prognosis simulation suggests that future bed-evolution will depend strongly on the peak value of discharge rather than the total runoff volume during flood events.

3. In the stream tube flow model, the river is divided into stream tubes whose boundaries are lines with $q_s = \text{constant}$. It can describe a real flow field for an approximately straight river reach. For a river reach with sharp bends or flood plains, the application of the stream tube flow model is limited due to existence of secondary currents.

To consider sediment dispersion caused by secondary currents at the interaction zone between the main channel and the flood plains a formula for calculating such dispersion was developed in the transport model. The grid was refined in the interaction zone to better reflect dispersion in this area. These improved the transport model by making it more applicable and suitable for simulating changes in morphology for river reaches with flood plains. Prediction of sediment accumulation on the flood plains at the Lauffen Reservoir between 1989 and 1994 was carried out using this model. The results show that 1.6% of sediment inflow during the three flood events is deposited on the flood plains. Deposition on the flood plains occurs only when the discharge exceeds $600 \text{ m}^3/\text{s}$. This discharge has a frequency of about 1.45 years, which is nearly identical to the field value observed (1.5 years).

4. The derived fractional erosion formula for simulating nonuniform sediment transport, including considerations of the stochastic nature of incipient motion, available bed material, suspended sediment concentration and fluctuating bed shear stress, is satisfactory for simulating selective transport processes. The successful tests using the data of Samaga's flume experiment and Tsinghua University's physical model are convincing examples.

The mathematical formulations for nonuniform sediment transport used in the model, which include selective transport, fractional erosion and sedimentation, the concept of the active layer and bed material sorting procedures, work well for unsteady flow conditions. The field study at the Lauffen Reservoir indicated that selective transport varies temporal and spatial grain size distributions of suspended sediment and bed material with changes in flow conditions, which directly influences sedimentation and erosion rates and changes river geometry.

5. The transport model for uniform sediment is appropriate for simulating or predicting long-term changes in river morphology. The uniform sediment transport model uses one representative grain diameter for both suspended load and bed material and hence is suitable for simulating river bed changes where the bed material contains slightly graded sediments. However, sediment in natural rivers is composed mainly of nonuniform sediment. Selective transport, fractional erosion and deposition, dominates nonuniform sediment transport processes. It affects changes in river geometry by varying the compositions of bed material and suspended sediment. A nonuniform sediment transport model is a useful and essential tool for river management purposes to investigate the effect of selective transport, improve our grasp

of this physical process and predict changes in river geometries realistically and correctly. A nonuniform sediment transport simulation requires more computer storage and computation in comparison with the uniform sediment transport simulation. With the fast development of computer technology these difficulties may soon be overcome.

5.2 Proposals

The tests and applications of the transport models for uniform and nonuniform sediment show that the models are widely applicable and suitable for simulating morphological changes in rivers. However, the models can be improved to increase the accuracy of predicted results through the following work:

- Sedimentation on flood plains results from sediment exchange due to convection and dispersion at the interface between the main channel and the flood plains. It will be necessary to carry out experiments to determine the coefficient, α , in the sediment dispersion formula.
- Frictional resistance will vary with composition changes in bed material during the sorting procedure. Resistance to flow influences the calculated water surface level which in turn influences the sediment transport simulation. It is essential that a variety of frictional resistance values be used where the bed material is obviously sorted, coarsened or fined.
- The model presented here could possibly be improved by also considering bed-load transport in the transport model. In natural rivers the bed-load component can be significant. Most of the river bed material consists of largely graded sediments. Selective transport has an extreme effect on the nonuniform sediment transport process and changes in river morphology. For example, bed armoring, one of the more important consequences of selective transport, limits erosion amounts. This may form a stable coarse armor layer and generate a corresponding stable bed slope.

Reference

- [1] P. Ackers and W.R. White. Sediment transport: a new approach and analysis. *Journal of Hydraulic Engineering, ASCE*, 99(HY11):2041–2060, 1973.
- [2] V. Alavian and V.H. Chu. Turbulent exchange flow in shallow compound channel. In *21st IAHR Congress, Vol. 3*, pages 447–451, Melbourne, Australia, Aug. 1985. IAHR.
- [3] J.R.L. Allen. River bedforms: Progress problems. In Collinson J.D. and J. Lewin, editors, *Modern and Ancient Fluvial System*, pages 19–33. International Association Sedimentologists Special Publication 6. Blackwell Scientific Publications, Oxford, 1983.
- [4] C.V. Alonse, D.K. Borah, and S.N. Prasad. Numerical model for routing graded sediment in alluvial channels. Final Report to the Vickburg Distictu. Technical report, U.S. army Corps of Engineers, U.S. Department of Agriculture Sedimentation Laboratory, Oxford, Miss, 1976.
- [5] E.D. Andrews. Effective and bankfull discharges of streams in Yampa River basin. *Jour. Hydro.*, 46:311–300, 1980.
- [6] R. Ariathurai and K. Arulanandan. Erosion rates of cohesive soils. *Journal of Hydraulic Engineering, ASCE*, 104(2):279–283, 1978.
- [7] U Arnold, E. Pasche, and G. Rouve. Mixing in rivers with compound cross section. In *21st IAHR Congress, Vol.2*, pages 168–172, Melbourne, Australia, Aug. 1985.
- [8] K. Ashida, M. Fujita, and B.Y. Liu. Suspended load transport in compound channels. In *6th Congress Asian and Pacific Regional Division*, pages 75–82, Tokyo, Japan, July 1988.
- [9] R.A. Bagnold. An approach to the sediment transport problem for general physics. In *Geological Survey Professional Paper 422-I*. United Stats Department of the Interior, Washington, D.C., 1966.
- [10] N Bayazit. Simulating of armor coat formation and destruction. In *Proc. XVIIth IAHR Congress*, pages 73–80, Sao Paulo, Brazil, 1975.
- [11] S. Beltaos. Transverse mixing in natural streams. In *Alberta Research Council Report No. SWE-78/01, pp.25-29.*, 1978.
- [12] J. P. Bennett and C. F. Nordin. Simulation of sediment transport and armoring. *Hydrolog. Sci. Bull.*, 22(4):555–569, 1977.
- [13] D.K. Borah, C.V. Alonso, and S.N. Prasad. Routing graded sediment in streams:formulations. *Journal of Haydraulic Engineering, ASCE*, 108(12):1486–1503, 1982.
- [14] D.K. Borah, C.V. Alonso, and S.N. Prasad. Routing graded sediments in streams: Applications. *Journal of Hydraulic Engineering, ASCE*, 108(12):1504–1517, 1982.
- [15] J.S. Bridge. Hydraulic interpretation of grain size distributions using physical model for bed-load transport. *Journal of Sedimentary Petrology*, 51(4):1109–1124, 1981.

- [16] J.S. Bridge and D.D. Dominic. Bed-load grain velocity and sediment transport. *Water Research Res.*, 20(4):476–490, 1984.
- [17] M.R. Carstens. Accelerated motion of spherical particles. *Tran. Am. Geophys. Union*, 33, 1952.
- [18] I. Celik and W. Rodi. A deposition-entrainment model for suspended sediment transport. Technical Report T6, Sonderforschungsbereich 210, Universität Karlsruhe, 1984.
- [19] I. Celik and W. Rodi. Mathematic modelling of suspended sediment transport in open channels. In *21st IAHR Congress, Vol.3*, pages 533–538, Melbourne, Australia, August 1985.
- [20] H.H. Chang. Mathematical model for erodible channels. *Journal of Hydraulic Engineering, ASCE*, 108(5), 1982.
- [21] H.H. Chang. *Fluvial processes in river engineering*. John Wiley & Sons, Inc, 1987.
- [22] H.H. Chang and J.C. Hill. Computer modeling of erodible flood channel and computer. *Journal of Hydraulic Engineering, ASCE*, 102(10):1461–1477, 1977.
- [23] H.H. Chang and J.C. Hill. Minimum stream power for rivers and deltas. *Journal of Hydraulic Engineering, ASCE*, 103(12):1375–1389, 1977.
- [24] Y.C. Chang. *Lateral mixing in meandering channels*. PhD thesis, Univ. of Iowa, Iowa city, 1971.
- [25] D. Cokljat and B.A. Younis. Compound channel flows: A parametric study using Reynolds-stress transport closure. *Journal of Hydraulic Research*, 33(5), 1995.
- [26] B.R. Colby, C. H. Hembree, and F. H. Rainwater. Sedimentation and chemical quality of surface waters in the winter river basin, Wyoming. *U.S. Geol. Surv. Wat. Supp. Pap.* 1373, 1956.
- [27] N.L. Coleman. Flume studies of sediment transfer coefficient. *Journal of Water Research*, 19(3), 1970.
- [28] P. Cormault. Determination experimentale du debit solide d'erosion de sediments fins choesifs. In *14th IAHR Congress, Vol. 4*, Paris, 1971.
- [29] H.A. Einstein. The bed-load function for sediment transportation in open channel flows. *U.S. Dept. Agric., Soil Conserv. Serv.*, 1026, 1950.
- [30] H.A. Einstein and N. Chien. Effects of heavy sediment concentration near the bed on velocity and sediment concentration. Technical Report No. 8, Univ. Calif. Inst. Eng., 1954.
- [31] J.W. Elder. The dispersion of marked fluid in turbulent shear flow. *J. Fluid. Mech.*, 5:544–560, 1959.
- [32] F. Engelund and E. Hansen. A monograph on sediment transport in alluvial streams. *Journal of Hydraulic Engineering, ASCE*, 98(1), 1967.
- [33] F. Engelund and J. Fredsoe. A sediment transport model for alluvial channels. *Nordic Hydrol., Lingby, Denmark*. 7, pages 293–300, 1976.

- [34] P. Evers. Untersuchung der Strömungsvergänge in gegliederten Gerinnen mit extremen Rauheitsunterschieden. Mitteilungen Heft 45, Institut für Wasserbau und Wasserwirtschaft, Rheinisch-Westfälische Technische Hochschule Aachen, 1983.
- [35] R.E. Falco. Coherent motions in the outer regions of turbulent boundary layers. *Physics of Fluids*, 20(10):124–132, 1977.
- [36] M. Falcon-ASCNAIO and J.F. Kennedy. Flow in alluvial river curves. *J. Fluid Mech.*, 133:1–16, 1983.
- [37] H.B. Fischer. Longitudinal dispersion in laboratory and natural streams. Rep. kh-r-12, Keck Lab., Calif. Inst. of Technol., Pasadena, 1966.
- [38] H.B. Fischer. The mechanics of dispersion in natural streams. *Journal of Hydraulic Engineering, ASCE*, 93:187–216, 1967.
- [39] H.B. Fischer, E.J. List, R.C.Y. Koh, J. Imberger, and N.H. Brooks. *Mixing in inland and Coastal Waters*. Academic Press, New York, 1979.
- [40] S. Fukuoka and K. Fujita. Prediction of flow resistance in compound channels and its application to design of river courses. *Proc. JSCE*, 411/II-12:268–273, 1989.
- [41] Bundesanstalt für Gewässerkunde (Hr. Zieger), 1996. Ergebnisse des Schwebstoffeßprogramms der BfG, Persönliche Mitteilung.
- [42] J. Gailani, C.K. Zoegler, and W. Lick. Transport of suspended solids in the lower Fox River. *Journal of Great Lakes Res.*, 1991.
- [43] J. Gessler. The beginning of bed-load movement of mixtures investigated as natural armoring in channels. Technical report, W. K. Laboratory of Hydraulics and Water Resources, California Institute of Technology, Pasadena, 1967.
- [44] J. Gessler. Self-stabilizing tendencies of alluvial channels. *Journal of Hydraulic Engineering, ASCE*, 96(WW2), 1970.
- [45] J. Gessler. Critical shear stress of sediment mixtures. In *Proc. XIV IAHR Congress*, Paris, 1971.
- [46] W.H. Graf. *Hydraulics of sediment transport*. McGraw-Hill Book Company, N.Y., 1971.
- [47] D.I. Graham, P.W. James, T.E.R. Jones, J.M. Davies, and E.A. Delo. Measurement and prediction of surface shear stress in annular flume. *Journal of Hydraulic Engineering, ASCE*, 118(9):1270–1286, 1992.
- [48] A. J. Grass. Initial instability of fine bed sands. *Journal of Hydraulic Engineering, ASCE*, 96(HY3), 1970.
- [49] A.J. Grass. Structure features of turbulent flow over smooth and rough boundaries. *J. Fluid. Mech.*, 50(2):233–255, 1971.
- [50] N. Hawley. Preliminary observations of sediment erosion from a bottom resting flume. *J. Great Lakes Res.*, 17(3):361–367, 1991.
- [51] M. Hino. Turbulent flow with suspended particles. *Journal of Hydraulic Engineering, ASCE*, 89:161–185, 1963.

- [52] J.O. Hinze. *Turbulence (second edition)*. McGraw-Hill Book Co., Inc., New York, 1975.
- [53] F.M. Holly Jr., J.C. Yang, P. Schovarz, J. Scheefer, S.H. Hsu, and R. Einhellig. CHARIMA numerical simulation of unsteady water and sediment movements in multi-connected networks of mobile-bed channels. IIHR Report No. 343, Iowa Insititute of Hydraulic Research, The Univerity of Iowa, 1990.
- [54] F.M. Holly Jr. Dispersion in rivers and coastal waters -1 . physical principles and dispersion equations. In P. Novak, editor, *Developments in Hydraulic Engineering -3*, pages 1–37. ELSEVIER APPLIED SCIENCE PUBLICATION, LONDON and NEW YORK, 1985.
- [55] G. Holtroff. Steady bed material transport in alluvial channel. *Journal of Hydraulic Engineering, ASCE*, 109(3), 1983.
- [56] S.M. Hsu and F.M. Holly Jr. Conceptual bed-load transport model and verification for sediment mixtures. *Journal of Hydraulic Engineering, ASCE*, 118(8), 1992.
- [57] H. Imamoto and T. Ishigaki. Flow visualisation in a transverse cross section of an open channel flow. *Journal of experimental heat transfer, thermal dynamics and fluid mechnics*, 5(3):268–273, 1992.
- [58] C. S. James. Seidiment transfer to overbank sections. *Journal of Hydraulic Research, IAHR*, 23(5), 1985.
- [59] H.E. Jobson and W.W. Sayre. Vertical transfer in open channel flow. *Journal of Hydraulic Engineering, ASCE*, 96(3):703–724, 1970.
- [60] M.F. Karim and J.F. Kennedy. Computer-based predictor for sediment discharge and factor of flluvial streams. IIHR Report 242, Iowa Institute of Hydraulic Research, the University of Iwoa, 1981.
- [61] M.F. Karim and John F. Kennedy. IALLUVIAL: A computer-based flow- and sediment-routing model for alluvial streams and its application to the Missoti River. IIHR Rep. No.250, Iowa Institute of Hydraulic Research, The university of Iwoa, Iwoa City, Iowa, 1982.
- [62] U. Kern. Transport von Schweb- und Schadstoffen in staugeregelten Fließgewässern am Beispiel des Neckars. Mitteilungen Helft 93, Institut für Wasserbau, Universität Stuttgart, 1997.
- [63] U. Kern and B. Westrich. Mobilität von Schadstoffen in den Sedimenten staugeregelter Flüsse - Zustand und Schadstoffpotential der Neckarsedimente (Abschlußbericht). Wissenschaftlicher Bericht 93/15 (HG 181), Institut für Wasserbau, Universität Stuttgart, 1993.
- [64] U. Kern and B. Westrich. Mobilität von Schadstoffen in den Sedimenten staugeregelter Flüsse - Naturversuche in der Stauhaltung Lauffen, Modellierung und Abschätzung des Remobilisierungsrisikos kontaminierter Altsedimente (Abschlußbericht). Wissenschaftlicher Bericht 96/23 (HG 237), Institut für Wasserbau, Universität Stuttgart, Stuttgart, 1996.
- [65] R.H. Kessel, K.C. Dunn, and R.C. McDonald. Lateral erosion and overbank deposition in the Mississippi River in Louisiana caused by the 1973 flooding. *Geology*, 11:461–464, 1974.

- [66] S.J. Kline, W.C. Peynolds, F.A. Schraub, and P.W. Rundstadler. The structure of turbulent boundary layers. *J. Fluid. Mech.*, 30:741–773, 1967.
- [67] R. Kohane. Berechnungsmethoden für Hochwasserabfluß in Fließgewässern mit oberströmten Vorländern. Mitteilungen Heft 73, Institut für Wasserbau Universität Stuttgart, 1991.
- [68] H. Könemann. Der wechselseitige Einfluss von Vorland und Flussbett auf das Widerstandsverhalten offener Gerinne mit gegliederten Querschnitten. Technical Report 25, Institut für Wasserbau der technischen Hochschule Darmstadt, 1980.
- [69] W. Kron. GENESIS - GENERation of SIMultaneous Streamflows. Bericht, Institut für Hydrologie und Wasserwirtschaft, Karlsruhe, 1996.
- [70] S. Krüger. Berechnungen mit einem numerischen Strömungsmodell für die Stauhaltung Lauffen am Neckar. Entwurf, Institut für Wasserbau, Universität Stuttgart, 1994.
- [71] C. Kuijper, J.M. Cornelisse, and J.C. Winterwerp. Research on erosive properties of cohesive sediments. *J. Geophysical Research*, 94(C10):14,341–14,350, 1989.
- [72] P. Larsen and N. Eisenhauer, editors. *Proceedings of the 5th International Symposium on River Sedimentation*, Karlsruhe, 1992. ISRS.
- [73] Y.L. Lau and B.G. Krishnapppan. Transverse dispersion in rectangular channels. *Journal of Haydraulic Engineering, ASCE*, 103(10):1173–1189, 1977.
- [74] Y.L. Lau and B.G. Krishnapppan. Modeling transverse mixing in natural streams. *Journal of Haydraulic Engineering, ASCE*, 107(2):209–226, 1981.
- [75] G. H. Lean and T. J. Weare. Modeling two-dimensional circulating flow. *Journal of Hydraulic Engineering, ASCE*, 105(1):17–26, 1979.
- [76] Hong-Yuan Lee, Hui-Ming Hsieh, Jinn-chuang Yang, and C.T. Yang. Quasi-two-dimensional simulation of scour and deposition in alluvial channels. *Journal of Hydraulic Engineering, ASCE*, 123(7):600–609, 1997.
- [77] Hong-Yuan Lee and A.J. Odgaard. Simulation of bed aromoring in alluvial channels. *Journal of Haydraulic Engineering, ASCE*, 112(9):794–801, 1986.
- [78] M.R. Leeder. On the interactions between turbulent flow, sediment transport and bedform mechanics in channelized flow. In Collinson J.D. and Lewin J., editors, *Modern and Ancient Fluvial Systems*. International Association Sedimentologists Special Publication 6, 5-18, Blackwell Scientific Publications, Oxford, 1983.
- [79] L.B. Leopld and Naddock. The hydraulic geometry of stream channels and physiographic implication. Geol. Surv. Prof. Pap., 252, United States Department of the Interior, Washington D.C., 1953.
- [80] L.B. Leopold. *A View of Rivers*. Harvard University Press, Cambridge, Massachusetts, London, England, 1994.
- [81] B. Lin and K. Shiono. Numerical moderling of solute transport in compound channel flows. *Journal of Hydraulic Research*, 33(6), 1995.

- [82] W.C. Little and R.G. Mayer. Stability of channel beds by armouring. *Journal of Hydraulic Engineering, ASCE*, 102(11):1647-1661, 1976.
- [83] G.K.Y. Luk and Y.L. Lau. Mathematical model of unsteady-state pollutants in natural streams. In *22st IAHR Congress*, pages 227-232, École Polytechnique Fédérale, Lausanne, 1987.
- [84] M.G. Macklin, B.T. Rumsby, and M.D. Newson. Historical floods and vertical accretion of fine-grained alluvium in the lower type valley, northeast England. In P. Billi, R.D. Hey, C.R. Thorne, and P. Tacconi, editors, *Dynamics of Gravel-Bed Rivers*. Wiley & Sons, Chichester, 1992.
- [85] H. Majumdar and M.R. Carstens. Diffusion of particles by turbulence: Effect of particle size. Technical Report WRC-0967, Water Research Center, Georgia Inst. Techn., Atlanta., 1967.
- [86] B.E. Maper. Sediment transport by streams in the Walla Walla River Basin, Washington and Oregon, July 1962 - June 1965. In *U.S. Geol. Surv. Wat. Supp. Pap.*, United States Department of the Interior, Washington, D.C., 1969.
- [87] V.J. Matyukhin and O.N. Prokoev. Experimental determination of the coefficient of vertical turbulent diffusion in water for settling particles. *Soviet Hydrol. (Am. Geophys. Union)*, 1966.
- [88] H. J. Mayer. Sedimentuntersuchungen im mittleren Neckar. *Deutsche gewässerkundliche Mitteilungen*, 32(1/2):27-34, 1988.
- [89] H.J. Mayer, M. Tippner, U. Schleichert, and D. Müller. Sedimentprofiluntersuchungen des Neckars (Bereich WSA Stuttgart). BfG-Bericht 0341, Bundesanstalt für Gewässerkunde, 1986.
- [90] A.J. Mehta. Laboratory studies on cohesive sediment deposition and erosion. In W. van Leussen, editor, *Physical Processes in Estuaries*, pages 427-445. Springer Verlag, Berlin, 1989.
- [91] A. Molinas and C.T. Yang. Computer program users manual for GSTARS. Technical report, U.S. Department of Interior Bureau of Reclamation Engineering and Research Centre, Denver Colo., 1986.
- [92] G. Müller. Schwermetallbelastung der Sedimente und Gewässergüte des Neckars 1972-1979-1985: Ein Vergleich. In G. Müller, editor, *Heidelberger Geowissenschaftliche Abhandlungen 5: 2. Neckar-Umwelt-Symposium, 22.-23. Oktober 1986 in Heidelberg*, pages 1-12, 1986.
- [93] P. Müller. Transport und selektive Sedimentation von Schwebstoffen bei gestautem Abfluß. Mitteilungen 56, Institut für Wasserbau, Universität Stuttgart, 1985.
- [94] H. Nakagawa and I. Nezu. Structure of space-time correlation of bursting phenomena. *J. Fluid. Mech.*, 104:1-43, 1981.
- [95] T. Nakato. Discussion of "modeling of river channel changes" by Chang, H.H. *Journal of Hydraulic Engineering, ASCE*, 113(2):262-265, 1987.

- [96] T. Nakato. Test of suspended sediment-transport formulas. *Journal of Hydraulic Engineering, ASCE*, 106(3):362-379, 1990.
- [97] T. Nakato, J.F. Kennedy, and J. Vadnal. A numerical model for flow and sediment transport in alluvial-river bends. IIHR Report No. 271, Iowa Institute of Hydraulic Research, University Iowa, Iowa City, Iowa, 1983.
- [98] G.C. Nanson. Point bar and flood plain formation of the meandering Beatton River, Northeastern British Columbia, Canada. *Sedimentology*, 27:3-29, 1986.
- [99] D. Naot, I. Nezu, and H. Nakagawa. Hydrodynamic behavior of compound rectangular open channels. *Journal of Hydraulic Engineering, ASCE*, 119(3):390-408, 1993.
- [100] I. Nezu and H. Nakagawa. Turbulence in open-channel flows. In *IAHR Monograph Series*, Rotterdam, Netherlands, 1993. Balkema.
- [101] G. Nicollet and M. Uan. Ecoulements à surface libre en lits composés. *Electricité de France, Direction des études et recherches*, E43/77/53, 1977.
- [102] P.I. Nokes and G.O. Hughes. 3d, turbulent mixing in uniform channel of irregular cross-section. *Journal of Hydraulic Research*, 32:67-86, 1994.
- [103] H.J.M. Ogink. The effective viscosity coefficient in 2-d depth-averaged flow models. In *21st IAHR Congress*, volume 3, Melbourne, Australia, August 1985.
- [104] T.M. Parchure and A.J. Mehta. Erosion of soft cohesive sediment deposits. *Journal of Hydraulic Engineering, ASCE*, 111(10):1308-1327, 1985.
- [105] I. Park and S.C. Jain. Numerical simulation of degradation of alluvial channels. *Journal of Hydraulic Engineering, ASCE*, 113(7):845-859, 1987.
- [106] E. Partheniades. Erosion and deposition of cohesive sediment. *Journal of Hydraulic Engineering, ASCE*, 91(HY1), 1965.
- [107] E. Pasche, G. Rouve, and P. Evers. Flow in compound channels with extreme flood-plain roughness. In *21st IAHR Congress*, pages 384-389, Melbourne, Australia, August 1985.
- [108] S.V. Patankar. A calculation procedure for two-dimensional elliptic situation. *Num. Heat. Transfer*, 2, 1979.
- [109] S.V. Patankar. *Numerical Heat Transfer and Fluid Flow*. McGraw-Hill, 1980.
- [110] S.V. Patankar and D.B. Spalding. A calculation procedure of mass, heat and momentum transfer in three-dimensional parabolic flows. *International Journal of Heat, Mass Transfer*, 15:1778-1806, 1972.
- [111] J.E. Pizutto. Flow variability and bankfull of sand-bed streams of the American Midwest. *Earth. Surf. Proc. Landf.*, 11:441-450, 1986.
- [112] P. Prinos and R.D. Townsend. Discharge in compound open channel. In *Proc. of 6th. Canadian Hydraulical Conf.*, pages 129-146, 1983.
- [113] P. Prinos and R.D. Townsend. Comparison of methods for predicting discharge in compound channels. *Advances in water resources*, 7:180-187, Dec. 1984.

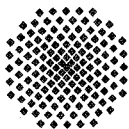
- [114] P. Prinos and R.D. Townsend. Structure of turbulence in compound channel flow. *Journal of Hydraulic Engineering, ASCE*, 111(5):1246–1261, 1985.
- [115] G.J. Proffitt and A.J. Sutherland. Transport of nonuniform sediment. *Journal of Hydraulic Research, IAHR*, 21(1):33–43, 1983.
- [116] J.L. Rahuel, F.M. Holly, J.P. Chollet, P.J. Belleudy, and G. Yang. Modeling of riverbed evolution for bedload sediment mixtures. *Journal of Hydraulic Engineering, ASCE*, 115(11):1521–1543, 1989.
- [117] N. Rajaratnam and R. Ahmadi. Interaction between main channel and flood plain flows. *Journal of Hydraulic Engineering, ASCE*, 103(5), 1979.
- [118] N. Rajaratnam and R. Ahmadi. Hydraulics of channels with flood-plains. *Journal of Hydraulic Research*, 19(1):43–60, 1981.
- [119] K.N. Rao, R. Narasimha, and Narayanan M.A.B. The burstion phenomenon in a turbulent boundary layer. *J. Fluid. Mech.*, 48:339–352, 1971.
- [120] I. Reid and L. E. Frostick. Fluvial sediment transport and deposition. In Kenneth Pye, editor, *Sediment transport and Deposition Processes*, chapter 4. ACKWELL SCIENTIFIC PUBLICATIONS, 1994.
- [121] J.S. Ribberink. *Mathematical modelling of one-dimensional morphological changes in rivers with non-uniform sediment*. PhD thesis, Delft, Techn. Univ., 1987.
- [122] H. Rouse. Modern conceptions of the mechanics of sediment suspension. *Transactions, ASCE*, 102:463–543, 1937.
- [123] J.C. Rutherford. *River Mixing*. J. Wiley and Sons, New York, 1994.
- [124] B.R. Samaga, K.G. Ranga Raju, and R.J. Garde. Bed-load transport of sediment mixtures. *Journal of Hydraulic Engineering, ASCE*, 112(HY11):1003–1018, 1986.
- [125] B.R. Samaga, Kittur G. Ranga Raju, and R.J. Garde. Suspended load transport of sediment mixtures. *Journal of Hydraulic Engineering, ASCE*, 112(HY11):1019–1035, 1986.
- [126] W.W. Sayre and Tsq-Ping Yeh. Transverse mixing characteristics of the Missouri River downstream from the Cooper Nuclear Station. IIHR Report No. 145, Iowa Institute of Hydraulic Research, The University of Iowa, Iowa City, Iowa, 1973.
- [127] W. Schmidt. Der Massenaustausch in freier Luft und verwandte Erscheinungen. *Probleme der kosmischen Physik*, 7, 1925.
- [128] B.E. Schönung. *Numerische Strömungsmechanik: Inkompressible Strömungen mit komplexen Berandungen*. Spring-Verlag, 1990.
- [129] H.W. Shen and C.S. Hung. Remodified Einstein procedure for sediment load. *Journal of Hydraulic Engineering, ASCE*, 109(4):565–578, 1983.
- [130] A. Shields. Anwendung der Ähnlichkeitsmechanik und Turbulenzforschung auf die Geschiebebewegung. Mitteilungen 26, Preussische Versuchsanstalt für Wasserbau und Schiffbau, 1936.

- [131] D.B. Simons and F. Sentuerk. *Sediment transport Technology: Water and Sediment Dynamics*. Water resource publications USA, 1992.
- [132] S.R. Singamsetti. Diffusion of sediment in a submerged jet. *Journal of Hydraulic Engineering, ASCE*, 92(2):153–168, 1966.
- [133] G.Di. Siolvio. Sediment exchange between stream and bottom: a four layer model. In *Proceedings of the International Grain Sorting Seminar*, Zürich, Oct. 1991. Versuchsanstalt für Wasserbau, Hydrologie und Glaziologie der Eidgenössischen Technischen Hochschule Zürich.
- [134] C.D. Smith. Effects of channel meanders on flood stage in valley. *Journal of Hydraulic Engineering, ASCE*, 104(1):49–58, 1978.
- [135] J.D. Smith and S.R. McLean. Mechanics of flow over ripples and dunes. *J. Geophy. Res.*, 94(12):1735–1746, 1977.
- [136] D.B. Spalding. A novel finite-difference-formulation for differential expressions involving both first and second derivatives. *Int. J. Num. Methods Eng.*, 4:551, 1972.
- [137] G. Steinbach and H. Hanisch. Traceversuche und mathematische Modelle zur Beschreibung des Stofftransportes im Rhein. Technical Report BfG-0626, BUNDESANSTALT FÜR GEWÄSSERKUNDE -BfG-, Koblenz, August 1991.
- [138] D. Stephenson and P. Kolovopoulos. Effects of momentum transfer in compound channels. *Journal of Hydraulic Engineering, ASCE*, 116(12):1512–1522, 1990.
- [139] A.J. Sutherland. Proposed mechanism of sediment entrainment of turbulent flows. *Journal of Geophysical Research*, 72:6183–6194, 1967.
- [140] A.J. Sutherland. Static armour layers by selective erosion. In C.R. Thorne, J.C. Bathurst, and R.D. Hey, editors, *Sediment Transport in Gravel-Bed Rivers*, pages 243–260. Wiley, Chichester, 1987.
- [141] Prabhata K. Swamee and Chandra Shekhar P. Ojha. Bed-load and suspended-load transport of nonuniform sediments. *Journal of Hydraulic Engineering, ASCE*, 117(6):774–787, 1991.
- [142] N. Tamai, T. Asaeda, and Ikeda. Study on generation of periodical large surface eddies in compound channel flow. *Water Resource Res.*, 22(7):1129–1138, 1986.
- [143] G.I. Taylor. Dispersion of soluble matter in solvent flowing slowly through a tube. *Dispersions of the Royal Society of London Series A*, 219:186–203, 1953.
- [144] C. Tchen. *Mean Value and Correlation Problems Connected with the Motion of Small Particles Suspended in a Turbulent Fluid*. PhD thesis, Technische Hogeschool, Delft, 1947.
- [145] C. Teisson. Cohesive suspended sediment transport: feasibility and limitations of numerical modeling. *Journal of Hydraulic Research*, 29(6):755–769, 1991.
- [146] W.A. Thomas and A.L. Prashum. Mathematical model of scour and deposition. *Journal of Hydraulic Engineering, ASCE*, 110(11):1613–1641, 1977.
- [147] A. Tominage and I. Nezu. Turbulent structure in compound open-channel flows. *Journal of Hydraulic Engineering, ASCE*, 117(11):21–41, 1991.

- [148] Cheng-Han Tsai and Wilber Lick. Resuspension of sediment from long island sound (U.S.A.). *Water science and technology*, 20(6/7):155–164, 1988.
- [149] Tsinghua University. A preliminary report on the model test for the TGP dam area sediment deposition. Technical report, Dept. of Hydr. Eng., 1994.
- [150] The Hydrologic Engineering Center US Army Corps of Engineers. *HEC-6 Scour and Deposition in River and Reservoirs*, 1977.
- [151] A. van Mazijk. *One-dimensional approach of transport phenomena of dissolved matter in rivers*. PhD thesis, Technical University Delft, NL, 1996.
- [152] A. van Niekerk, K.R. Vogel, R.L. Slingerland, and J.S. Bridge. Routing of heterogeneous sediments over movable bed: Model development. *Journal of Hydraulic Engineering, ASCE*, 118(HY2), 1992.
- [153] L.C. van Rijn. Sediment transport. Part I : Bed load transport. *Journal of Hydraulic Engineering, ASCE*, 110(10):1431–1456, 1984.
- [154] L.C. van Rijn. Sediment transport. Part II : Suspended load transport. *Journal of Hydraulic Engineering, ASCE*, 110(11):1613–1732, 1984.
- [155] L.C. van Rijn. Mathematical modeling of suspended sediment in nonuniform flows. *Journal of Hydraulic Engineering, ASCE*, 112(6):433–455, 1986.
- [156] V.A. Vanoni. Sediment transportation mechanics: Suspension of sediment (progress report of task committee). *Journal of Hydraulic Engineering, ASCE*, 89(5), 1963.
- [157] V.A. Vanoni. Measurement of critical shear stresses for entraining fine sediments in a boundary layer. California Institute Technology Report, KH-R-7, California Institute, 1964.
- [158] V.A. Vanoni. Sediment transportation mechanics: Initial of motion (progress report of task committee). *Journal of Hydraulic Engineering, ASCE*, 92(2), 1966.
- [159] V.A. Vanoni. Sediment engineering. ASCE-manuals and reports, Amer. Soc. Civ. Eng., New York, USA, 1975.
- [160] V.A. Vanoni and G.N. Nomicos. Resistance properties of sediment-laden streams. *Trans. Am. Soc. Civil. Engrs.*, 125(1), 1960.
- [161] D.E. Walling and S.B. Bradley. Rates and patterns of contemporary flood plain sedimentation: a case study of the River Clume, Devon, UK. *Geojournal*, 19:153–162, 1989.
- [162] S. Y. Wang and S.E. Adeff. Three-dimensional modeling of river sedimentation processes. In S.Y. Wang, H.W. Shen, and L.Z. Ding, editors, *Proceedings of the Third International Symposium on River Sedimentation*, pages 1496–1505, The University of Mississippi, March 1989.
- [163] S.Y. Wang, H.W. Shen, and L.Z. Ding, editors. *Proceedings of the Third International Symposium on River Sedimentation*, The University of Mississippi, 1986.
- [164] Z. Y. Wang, W. Kron, X. Lu, and E. Plate. Flume experiments on sediment transport, erosion and siltation of a channel bed in unsteady and non-uniform flow conditions. Bericht, Institut für Hydrologie und Wasserwirtschaft, Karlsruhe, 1993.

- [165] Z.Y. Wang and P. Larsen. Turbulent structure of water and clay suspension with bed load. *Journal of Hydraulic Engineering, ASCE*, 120(5):577–600, 1994.
- [166] B. Westrich. Massenaustausch in Strömungen mit Totwasserzonen unter stationären Fließbedingungen. Mitteilungen SFB /80 /ET / 95, Universität Karlsruhe, April 1977.
- [167] B. Westrich. *Fluvialer Feststofftransport - Auswirkungen auf die Morphologie und Bedeutung für die Gewässergüte*. Schriftenreihe GWF Wasser, Abwasser, Band 22. Oldenbourg Verlag, München, 1988.
- [168] B. Westrich. Schadstofftransport in Flüssen und besonderer Berücksichtigung des Feststoffeinflusses (Zwischenbericht). Wissenschaftlicher Bericht 90/28(hg 138), Institut für Wasserbau, Universität Stuttgart, 1990.
- [169] B. Westrich and M. Juraschek. Flow transport capacity for suspended sediment. In *XXIth IAHR Congress, Vol.3*, Melbourne, Australia, 1985.
- [170] B. Westrich and H. Kobus. Massenaustausch in Strömungen mit Totwasserzone. Technical Report SFB /80 /ET / 164, Universität Karlsruhe, Dez. 1978.
- [171] Bernd Westrich, Yichun Xu, and Samer Al-zubi. Numerical modelling of suspended sediment transport in compound channels. In *2nd International Conference on River Flood Hydraulics*, York, England, March 1994.
- [172] I.R. Wood and T. Liang. Dispersion in open channel with a step in the cross-section. *Journal of Hydraulic Research*, 27(6):587–601, 1989.
- [173] H. Xie. Characteristics of overbank flow and related hydraulic computations. In *Proceedings of the International Symposium on River Sedimentation*. Chinese Soc. of Hydr. Eng. Beijing, 1980.
- [174] Yichun Xu and Bernd Westrich. Simulation of suspended-load transport and sediment sorting on sediment mixtures. In F.M. Holly Jr and A. Alsaffar, editors, *Proceedings of XXVII Congress of International Association for Hydraulic Research, Theme A.*, San Francisco, Aug. 1997.
- [175] M.S. Yalin and B.M. Krishnappan. A probabilistic method for determining the distribution of suspended solids in open channel. In *Proc. of Int. Symp. on River Mechanics, IAHR*, pages A–52, 1–12, 1973.
- [176] C.T. Yang. Incipient motion and sediment transport. *Journal of Hydraulic Engineering, ASCE*, 99(HY10):1679–1704, 1973.
- [177] C.T. Yang. Sediment transport and unit stream power function. *Journal of Hydraulic Engineering, ASCE*, 108(6):1679–1704, 1982.
- [178] C.T. Yang. Unit stream power equation for gravel. *Journal of Hydraulic Engineering, ASCE*, 110(12):1679–1704, 1984.
- [179] Ben Chie Yen. Hydraulics of flood plains: Methodology for backwater computation. Wissenschaftlicher Bericht No.84/5(HWV 053), Institut für Wasserbau, Universität Stuttgart, 1984.

- [180] Ben Chie Yen, R. Camacho, R. Kohane, and B. Westrich. Significance of flood plains in backwater computation. In *21st IAHR Congress, Vol. 3 (Theme B)*, pages 440–445, Melbourne, Australia, August 1985.
- [181] C.L. Yen, H.Y. Lee, and S.Y. Chang. A study on aggregation/degradation of coarse sediment in alluvial stream. Res. Report 88, Hydr. Res. Lab., Nat. Taiwan Univ., Taiwan, 1988.
- [182] C.L. Yen, H.Y. Lee, and S.Y. Chang. Recovery of channel bed in aggregation/degradation process. In *23rd IAHR Congress*, pages B323–B329. IAHR, 1989.
- [183] N. Yotsukura and E.D. Cobb. Transverse diffusion of solution in natural streams. *United States Geological Survey (USGS), Professional Paper 582-C, Geological Survey, United States Department of Interior, Washington, DC*, 1972.
- [184] N. Yotsukura and W. W. Sayer. Transverse mixing in natural channels. *Water Resources Research*, 12(4), 1976.
- [185] Jianjun Zhou and Bingnan Lin. 2-d mathematical model for suspended sediment, Part I - Model theories and validations. *Journal of basis science and engineering*, 3(1), 1995.
- [186] C.K. Ziegler and W. Lick. A numerical model of the resuspension, deposition and transport of fine-grained sediments in shallow water. Technical Report ME-86-3, University of California, Santa Barbara, California, 1986.
- [187] C.K. Ziegler and B. S. Nisbet. Fine-grained sediment transport in Pawtuxet River, Rhode Island. *Journal of Hydraulic Engineering, ASCE*, 120(5):561–577, 1994.
- [188] C.K. Ziegler and B.S. Nisbet. Long-term simulation of fine-grained sediment transport in large reservoir. *Journal of Hydraulic Engineering, ASCE*, 121(11), 1995.



Direktoren

o. Prof. Dr.-Ing. habil. Jürgen Giesecke
o. Prof. Dr.h.c. Helmut Kobus, Ph.D.

Vorstand

o. Prof. Dr.-Ing. habil. J. Giesecke
o. Prof. Dr.h.c. H. Kobus, Ph.D.
Prof. Dr.-Ing. Dr. A. Bárdossy
(Wassermengenwirtschaft)
Prof. Dr.-Ing. habil. B. Westrich
Dr.-Ing. B. Barczewski
Dr.-Ing. H.-P. Koschitzky
Dr.-Ing. W. Marx

Lehrstuhl für Wasserbau und Wasserwirtschaft

Leiter: o. Prof. Dr.-Ing. habil. Jürgen Giesecke
Stellv.: Dr.-Ing. Walter Marx, AOR
Prof. Dr.-Ing. Dr. András Bárdossy
(Wassermengenwirtschaft)

Lehrstuhl für Hydraulik und Grundwasser

Leiter: o. Prof. Dr.h.c. Helmut Kobus, Ph.D.
Stellv.: Dr.-Ing. Hans-Peter Koschitzky, AOR

VEGAS, Versuchseinrichtung zur Grundwasser- und
Altlastensanierung

Wiss. Leiter: Dr.-Ing. Baldur Barczewski

Techn. Leiter: Dr.-Ing. Hans-Peter Koschitzky

Versuchsanstalt

Leiter: apl. Prof. Dr.-Ing. habil. Bernhard Westrich

Verzeichnis der Mitteilungshefte

- 1 Röhnisch, Arthur: *Die Bemühungen um eine Wasserbauliche Versuchsanstalt an der Technischen Hochschule Stuttgart*, und
Fattah Abouleid, Abdel: *Beitrag zur Berechnung einer in lockeren Sand gerammten, zweifach verankerten Spundwand*, 1963
- 2 Marotz, Günter: *Beitrag zur Frage der Standfestigkeit von dichten Asphaltbelägen im Großwasserbau*, 1964
- 3 Gurr, Siegfried: *Beitrag zur Berechnung zusammengesetzter ebener Flächentragwerke unter besonderer Berücksichtigung ebener Stauwände, mit Hilfe von Randwert- und Lastwertmatrizen*, 1965
- 4 Plica, Peter: *Ein Beitrag zur Anwendung von Schalenkonstruktionen im Stahlwasserbau*, und Petrikat, Kurt: *Möglichkeiten und Grenzen des wasserbaulichen Versuchswesens*, 1966
- 5 Plate, Erich: *Beitrag zur Bestimmung der Windgeschwindigkeitsverteilung in der durch eine Wand gestörten bodennahen Luftschicht*, und
Röhnisch, Arthur; Marotz, Günter: *Neue Baustoffe und Bauausführungen für den Schutz der Böschungen und der Sohle von Kanälen, Flüssen und Häfen; Gesteungskosten und jeweilige Vorteile*, sowie Unny, T.E.: *Schwingungsuntersuchungen am Kegelstrahlschieber*, 1967

- 6 Seiler, Erich: *Die Ermittlung des Anlagenwertes der bundeseigenen Binnenschiffahrtsstraßen und Talsperren und des Anteils der Binnenschifffahrt an diesem Wert*, 1967
- 7 *Sonderheft anlässlich des 65. Geburtstages von Prof. Arthur Röhnisch mit Beiträgen von Benk, Dieter; Breitling, J.; Gurr, Siegfried; Haberhauer, Robert; Honekamp, Hermann; Kuz, Klaus Dieter; Marotz, Günter; Mayer-Vorfelder, Hans-Jörg; Miller, Rudolf; Plate, Erich J.; Radomski, Helge; Schwarz, Helmut; Vollmer, Ernst; Wildenhahn, Eberhard*; 1967
- 8 Jumikis, Alfred: *Beitrag zur experimentellen Untersuchung des Wassernachschubs in einem gefrierenden Boden und die Beurteilung der Ergebnisse*, 1968
- 9 Marotz, Günter: *Technische Grundlagen einer Wasserspeicherung im natürlichen Untergrund*, 1968
- 10 Radomski, Helge: *Untersuchungen über den Einfluß der Querschnittsform wellenförmiger Spundwände auf die statischen und rammtechnischen Eigenschaften*, 1968
- 11 Schwarz, Helmut: *Die Grenztragfähigkeit des Baugrundes bei Einwirkung vertikal gezogener Ankerplatten als zweidimensionales Bruchproblem*, 1969
- 12 Erbel, Klaus: *Ein Beitrag zur Untersuchung der Metamorphose von Mittelgebirgsschneedecken unter besonderer Berücksichtigung eines Verfahrens zur Bestimmung der thermischen Schneequalität*, 1969
- 13 Westhaus, Karl-Heinz: *Der Strukturwandel in der Binnenschifffahrt und sein Einfluß auf den Ausbau der Binnenschiffskanäle*, 1969
- 14 Mayer-Vorfelder, Hans-Jörg: *Ein Beitrag zur Berechnung des Erdwiderstandes unter Ansatz der logarithmischen Spirale als Gleitflächenfunktion*, 1970
- 15 Schulz, Manfred: *Berechnung des räumlichen Erddruckes auf die Wandung kreiszylindrischer Körper*, 1970
- 16 Mobasseri, Manoutschehr: *Die Rippenstützmauer. Konstruktion und Grenzen ihrer Standsicherheit*, 1970
- 17 Benk, Dieter: *Ein Beitrag zum Betrieb und zur Bemessung von Hochwasserrückhaltebecken*, 1970
- 18 Gál, Attila: *Bestimmung der mitschwingenden Wassermasse bei überströmten Fischbauchklappen mit kreiszylindrischem Staublech*, 1971, *vergriffen*
- 19 Kuz, Klaus Dieter: *Ein Beitrag zur Frage des Einsetzens von Kavitationerscheinungen in einer Düsenströmung bei Berücksichtigung der im Wasser gelösten Gase*, 1971, *vergriffen*

- 20 Schaak, Hartmut: *Verteilungen von Wasserkraftanlagen*, 1971
- 21 *Sonderheft zur Eröffnung der neuen Versuchsanstalt des Instituts für Wasserbau der Universität Stuttgart mit Beiträgen von*
Brombach, Hansjörg; Dirksen, Wolfram; Gál, Attila; Gerlach, Reinhard; Giesecke, Jürgen; Holthoff, Franz-Josef; Kuz, Klaus Dieter; Marotz, Günter; Minor, Hans-Erwin; Petrikat, Kurt; Röhnisch, Arthur; Rueff, Helge; Schwarz, Helmut; Vollmer, Ernst; Wildenhahn, Eberhard; 1972
- 22 Wang, Chung-su: *Ein Beitrag zur Berechnung der Schwingungen an Kegelstrahlschiebern*, 1972
- 23 Mayer-Vorfelder, Hans-Jörg: *Erdwiderstandsbeiwerte nach dem Ohde-Variationsverfahren*, 1972
- 24 Minor, Hans-Erwin: *Beitrag zur Bestimmung der Schwingungsanfachungsfunktionen überströmter Stauklappen*, 1972
- 25 Brombach, Hansjörg: *Untersuchung strömungsmechanischer Elemente (Fluidik) und die Möglichkeit der Anwendung von Wirbelkammerelementen im Wasserbau*, 1972, vergriffen
- 26 Wildenhahn, Eberhard: *Beitrag zur Berechnung von Horizontalfilterbrunnen*, 1972
- 27 Steinlein, Helmut: *Die Eliminierung der Schwebstoffe aus Flußwasser zum Zweck der unterirdischen Wasserspeicherung, gezeigt am Beispiel der Iller*, 1972
- 28 Holthoff, Franz Josef: *Die Überwindung großer Hubhöhen in der Binnenschifffahrt durch Schwimmerhebwerke*, 1973
- 29 Röder, Karl: *Einwirkungen aus Baugrundbewegungen auf trog- und kastenförmige Konstruktionen des Wasser- und Tunnelbaues*, 1973
- 30 Kretschmer, Heinz: *Die Bemessung von Bogenstaumauern in Abhängigkeit von der Talform*, 1973
- 31 Honekamp, Hermann: *Beitrag zur Berechnung der Montage von Unterwasserpipelines*, 1973
- 32 Giesecke, Jürgen: *Die Wirbelkammertriode als neuartiges Steuerorgan im Wasserbau*, und
Brombach, Hansjörg: *Entwicklung, Bauformen, Wirkungsweise und Steuereigenschaften von Wirbelkammerverstärkern*, 1974
- 33 Rueff, Helge: *Untersuchung der schwingungserregenden Kräfte an zwei hintereinander angeordneten Tiefschützen unter besonderer Berücksichtigung von Kavitation*, 1974

- 34 Röhnisch, Arthur: *Einpreßversuche mit Zementmörtel für Spannbeton - Vergleich der Ergebnisse von Modellversuchen mit Ausführungen in Hüllwellrohren*, 1975
- 35 *Sonderheft anlässlich des 65. Geburtstages von Prof. Dr.-Ing. Kurt Petrikat mit Beiträgen von:* Brombach, Hansjörg; Erbel, Klaus; Flinspach, Dieter; Fischer jr., Richard; Gál, Attila; Gerlach, Reinhard; Giesecke, Jürgen; Haberhauer, Robert; Hafner Edzard; Hausenblas, Bernhard; Horlacher, Hans-Burkhard; Hutarew, Andreas; Knoll, Manfred; Krummet, Ralph; Marotz, Günter; Merkle, Theodor; Miller, Christoph; Minor, Hans-Erwin; Neumayer, Hans; Rao, Syamala; Rath, Paul; Rueff, Helge; Ruppert, Jürgen; Schwarz, Wolfgang; Topal-Gökceli, Mehmet; Vollmer, Ernst; Wang, Chung-su; Weber, Hans-Georg; 1975
- 36 Berger, Jochum: *Beitrag zur Berechnung des Spannungszustandes in rotationssymmetrisch belasteten Kugelschalen veränderlicher Wandstärke unter Gas- und Flüssigkeitsdruck durch Integration schwach singulärer Differentialgleichungen*, 1975
- 37 Dirksen, Wolfram: *Berechnung instationärer Abflußvorgänge in gestauten Gerinnen mittels Differenzenverfahren und die Anwendung auf Hochwasserrückhaltebecken*, 1976
- 38 Horlacher, Hans-Burkhard: *Berechnung instationärer Temperatur- und Wärmespannungsfelder in langen mehrschichtigen Hohlzylindern*, 1976
- 39 Hafner, Edzard: *Untersuchung der hydrodynamischen Kräfte auf Baukörper im Tiefwasserbereich des Meeres*, 1977, ISBN 3-921694-39-6
- 40 Ruppert, Jürgen: *Über den Axialwirbelkammverstärker für den Einsatz im Wasserbau*, 1977, ISBN 3-921694-40-X
- 41 Hutarew, Andreas: *Beitrag zur Beeinflußbarkeit des Sauerstoffgehalts in Fließgewässern an Abstürzen und Wehren*, 1977, ISBN 3-921694-41-8, vergriffen
- 42 Miller, Christoph: *Ein Beitrag zur Bestimmung der schwingungserregenden Kräfte an unterströmten Wehren*, 1977, ISBN 3-921694-42-6
- 43 Schwarz, Wolfgang: *Druckstoßberechnung unter Berücksichtigung der Radial- und Längsverschiebungen der Rohrwandung*, 1978, ISBN 3-921694-43-4
- 44 Kinzelbach, Wolfgang: *Numerische Untersuchungen über den optimalen Einsatz variabler Kühlsysteme einer Kraftwerkskette am Beispiel Oberrhein*, 1978, ISBN 3-921694-44-2
- 45 Barczewski, Baldur: *Neue Meßmethoden für Wasser-Luftgemische und deren Anwendung auf zweiphasige Auftriebsstrahlen*, 1979, ISBN 3-921694-45-0
- 46 Neumayer, Hans: *Untersuchung der Strömungsvorgänge in radialen Wirbelkammerverstärkern*, 1979, ISBN 3-921694-46-9

- 47 Elalfy, Youssef-Elhassan: *Untersuchung der Strömungsvorgänge in Wirbelkammerdioden und -drosseln*, 1979, ISBN 3-921694-47-7
- 48 Brombach, Hansjörg: *Automatisierung der Bewirtschaftung von Wasserspeichern*, 1981, ISBN 3-921694-48-5
- 49 Geldner, Peter: *Deterministische und stochastische Methoden zur Bestimmung der Selbstdichtung von Gewässern*, 1981, ISBN 3-921694-49-3
- 50 Mehlhorn, Hans: *Temperaturveränderungen im Grundwasser durch Brauchwassereingleitungen*, 1982, ISBN 3-921694-50-7, vergriffen
- 51 Hafner, Edzard: *Rohrleitungen und Behälter im Meer*, 1983, ISBN 3-921694-51-5
- 52 Rinnert, Bernd: *Hydrodynamische Dispersion in porösen Medien: Einfluß von Dichteunterschieden auf die Vertikalvermischung in horizontaler Strömung*, 1983, ISBN 3-921694-52-3
- 53 Lindner, Wulf: *Steuerung von Grundwasserentnahmen unter Einhaltung ökologischer Kriterien*, 1983, ISBN 3-921694-53-1, vergriffen
- 54 Herr, Michael; Herzer, Jörg; Kinzelbach, Wolfgang; Kobus, Helmut; Rinnert, Bernd: *Methoden zur rechnerischen Erfassung und hydraulischen Sanierung von Grundwasserkontaminationen*, 1983, ISBN 3-921694-54-X
- 55 Schmitt, Paul: *Wege zur Automatisierung der Niederschlagsermittlung*, 1984, ISBN 3-921694-55-8
- 56 Müller, Peter: *Transport und selektive Sedimentation von Schwebstoffen bei gestau tem Abfluß*, 1985, ISBN 3-921694-56-6
- 57 El-Qawasmeh, Fuad: *Möglichkeiten und Grenzen der Tropfbewässerung unter besonderer Berücksichtigung der Verstopfungsanfälligkeit der Tropfelemente*, 1985, ISBN 3-921694-57-4
- 58 Kirchenbaur, Klaus: *Mikroprozessorgesteuerte Erfassung instationärer Druckfelder am Beispiel seegangsbelasteter Baukörper*, 1985, ISBN 3-921694-58-2
- 59 Kobus, Helmut (Hrsg.): *Modellierung des großräumigen Wärme- und Schadstofftransports im Grundwasser*, Tätigkeitsbericht 1984/85 (DFG-Forschergruppe an den Universitäten Hohenheim, Karlsruhe und Stuttgart), 1985, ISBN 3-921694-59-0
- 60 Spitz, Karlheinz: *Dispersion in porösen Medien: Einfluß von Inhomogenitäten und Dichteunterschieden*, 1985, ISBN 3-921694-60-4
- 61 Kobus, Helmut: *An Introduction to Air-Water Flows in Hydraulics*, 1985, ISBN 3-921694-61-2

- 62 Kaleris, Vassilios: *Erfassung des Austausches von Oberflächen- und Grundwasser in horizontalebene Grundwassermodellen*, 1986, ISBN 3-921694-62-0
- 63 Herr, Michael: *Grundlagen der hydraulischen Sanierung verunreinigter Porengrundwasserleiter*, 1987, ISBN 3-921694-63-9
- 64 Marx, Walter: *Berechnung von Temperatur und Spannung in Massenbeton infolge Hydratation*, 1987, ISBN 3-921694-64-7
- 65 Koschitzky, Hans-Peter: *Dimensionierungskonzept für Sohlbelüfter in Schußbrinnen zur Vermeidung von Kavitationsschäden*, 1987, ISBN 3-921694-65-5
- 66 Kobus, Helmut (Hrsg.): *Modellierung des großräumigen Wärme- und Schadstofftransports im Grundwasser*, Tätigkeitsbericht 1986/87 (DFG-Forschergruppe an den Universitäten Hohenheim, Karlsruhe und Stuttgart) 1987, ISBN 3-921694-66-3
- 67 Söll, Thomas: *Berechnungsverfahren zur Abschätzung anthropogener Temperaturanomalien im Grundwasser*, 1988, ISBN 3-921694-67-1
- 68 Dittrich, Andreas; Westrich, Bernd: *Bodenseeufererosion, Bestandsaufnahme und Bewertung*, 1988, ISBN 3-921694-68-X, vergriffen
- 69 Huwe, Bernd; van der Ploeg, Rienk R.: *Modelle zur Simulation des Stickstoffhaushaltes von Standorten mit unterschiedlicher landwirtschaftlicher Nutzung*, 1988, ISBN 3-921694-69-8, vergriffen
- 70 Stephan, Karl: *Integration elliptischer Funktionen*, 1988, ISBN 3-921694-70-1
- 71 Kobus, Helmut; Zilliox, Lothaire (Hrsg.): *Nitratbelastung des Grundwassers, Auswirkungen der Landwirtschaft auf die Grundwasser- und Rohwasserbeschaffenheit und Maßnahmen zum Schutz des Grundwassers*. Vorträge des deutsch-französischen Kolloquiums am 6. Oktober 1988, Universitäten Stuttgart und Louis Pasteur Strasbourg (Vorträge in deutsch oder französisch, Kurzfassungen zweisprachig), 1988, ISBN 3-921694-71-X
- 72 Soyeaux, Renald: *Unterströmung von Stauanlagen auf kluftigem Untergrund unter Berücksichtigung laminarer und turbulenter Fließzustände*, 1991, ISBN 3-921694-72-8
- 73 Kohane, Roberto: *Berechnungsmethoden für Hochwasserabfluß in Fließgewässern mit überströmten Vorländern*, 1991, ISBN 3-921694-73-6
- 74 Hassinger, Reinhard: *Beitrag zur Hydraulik und Bemessung von Blocksteinrampen in flexibler Bauweise*, 1991, ISBN 3-921694-74-4
- 75 Schäfer, Gerhard: *Einfluß von Schichtenstrukturen und lokalen Einlagerungen auf die Längsdispersion in Porengrundwasserleitern*, 1991, ISBN 3-921694-75-2

- 76 Giesecke, Jürgen: *Vorträge, Wasserwirtschaft in stark besiedelten Regionen; Umweltforschung mit Schwerpunkt Wasserwirtschaft*, 1991, ISBN 3-921694-76-0
- 77 Huwe, Bernd: *Deterministische und stochastische Ansätze zur Modellierung des Stickstoffhaushalts landwirtschaftlich genutzter Flächen auf unterschiedlichem Skalenniveau*, 1992, ISBN 3-921694-77-9
- 78 Rommel, Michael: *Verwendung von Kluftdaten zur realitätsnahen Generierung von Kluftnetzen mit anschließender laminar-turbulenter Strömungsberechnung*, 1993, ISBN 3-92 1694-78-7
- 79 Marschall, Paul: *Die Ermittlung lokaler Stofffrachten im Grundwasser mit Hilfe von Einbohrloch-Meßverfahren*, 1993, ISBN 3-921694-79-5
- 80 Ptak, Thomas: *Stofftransport in heterogenen Porenaquiferen: Felduntersuchungen und stochastische Modellierung*, 1993, ISBN 3-921694-80-9
- 81 Haakh, Frieder: *Transientes Strömungsverhalten in Wirbelkammern*, 1993, ISBN 3-921694-81-7
- 82 Kobus, Helmut; Cirpka, Olaf; Barczewski, Baldur; Koschitzky, Hans-Peter: *Versuchseinrichtung zur Grundwasser und Altlastensanierung VEGAS, Konzeption und Programmrahmen*, 1993, ISBN 3-921694-82-5
- 83 Zang, Weidong: *Optimaler Echtzeit-Betrieb eines Speichers mit aktueller Abflußregenerierung*, 1994, ISBN 3-921694-83-3
- 84 Franke, Hans-Jörg: *Stochastische Modellierung eines flächenhaften Stoffeintrages und Transports in Grundwasser am Beispiel der Pflanzenschutzmittelproblematik*, 1995, ISBN 3-921694-84-1
- 85 Lang, Ulrich: *Simulation regionaler Strömungs- und Transportvorgänge in Karst-aquiferen mit Hilfe des Doppelkontinuum-Ansatzes: Methodenentwicklung und Parameteridentifikation*, 1995, ISBN 3-921694-85-X, vergriffen
- 86 Helmig, Rainer: *Einführung in die Numerischen Methoden der Hydromechanik*, 1996, ISBN 3-921694-86-8
- 87 Cirpka, Olaf: *CONTRACT: A Numerical Tool for Contaminant Transport and Chemical Transformations - Theory and Program Documentation -*, 1996, ISBN 3-921694-87-6
- 88 Haberlandt, Uwe: *Stochastische Synthese und Regionalisierung des Niederschlages für Schmutzfrachtberechnungen*, 1996, ISBN 3-921694-88-4
- 89 Croisé, Jean: *Extraktion von flüchtigen Chemikalien aus natürlichen Lockergesteinen mittels erzwungener Luftströmung*, 1996, ISBN 3-921694-89-2

- 90 Jorde, Klaus: *Ökologisch begründete, dynamische Mindestwasserregelungen bei Ausleitungskraftwerken*, 1997, ISBN 3-921694-90-6
- 91 Helmig, Rainer: *Gekoppelte Strömungs- und Transportprozesse im Untergrund - Ein Beitrag zur Hydrosystemmodellierung*-, 1998, ISBN 3-921694-91-4
- 92 Emmert, Martin: *Numerische Modellierung nichtisothermer Gas-Wasser Systeme in porösen Medien*, 1997, ISBN 3-921694-92-2
- 93 Kern, Ulrich: *Transport von Schweb- und Schadstoffen in staugeregelten Fließgewässern am Beispiel des Neckars*, 1997, ISBN 3-921694-93-0
- 94 Förster, Georg: *Druckstoßdämpfung durch große Luftblasen in Hochpunkten von Rohrleitungen* 1997, ISBN 3-921694-94-9
- 95 Cirpka, Olaf: *Numerische Methoden zur Simulation des reaktiven Mehrkomponententransports im Grundwasser*, 1997, ISBN 3-921694-95-7
- 96 Färber, Arne: *Wärmetransport in der ungesättigten Bodenzone: Entwicklung einer thermischen In-situ-Sanierungstechnologie*, 1997, ISBN 3-921694-96-5
- 97 Betz, Christoph: *Wasserdampfdestillation von Schadstoffen im porösen Medium: Entwicklung einer thermischen In-situ-Sanierungstechnologie*, 1998, ISBN 3-921694-97-3
- 98 Xu, Yichun: *Numerical Modeling of Suspended Sediment Transport in Rivers*, 1998, ISBN 3-921694-98-1